Coordination between the microbiota and the root endodermis is required for plant mineral nutrient homeostasis

Isai Salas-González[1,6†], Guilhem Reyt[2,3†], Paulina Flis[2,3†], Valéria Custódio[4‡], David Gopaulchan[2,3], Niokhor Bakhoum[2,3], Tristan P. Dew[2,3], Kiran Suresh[5], Rochus Benni Franke[5], Jeffery L. Dangl[1,6], David E. Salt[2,3] and Gabriel Castrillo[2,3*]

[1]Curriculum in Bioinformatics and Computational Biology, Department of Biology, University of North Carolina at Chapel Hill, Chapel Hill, North Carolina, USA.

[2]School of Biosciences, University of Nottingham, Sutton Bonington, United Kingdom

[3]Future Food Beacon of Excellence, University of Nottingham, Sutton Bonington, United Kingdom

[4]Instituto de Tecnologia Química e Biológica António Xavier, Universidad de Nova de Lisboa, Lisboa, Portugal

[5]Institute of Cellular and Molecular Botany, University of Bonn. Germany

[6] Howard Hughes Medical Institute, University of North Carolina at Chapel Hill, Chapel Hill, North Carolina, USA

*Correspondence to: gabriel.castrillo@nottingham.ac.uk

†These authors contributed equally to this work.

‡Current address: Future Food Beacon of Excellence and the School of Biosciences, University of Nottingham, Sutton Bonington, United Kingdom

Abstract

Plant roots and animal guts have evolved specialized cells layers to control mineral nutrient homeostasis that must tolerate the resident microbiota while keeping homeostatic integrity. Whether and how the root diffusion barriers in the endodermis, critical for the mineral nutrient balance of plants, coordinates with the microbiota, is unknown. We demonstrate that genes controlling endodermal function in the model plant *Arabidopsis thaliana* contribute to the plant microbiome assembly. We characterize a regulatory mechanism of endodermal differentiation driven by the microbiota with profound effects on nutrient homeostasis. Furthermore, we demonstrate that this mechanism is linked to the microbiota's capacity to repress responses to the phytohormone abscisic acid in the root. Our findings establish the endodermis as a regulatory hub coordinating microbiota assembly and homeostatic mechanisms.

Plant roots, analogous to animal guts, selectively absorb mineral nutrients and water from the environment and transport them into the vascular systems for long distance transport to other tissues and organs (*1*, *2*). These processes are tightly controlled by specialized cell layers, the root endodermis and exodermis (when present) in plants and the intestinal epithelium in animals. These cells act as control points for the diffusion of water, solutes and immune ligands. Diffusion barriers must permit the presence of the metabolically active resident microbiota and still protect homeostatic integrity. In animals, mechanisms by which the intestinal epithelium functions with the microbiota present have been partially elucidated (*2*) and serious diseases caused by its malfunction have been described (*3*). In contrast, in plants the mechanisms of the deposition of the root diffusion barriers has been described only under axenic conditions (*4*), but the integration of the microbiota into its function is unknown. The endodermis has two types of root diffusion barriers, the Casparian strips, consisting of fine bands of lignin that encircle endodermal cells, and the deposition of suberin within the space between the cell wall and the plasma membrane of endodermal cells. Endodermal suberization follows a defined program by which a few cells first

suberize in a “patchy” manner that later expands into a zone of continuous suberization (*5*). Suberin deposition changes in response to nutritional stress, and is regulated by the plant hormones ethylene and abscisic acid (ABA) (*5*). The activation of a surveillance system to check the integrity of the Casparian strips, controlled by the *Schengen* pathway, induces lignification and suberization of the endodermis (*6*). The discovery that the endodermis restricts the diffusion of microbe-associated molecular patterns (*7)* important for the establishment of the root microbiome (*8*) suggests its role as a regulatory hub coordinating the plant ionome, plant mineral nutrient and trace element composition (*9*), and assembly of the microbiota. This coordination might influence plant performance under changeable environments with consequences on agronomic yields and food nutritional quality.

Genes controlling endodermal function influence microbiome assembly

We compared the bacterial community composition of wild-type *Arabidopsis thaliana* (Arabidopsis) (accession Col-0) plants with five groups of root diffusion barrier mutants and transgenic lines over- or mis-expressing relevant genes (fig. S1A and table S1). Arabidopsis plants lack an exodermis, thus this collection of genotypes represents clean combinatorial impairments in different sectors of the endodermal root diffusion barrier network (fig. S1A). We grew plants in a natural soil and determined their shoot area, as well as root, shoot and soil bacterial community profiles using 16S rRNA amplicon sequencing. We observed that genotypes with strong impairment in the root diffusion barriers (groups 5 and 6) showed a significant reduction in shoot area (fig. S1B) that might be the result of complex interactions between soil properties, the microbiome presence and the root diffusion barriers.

General microbiome characteristics were in line with previous findings (*10*, *11*) (fig. S1C and S1D). Canonical analysis of principal coordinates (CAP) showed significant differences in bacterial community compositions across the root diffusion barrier genotypes (Fig. 1A, S1E). As

expected from a plant-derived mechanism, we consistently observed these differences in root and shoot, but not in the soil fraction (root and shoot PERMANOVA $p < 1e\text{-}4$, soil PERMANOVA $p = 0.25$) (Fig. 1A, S1E, and S1F). Genotypes bearing significantly different bacterial communities represent the majority of the root diffusion barrier plant groups analyzed (Fig. 1A, S1E, S1F, and S1G) indicating that certain genes broadly distributed across the root diffusion barrier regulatory network contribute to the composition of the plant microbiome.

To further understand the interaction between the root diffusion barriers and the plant microbiome, we built a bacterial synthetic community consisting of 41 taxonomically diverse bacteria isolated from the roots and shoots of Arabidopsis grown in natural soils (*12*, *13*). This synthetic community approximates the endophytic compartment community composition observed in natural Arabidopsis populations (fig. S2A). We inoculated seedlings of wild type plants and a selection of seven root diffusion barrier genotypes, representing the different functional groups, grown on agar plates. We recapitulated, in all genotypes, microbiome composition differences observed in a natural soil (Fig. 1B, S2B, S2C, and S2D), regardless of the differences observed in the root metabolome (fig. S2E and S2F), and the root diffusion barrier hormonal control in some of them (fig. S2G). Thus, we confirmed that plants with atypical root diffusion barriers assemble an altered microbiota, even on agar plates that minimize developmental and physiological differences among the root diffusion barrier genotypes (fig. S2H and S2I).

We determined the leaf ionomic profiles of the different genotypes grown in a natural soil and on agar plates. We noticed that some of the genotypes with an atypical shoot ionome also assemble a distinct root and shoot microbiome (Fig. 1C, 1D, S3A and S3B). We found a significant correlation (Mantel test $p < 0.05$) between the root bacterial community dissimilarity and the shoot ionome dissimilarity (Fig. 1E and 1F) in both natural soil and agar systems. This correlation is less obvious with the shoot microbiome of plants grown in a natural soil (fig. S3C), and it does not

exist in the case of the soil microbiome (fig. S3C) and shoot and agar microbiome of plants grown on agar plates (fig. S3D). As a control, we repeated the same analysis with soil elemental profiles, which were different from the plant shoot ionome (fig. S3E, S3F), and we did not detect a significant correlation with the microbiome (fig. S3G).

Our results (Fig. 1) indicate that endodermal root diffusion barrier components regulate plant microbiome configuration in Arabidopsis plants. This effect suggests that the same mechanisms that maintain mineral nutrient homeostasis contribute to microbiome composition as well.

Individual bacterial strains modify root diffusion barriers

To explore the interplay between the root diffusion barriers and the plant microbiome, we analyzed the microbiota's ability to influence the deposition of root diffusion barriers in the endodermis. We determined how the deposition of the Casparian strips and suberin synthesis changes in response to a collection of 416 individual bacterial strains (fig. S4A and S4B) isolated from the roots and shoots of Arabidopsis grown in natural soils (*12*, *13*). We individually screened the bacterial strains for their ability to modify the function of the Casparian strip in blocking the diffusion of propidium iodide, a fluorescent apoplastic tracer, into the root tissue layers (*14*) (fig. S4C). We found that 25% and 1.9% of the isolates analyzed induced a significant early and late block in the diffusion of propidium iodide, respectively (Fig. 2A). Using a representative subset (n=41) of the bacterial strains (Fig. 2B) we proved that these effects were not a mere consequence of root growth modification (Fig. 2A, S5A, S5B, S5C, and S5D). Indeed, we noticed that some bacteria have the capacity to induce changes in the endodermal lignification independently of the appearance of the first root hair, a marker of root development (fig. S5C, S5D, S5E, and S5F). These results indicate that members of the root microbiome have the capacity to modify Casparian strip formation.

105 To test whether this bacterial effect also occurs in the deposition of endodermal suberin, we
106 analyzed the expression of the suberization reporter *pGPAT5::mCITRINE-SYP122* (*15*) in plant
107 roots in response to 416 individual bacterial isolates (fig. S4A, S4B and S4C). The majority of the
108 bacteria analyzed (71%) significantly expanded the root zone where *GPAT5* expression follows
109 a patchy pattern (Fig. 2A). Accordingly, the root zone with continuous activation of *GPAT5* is
110 reduced (Fig. 2A). We ruled out that the bacterial effect on endodermal suberization was
111 exclusively linked to the bacterial capacity to induce changes in root growth (Fig. 2A, S5A, S5G,
112 and S5H). This suberin deposition phenotype showed a strong phylogenetic signal (Pagel's λ =
113 0.78, p = 4.3 e-40) highlighting that closely related strains exhibit similar effects on root
114 suberization (Fig. 2A).
115
116 We demonstrated that the bacterial effects on Casparian strip function and endodermal
117 suberization are not linked. We found no correlation (r = -0.07, p = 0.13) between these two
118 parameters (fig. S5I). The small variation found in Casparian strip function does not explain the
119 large effect detected in the case of suberin deposition in response to the bacterial collection (fig.
120 S5J). These results indicate that Casparian strip synthesis is more resilient to the effect of
121 individual bacteria than endodermal suberization, and that members of the plant microbiome can
122 modify suberin deposition independently of the Casparian strip.
123
124 Next, we used the representative subset (n=41) of the bacterial strains in plant-association assays
125 to test whether their effect on suberization regulates plant mineral nutrient homeostasis (Fig. 2B,
126 S6A, and S6B). We observed that root suberin, stained with Fluorol Yellow (*16*) and quantified as
127 the distance from the root tip to the continuously suberized zone, recapitulated the gradient of
128 suberization found in our previous screening (Fig. 2C, S6A, S6C, S6D, and S6E). We identified
129 strains that increase deposition of suberin (Fig. 2C and S6C) and strains that inhibit suberization
130 to levels found in the line *pCASP1::CDEF1* expressing the cuticle destructing factor1 (*CDEF1*)

that degrades endodermal suberin (*16*) (Fig. 2C and S4C). This suggests that members of the plant microbiota might interfere with the mechanisms controlling endodermal suberization such as the hormonal control (*5*) or immune system activation (*17*). Several controls validated that in general, the bacterial effect on suberization is not due to an indirect effect on plant development (fig. S5G, S6D, S6E, and S6F). These results indicate that strains from the plant microbiome can modify suberin accumulation in the endodermis over a wide range.

We asked if the bacterially-induced changes in the root diffusion barriers function affect plant mineral nutrient homeostasis. Analyses of shoots from plants inoculated with the selected strains showed strong perturbation in the ionome (Fig. 2D). We identified clusters of mineral nutrients whose concentrations significantly increased, decreased, or were not changed across the bacterial strain treatments (Fig. 2D). The variations in suberin accumulation induced by single isolates was highly correlated with the accumulation of a significant number of nutrients in the shoot (Fig. 2E and fig. S7A). Various controls excluded that the differences observed were an indirect fertilizing effect caused by the bacteria present in the leaves (fig. S7B, S7C, and S7D). These findings strongly suggest that the mechanisms that influence suberin deposition mediated by members of the plant microbiota also influence mineral nutrient homeostasis in the plant.

We next asked, whether bacterial abundance explains the observed suberin phenotypes. We found a positive correlation between root bacterial colonization capacity and suberin deposition in the plant (fig S6D, S7E). This correlation suggests that bacterial colonization might be a predictor of a positive bacterial effect on suberin deposition.

A bacterial synthetic community modifies suberin plasticity

To investigate the role of a more complex plant microbiome in regulating suberin deposition, we used the bacterial synthetic community consisting of 41 taxonomically diverse bacteria (Fig. 2B,

157 S2A, and S4A) able to colonize the rhizoplane and the endophytic compartment of the root (fig.
158 S8A). We grew wild-type plants axenically or inoculated with the synthetic community under
159 nutritional stresses known to induce obvious perturbations in suberin deposition (*5*) (fig. S6B). We
160 recapitulated the suberin plasticity found in response to nutritional stresses in plants growing
161 axenically (*5*) (Fig. 3A, 3B and S8B). In contrast, nutrient stressed plants inoculated with the
162 synthetic community showed significant reductions in the levels of plasticity of suberin deposition,
163 as evidenced by a longer distance to the continuous zone (Fig. 3A, 3B and S8B). This was
164 particularly evident in the case of low K, and high NaCl (Fig. 3A, 3B and S8B). This effect was
165 robust over a wide range of synthetic community inoculum concentrations (fig. S8C). We
166 confirmed, using direct chemical quantification, that the synthetic community reduces the suberin
167 content in the root and introduces minor changes in the suberin polyester composition (fig. S8D).
168 Thus, we hypothesize that this microbiome effect on root suberization could be a regulatory
169 component of the root diffusion barriers with consequences for mineral nutrient homeostasis and
170 plant performance during nutritional stress. Indeed, we found that plants inoculated with the
171 synthetic community coped better with the nutritional stresses (Fig. 3A, 3C and S8E). Inoculated
172 stressed plants had larger rosettes with a significantly greater dry weight compared with axenic
173 stressed plants (Fig. 3A, 3C and S8E). We linked this beneficial microbiome effect to endodermal
174 suberization. Different *CDEF1* expressing lines lacking the ability to accumulate suberin were
175 insensitive to the microbiome effect (fig. S8F and S8G).
176
177 We then analyzed elemental profiles of plant leaves grown under nutritional stresses (fig. S6B).
178 All tested stress conditions induced significant changes in the plant ionome (Fig. 3D, S9A, and
179 S9B). In accordance with our previous results (Fig. 2D), plants inoculated with the synthetic
180 community exhibited distinct ionomes compared to axenic plants (Fig. 3D, S9A, and S9B),
181 indicating a bacterial effect on mineral nutrient homeostasis. We confirmed that ionomic
182 differences observed were not due to a bacterial fertilizing effect (fig. S9A and S9B). The bacterial

183 synthetic community induced a significant reconfiguration of the plant ionome even under replete
184 nutrient conditions (Fig. 3D). We verified that this bacterial effect on the plant ionome is linked to
185 root suberization. In line with our previous results (fig. S8F and S8G), we observed that lines
186 expressing *CDEF1* grown axenically, with a constitutively lower amount of endodermal suberin,
187 produced changes in a sector of the plant ionome that recapitulated the synthetic community
188 effect on wild-type plants (fig. S9C). Furthermore, the synthetic community's ability to induce
189 changes in this sector of the plant ionome is reduced in these lines (fig. S9C). This, in conjunction
190 with the beneficial microbiome effect (Fig. 3A, C), indicates that microbiome-mediated suberin
191 deposition optimizes a sector of the plant ionome facilitating plant acclimation to nutrient stresses.
192
193 **The microbiome modulates suberization through abscisic acid response repression**
194 To understand how the microbiota modulates suberin deposition we analyzed the transcriptome
195 of plants grown with the synthetic community. We contrasted sets of differentially expressed
196 genes in roots of wild-type plants and the mutant *myb36-2* which displays an enhanced
197 accumulation of suberin due to the constitutive activation of the Schengen pathway (*18*). We
198 identified differentially expressed genes that respond either to the synthetic community, to the
199 Schengen pathway or to both (Fig. 4A and S10A). We found that clusters C1 and C2 contain
200 genes with a synthetic community effect (Fig. 4A and S10A). Consistent with microbiome
201 influence on suberization, these clusters are enriched with genes related to defense, ion transport
202 and nutrient responses (fig. S10B). In line with previous observations (Fig. 3A, 3B), genes related
203 to phenylpropanoid metabolism and fatty acid elongation, critical for the synthesis of suberin (*19*),
204 are repressed by the synthetic community (fig. S10C and S10D). Further, the synthetic
205 community supresses the transcriptional response to ABA (cluster C2), a hormone known to
206 induce suberin accumulation (*5*) (Fig. 4A, 4B, S10E, and S10F). We therefore hypothesized that
207 the microbiome modulates suberization via an ABA-dependent pathway. Indeed, we found that
208 the ABA mutants *aba2-1* (*20*) and *abi4-1* (*21*), mimicked the bacterially-induced reduction in

suberin observed in wild-type plants (Fig. 4C, S10G, and S10H) and that they don't respond to the microbiome effect on suberization and plant growth (Fig. 4C, S10G, and S10H). We observed similar results when we used the line *pCASP1::abi1-1*, impaired in endodermal ABA signalling (*5*) (fig. S10I). Furthermore, we found that the synthetic community suppresses fluorescence in the root of the two ABA reporter lines *6xABRE_A::erGFP* and *6xABRE_R::erGFP* (*22*) in two different nutritional conditions (fig. S10J and S10K). Therefore, we concluded that the microbiome controls endodermal suberization through the inhibition of the ABA signalling pathway in the plant and locally in the endodermis. Reinforcing this conclusion, we didn't observe a synthetic community effect on the transcriptional response to ethylene, another hormone controlling suberization (*5*), and the ethylene mutants analyzed did respond to the microbiome's effect on suberization (Fig. 4C, S10E, S10F, S10G, and S10H).

We found that ABA mutants had different leaf ionomes compared to plants grown axenically (fig. S11A). This supports the idea that the microbiota also control other non-suberin based ionomic mechanisms (*10*, *23*). We hypothesized that the microbiome effect on suberization could represent an uncharacterized regulatory branch of endodermal suberization, independent of the Schengen pathway. Indeed, the *sgn3-3* mutant, with an impaired Schengen pathway (*24*), is responsive to the synthetic community (fig. S10H, S11A and S11B). We confirmed these results in the *sgn3-3 myb36-2* double mutant where we observed less suberization and larger rosettes in synthetic community-inoculated plants compared to axenic plants (fig. S10H, S11A and S11B). Therefore, the root microbiota effect on suberin is a signalling branch of endodermal suberization that impacts ABA signalling and is independent of the Schengen pathway (Fig. 4D).

We observed that the Schengen pathway exerts an epistatic effect on the microbiome-controlled branch of suberization (Fig. 4D). We identified genes whose repression by the synthetic community could be overridden by Schengen pathway activation in *myb36-2* (fig. S11C and

S11D). We also noticed that the transcriptional response to ABA in *myb36-2* was not repressed by the synthetic community (Figure 4B). The synthetic community failed to reduce the suberin levels in the mutants *myb36-2* and *esb1-1,* both expressing constitutive activation of the Schengen pathway (*25*) (fig. S10H and S11B).

Finally, we tested whether the synthetic community's control over suberization translates to a natural microbial community. Wild-type plants inoculated with both synthetic and natural microbiomes similarly exhibited larger leaves (fig. S12A and S12B), and less suberin compared to axenic plants in response to salinity stress (Fig. 4E and S12C). We did not observe any microbiome effect on the ABA mutant *aba2-1* (Fig. 4E, S12A, S12B, and S12C). These results demonstrate that the plant microbiota is an essential component of the root diffusion barrier regulatory network in natural conditions.

Conclusions

We demonstrate that the genes regulating root diffusion barriers influence the composition of the plant microbiota, and reciprocally that microbes colonizing the root influence root diffusion barrier function. We establish that suberization of the endodermis, important for plant adaptation to nutritional stresses under axenic conditions (*5*), is reduced by the root microbiome through repression of the plants ABA transcriptional response. We reveal that coordination between root diffusion barriers and the microbiome leads to a balancing of the plant ionome that allows the plant to successfully absorb environmental perturbations such as low iron or high salinity. Our findings define a mechanism allowing plants to cope with fluctuations in mineral nutrient supply in nature, and generalize the role of the microbiome in controlling diffusion barrier functions across kingdoms. Our findings improve our understanding of how diffusion barriers in multicellular organisms integrate microbial function to maintain mineral nutrient homeostasis (Fig. 4D). We envision future applications of microbial-based strategies for the modulation of suberin production

in crops. We anticipate the opening of unexplored avenues leading to the development of plants more adapted to extreme environmental conditions, with more capacity for carbon sequestration, high content of beneficial mineral nutrients and less toxic elements.

References and Notes

1. M. Barberon, N. Geldner, *Plant Physiol*. **166**, 528–37 (2014).
2. J. M. Allaire, et al., *Trends Immunol*. **39,** 677–696 (2018).
3. M. Coskun, et al., *Front. Med*. **1**, 24 (2014).
4. I. C. R. Barbosa, N. Rojas-Murcia, N. Geldner, *Curr. Opin. Biotechnol*. **56**, 121–129 (2019).
5. M. Barberon, et al., *Cel*l. **164**, 447–459 (2016).
6. V. G. Doblas, et al., *Science.* **355**, 280–284 (2017).
7. A. Feng Zhou, et al., *Cell*. **180**, 440–453 (2020).
8. K. Yu, et al., *Curr. Biol*. **29**, 3913–3920 (2019).
9. D. E. Salt, I. Baxter, B. Lahner*, Annu. Rev*. *Plant Biol*. **59**, 709–733 (2008).
10. G. Castrillo, et al., *Nature*. **543**, 513–518 (2017).
11. O. M. Finkel, et al., *PLoS Biol*. **17**, e3000534 (2019).
12. A. Levy, et al., *Nat. Genet*. **50**, 138–150 (2018).
13. Y. Bai, et al., *Nature*. **528**, 364–369 (2015).
14. J. Alassimone, S. Naseer, N. Geldner, *Proc. Natl. Acad. Sci. U. S. A*. **107**, 5214–5219 (2010).
15. T. G. Andersen, et al., *Nature*. **555**, 529–533 (2018).
16. S. Naseer, et al., *Proc. Natl. Acad. Sci. U. S. A*. **109**, 10101–10106 (2012).
17. A. Emonet, et al., *bioRxiv*, in press, doi:10.1101/2020.08.03.233817 (2020).
18. T. Kamiya, et al., *Proc. Natl. Acad. Sci. U. S. A.* **112**, 10533–8 (2015).
19. J. Liu, A. Osbourn, P. Ma, *Mol. Plant*. **8**, 689–708 (2015).

20. M. González-Guzmán, et al., *Plant Cell*. **14**, 1833–1846 (2002).
21. E. M. Söderman, et al., *Plant Physiol*. **124**, 1752–1765 (2000).
22. R. Wu, et al., *Plant Physiol.* **177**, 1650–1665 (2018).
23. K. Hiruma, et al., *Cel*l. **165**, 464–74 (2016).
24. S. Fujita, et al., *EMBO J*., 1–18 (2020).
25. P. Wang, et al., *Sci. Rep*. **9**, 4227 (2019).
26. L. Song, et al., Science. **354** (2016).
27. K. N. Chang, et al., *Elife*. doi:10.7554/eLife.00675. (2013).

Acknowledgments

We thank Dr Kamal Swarup and Rosalba Pérez-Torres for technical assistance; Dr Priya Ramakrishna for her help in the soil extraction; Prof Paul Schulze-Lefert, MPIPZ, Germany and Prof Julia Vorholt, ETH Zurich, Switzerland for their strain collections; Prof Malcolm Bennet, Dr Connor Fitzpatrick and Dr Omri M. Finkel for critical comments on the manuscript. **Funding:** This work was supported by the Deutsche Forschungsgemeinschaft (DFG), grant FR1721/2-1 to R.B.F. I. S-G. and J.L.D are supported by funds from the Howard Hughes Medical Institute and from National Science Foundation grant IOS-1917270 awarded to J.L.D. J.L.D is an investigator of the HHMI. G.R. and D.E.S are supported by the UK BBSRC grant BB/N023927/1, the Biological Sciences Research Council grant BB/L027739/1, and the University of Nottingham Future Food Beacon of Excellence. G.C is supported by a Nottingham Research Fellowship, The Royal Society grant RGS\R1\201229, and the Future Food Beacon of Excellence, University of Nottingham; **Author contributions:** Conceptualization, I.S-G., G.R., P.F., D.E.S. and G.C.; Data curation, I.S-G and G.C.; Formal analysis, I.S-G.; Investigation, I.S-G., G.R., P.F., V.C., D.G., N.B., T.P.D., K.S., R.B.F. and G.C.; Methodology, G.C.; Project administration, G.C.; Software, I.S-G.; Supervision, G.C.; Visualization, I.S-G., G.R. and G.C.; Writing – Original Draft, I.S-G. and G.C.; Writing – Review & Editing, G.R., P.F., V.C., D.G., N.B., J.L.D., and D.E.S; **Competing**

interests: Authors declare no competing interests; **Data and materials availability:** DNA sequence data is available at the NCBI bio-project repository ID PRJNA630964. RNA-Seq raw sequence data and read counts are available at the NCBI Gene Expression Omnibus accession number GSE151376. All data and code needed to reproduce all analyses can be found at https://github.com/isaisg/rootbarriersmicro. All other data are present either in the main paper or the Supplement.

Supplementary Materials:

Materials and Methods

Figures S1-S12

Table S1-S2

References (1-69)

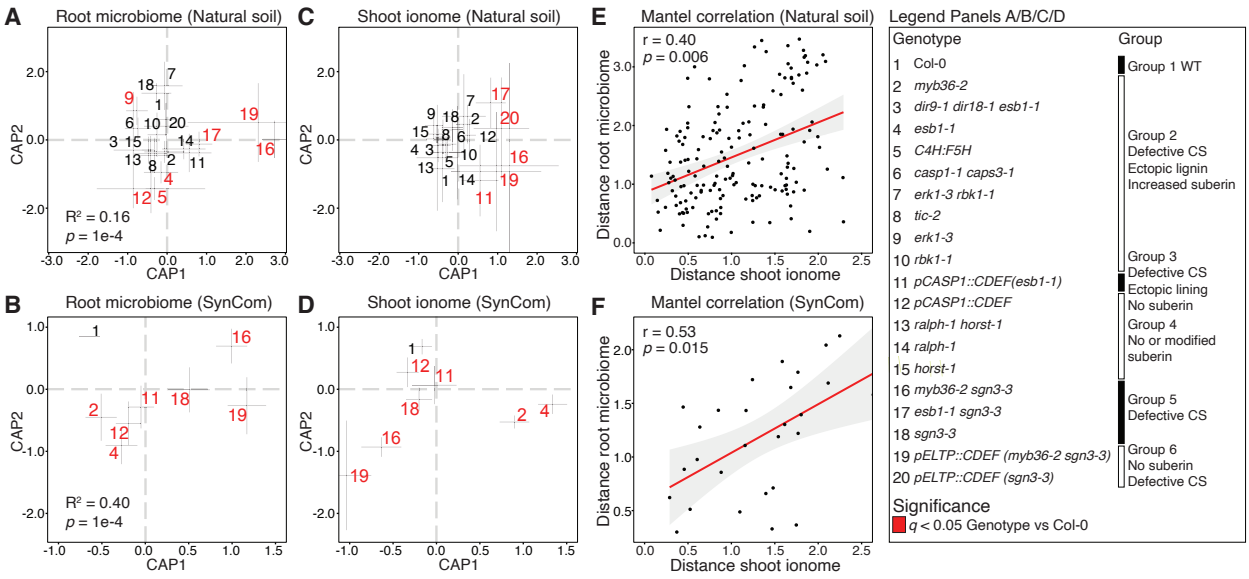

Fig. 1. Plants with modified root diffusion barriers assemble a distinct microbiome.

A, B. Canonical analysis of principal coordinates (CAP) of root microbiome composition showing the projected microbiome assembly of the root diffusion barrier genotypes (numbers) in plants grown in **A.** a natural soil and **B.** agar plates inoculated with a bacterial synthetic community (SynCom). **C, D.** CAP analysis of shoot mineral nutrient composition (ionome) showing the projected ionomic profiles of plant genotypes (numbers) in plants grown in **C.** a natural soil and **D.** agar plates inoculated with a bacterial synthetic community. Numbers in red are statistically significant as compared with Col-0 ($q < 0.05$). **E, F.** Pairwise correlation analysis between the shoot ionome and the root microbiome composition in plants grown in **E.** a natural soil and **F.** agar plates inoculated with a bacterial synthetic community. Panel shows the Mantel r statistic, and its *p*-value.

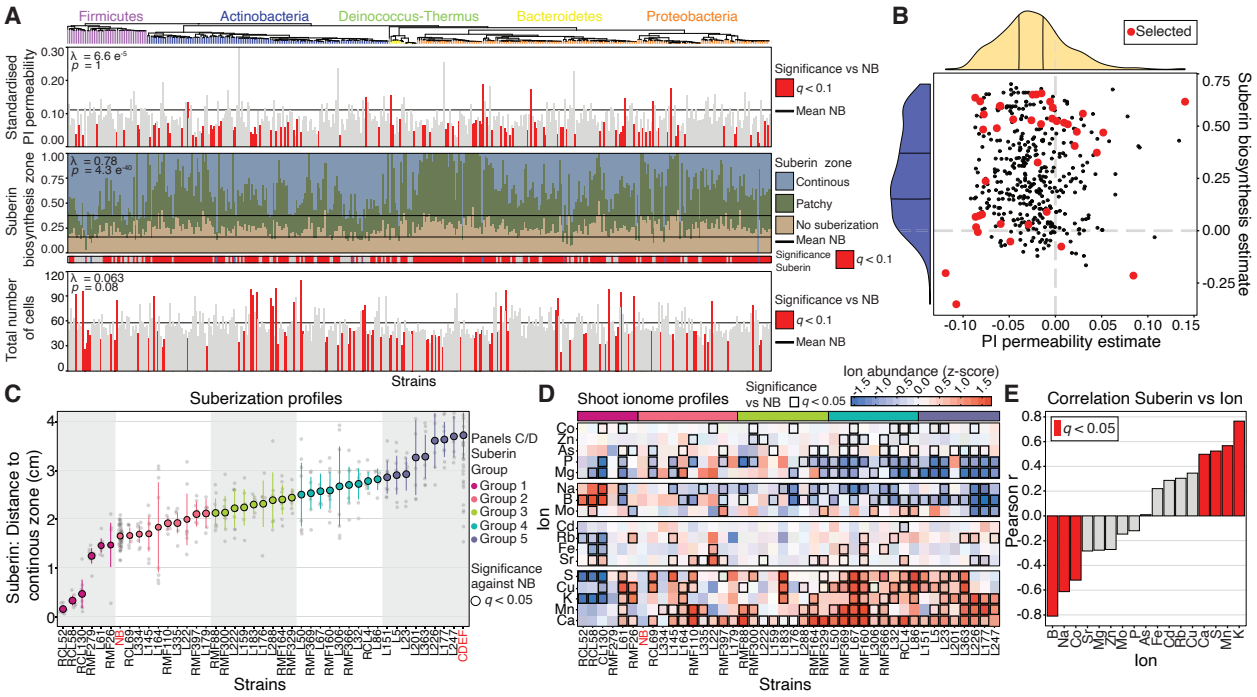

Fig. 2. Bacterial isolates modify endodermal function.

A. Bar graphs representing bacterial isolates average effect on propidium iodide (PI) permeability, suberin biosynthesis, and the total number of cells in the root. Significantly different values from the no bacterial control (horizontal lines in each panel) are in red. For the suberin biosynthesis this information is in the bottom bar (Significance Suberin). The data are sorted according to the bacterial collection phylogeny, as indicated by the tree (phylum) on the top. The *p* - and the λ–values from Pagel's λ test for phylogenetic signal are also shown. **B.** Selection of a representative number of bacterial strains. At the top of each axis is the corresponding data distribution divided into tertiles. Red dots represent the selected bacteria. **C.** Distinct suberization (distances from the root tip to the continuous zone of suberization) profiles in Col-0 exposed to the bacterial isolates. Controls used, plants grown in axenic conditions (NB) and the line *pCASP1::CDEF1*, are in red. Colours represent groups of bacteria, with a differential effect on suberization. **D.** Heatmap showing the standardized mineral nutrient concentrations in plant inoculated or not (NB) with the bacterial strains. The columns have been ordered to match the bacterial effect on endodermal suberization (Figure 2C). Significant ($q < 0.05$) values in relation to NB are outlined in black. **E.** Bar graph showing the correlation coefficient calculated between each mineral nutrient abundance and the suberization in plant exposed to bacterial strains (fig. S7A). Bars in red are significant ($q < 0.05$).

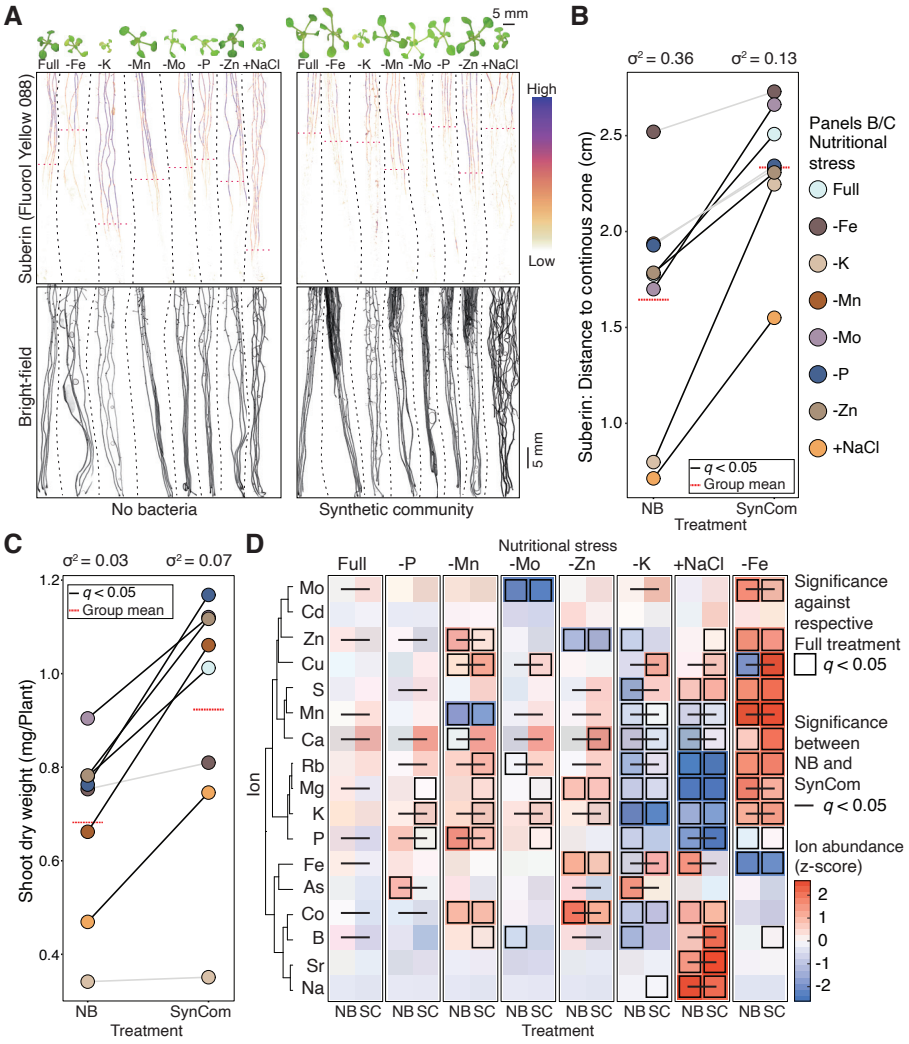

Fig. 3. A synthetic community (SynCom) controls endodermal suberization to enhance plant adaptation to nutrient stresses.

A. (Top) Endodermal suberization in plants inoculated or not with the SynCom, and exposed to nutritional stresses. As a control we used replete nutrient conditions (Full). The red line highlights the initiation of the continuous zone of suberization. (Bottom) Root systems from the same plants (Bright-field). Representative plant rosettes are in the upper part of the figure. **B.C.** Comparative analysis of suberin deposition (B) and shoot dry weight (C) in plants inoculated with the SynCom or grown axenically (NB), under nutrient stresses. Colored points represent the average value for each condition. The line connecting both points is the difference between NB and SynCom treatments. A black line indicates statistical significance ($q < 0.05$). The average values (horizontal red line) and variance (top) are depicted for each bacterial treatment. **D.** Heatmap showing the standardized mineral nutrient concentrations in plants inoculated or not (NB) with the bacterial synthetic community (SC) and exposed to the nutrient stresses. Significant intra stress comparisons (stress vs full) are outlined in black ($q < 0.05$) and significant comparisons between no bacteria and SynCom treatment within stress, are represented with a horizontal black line ($q < 0.05$).

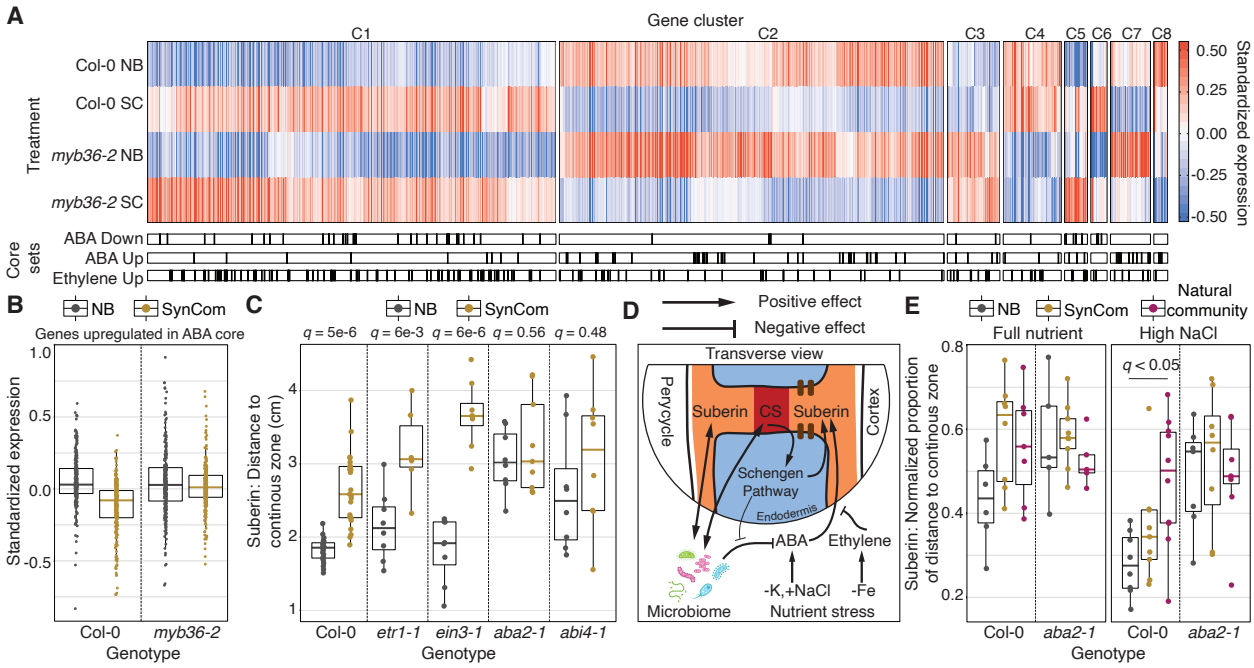

Fig. 4. Microbiome effect on suberization represents an uncharacterized regulatory pathway.

A. Heatmap of the 4538 differentially expressed genes identified in the RNA-seq in Col-0 and *myb36-2* roots uninoculated (NB) or inoculated with the synthetic community (SynCom). Clusters (C) are designated with numbers. Bars on the bottom indicate the representation of the ABA (ABA Up and ABA Down) and ethylene core genes identified from the literature (*26*, *27*). **B.** Boxplots displaying the standardized expression of the ABA-induced core genes extracted from the literature (*26*) in the RNA-Seq. **C.** Suberin quantification in Col-0, ethylene (*etr1-1* and *ein3-1*), and ABA (*aba2-1* and *abi4-1*) mutants, exposed (SC) or not (NB) to the SynCom. Statistical significance was determined using intra-genotype *t*-tests. *q*-values are shown. **D.** Schematic overview of the microbiome regulatory branch integration within the endodermal suberization regulatory network. **E**. Suberin quantification in Col-0, and *aba2-1*, inoculated with the SynCom, a natural community, or grown axenically (NB) in the perlite system under full nutrient conditions or 70 mM NaCl.

Science
AAAS

Supplementary Materials for

Coordination between the microbiota and the root endodermis is required for plant mineral nutrient homeostasis

Isai Salas-González, Guilhem Reyt, Paulina Flis, Valéria Custódio, David Gopaulchan, Niokhor Bakhoum, Tristan P. Dew, Kiran Suresh, Rochus Benni Franke, Jeffery L. Dangl, David E. Salt and Gabriel Castrillo

Correspondence to: gabriel.castrillo@nothingham.ac.uk

This PDF file includes:

Materials and Methods

1. Census study in a natural soil.

a. Soil collection

For experiments in a natural soil, we collected the soil from a location free of pesticide and fertilizer at Sutton Bonington Campus (University of Nottingham, UK; +52° 49′ 59.75″N, −1° 14′ 56.62″W). Before collecting the soil, all tools used were washed with water and disinfected with 70% ethanol, and the staff wore gloves the whole time. Approximately the first 10 cm of the soil, containing the local vegetation, was discarded and the collected soil was placed in a clean plastic box at 4°C until use.

b. Soil preparation.

Collected soil was dried at room temperature in clean plastic trays for approximately 5 days and sifted using a plastic sieve to remove rocks and vegetative debris. The soil was then mixed in a proportion 2:1 (v/v) with autoclaved dry pavior sand to improve soil drainage. A square of sterilized Miracloth (Millipore) was placed at the bottom of round plastic pots (9 cm diameter) to prevent soil leakage. All pots were then filled with the soil mixture and used to grow *Arabidopsis thaliana* plants.

c. Plant growth conditions

All *Arabidopsis thaliana* mutants used in this study were in the Columbia (Col-0) background (table S1). To determine the role of the root diffusion barrier regulatory network in controlling microbiome composition, we analyzed a collection of mutants (*esb1-1*, *myb36-2* (GK-543B11), *sgn3-3* (salk_043282), *myb36-2 sgn3-3*, *casp1-1 casp3-1* (SAIL_265_H05/SALK_011092), *erk1-3* (SALK_060966), *rbk1-1* (SALK_043441), *erk1-3 rbk1-1*, *tic-2* (SAIL_753_E03), *dir9-1 dir18-1 esb1-1* (GABI_323A02/SALK_115430), *esb1-1 sgn3-3*, *ralph-1* (SM.37066), *horst-1* (SALK_107454), *ralph-1 horst-1*, and lines (*C4H::F5H*, *pCASP1::CDEF1(wild-type)*, *pCASP1::CDEF1(esb1-1)*, *pELTP::CDEF1(sgn3-3)*, *pELTP::CDEF1(myb36-2 sgn3-3)*) with atypical root diffusion barrier function.

All seeds were surface-sterilized with 70% bleach, 0.2% Tween-20 for 8 min, and rinsed 3 times with sterile distilled water to eliminate any seed-borne microbes on the seed surface. Seeds were stratified at 4°C in the dark for 2 days and then germinated in sterile pots filled with soil mixture prepared as described in material and methods 1b. As controls, we used pots without plants as ‘bulk soil’ and pots with wild-type plants Col-0. All pots were randomized using a true random generator (random.org), and trays were reshuffled every week in the growth chamber without

paying attention to the pot labels. All pots, including controls, were watered twice a week from the top with sterile distilled water to avoid chlorine and other tap water additives.

Plants were grown in a growth chamber (Conviron) with an 8-h light/16-h dark regime at 21°C day/19°C night for 11 weeks. This experiment was repeated twice.

d. Rosette area determination.

The area of the plant rosettes was quantified from pictures of the different root diffusion barrier genotypes grown in a natural soil for 11 weeks. The quantification was performed using the tool Measurement Log on Photoshop. We used a customize scale to transform pixels into cm.

e. Rosette area determination. Statistics

For each of the 19 Arabidopsis root diffusion barrier mutants and lines, we compared the rosette area against the Col-0 genotype using a leveneTest car v.3.0.3 package (https://cran.r-project.org/web/packages/car/car.pdf), in R, followed by a *t*-test controlling or not for different variances between the two groups (1 of the 19 genotypes of interest and Col-0). We used the false discovery rate (FDR) method to adjust the *p*-values obtained for all comparisons. Genotypes with a corrected *p*-value < 0.1 were considered significantly different from Col-0. To visualize the results, we plotted the estimated mean with 95% confidence interval of each genotype.

f. DNA extraction

For this experiment, roots, shoots and soil were harvested separately from the individual randomized pots. Approximately the whole root system, 4-5 leaves from 11-week-old plants, and soil were harvested and placed in 50 mL Falcon tubes containing sterile water. Root and leaf samples were then rinsed at least three times with sterile distilled water to remove weakly associated microbes and soil particles. Soil samples were filtered using a sterile cell strainer

(Fisherbrand, Fisher Scientific) to remove big soil particles and centrifuged at max speed for 20 min in an Eppendorf 5810R centrifuge, at room temperature. The supernatant was then discarded and the pellet was resuspended in 1 mL of sterile water and transferred into clean 1.5 mL Eppendorf tubes. Samples were centrifuged again in a microcentrifuge (Fisher Scientific, accuSpin Micro 17) at maximum speed, and the supernatant was decanted. All samples were stored at -80 °C until further analysis.

For DNA extraction, root and leaf samples were lyophilized using an Alpha 2-4 LD freeze dry system, and pulverized using a TissueLyser II (Qiagen), 2 cycles of 30 seconds, frequency 30 s^{-1}. For the DNA extraction we used 96-well-format MoBio PowerSoil Kit (MOBIO Laboratories; Qiagen) following the manufacturer's instruction. Before starting the extraction, all samples, including soil, were randomized by placing them in a plastic bag that was shaken several times. Samples were then taken individually from the bag and loaded in the DNA extraction plates. This random distribution was maintained throughout library preparation and sequencing.

g. Bacterial 16S rRNA sequencing.

For natural soil experiments 16S *rRNA* sequencing, the V3-V4 region of the bacterial 16S *rRNA* gene was amplified using the primers 338F (5′-ACTCCTACGGGAGGCAGCA-3′) and 806R (5′-GGACTACHVGGGTWTCTAAT-3′). Two barcodes and six frameshifts were added to the 5' end of 338F and six frameshifts were added to the 806R primers, based on the protocol by Lundberg et al. (*28*). PCR reactions with ~20 ng DNA template were performed in triplicate and included a unique mixture of three frameshifted primer combinations for each plate. PCR blockers mPNA and pPNA were used to reduce contamination by plant host plastid and mitochondrial 16S *rRNA* amplicon. PCR conditions were as follows: 5 µL Kapa Enhancer, 5 µL Kapa Buffer A, 1.25 µL 5 µM 338F, 1.25 µL 5 µM 806R, 0.375 µL mixed plant rRNA gene-blocking peptide nucleic acids (PNAs; 1:1 mix of 100 µM plastid PNA and 100 µM mitochondrial PNA), 0.5 µL Kapa dNTPs,

0.2 µL Kapa Robust Taq, 8 µL dH_2O, 5 µL DNA; temperature cycling: 95°C for 60 s; 24 cycles of 95°C for 15 s; 78°C (PNA) for 10 s; 50°C for 30 s; 72°C for 30 s; 12°C until use.

PCR reactions were clean-up using AMPure XP magnetic beads (Beckman Coulter) to remove primer dimers. The PCR product was indexed using a primer that contains forward Illumina adapter (5′-AATGATACGGCGACCACCGAGATCTACACGCCTCCCTCGC GCCATCAGAGATGTG-3′) and 96 indexed reverse primers (5′-CAAGCAGAAGACGG CATACGAGATXXXXXXXXXGTGACTGGAGTTCAGACGTGTGCTC-3′) with reverse Illumina adapter. We used Kapa HiFi Hotstart Readymix and the following temperature cycling: 95°C for 60 s; 9 cycles of 95°C for 15 s; 78°C (PNA) for 10 s; 60°C for 30 s; 72°C for 35 s; 12°C until use. PCR products were purified using AMPure XP magnetic beads (Beckman Coulter) and quantified with a Qubit 2.0 fluorometer (Invitrogen). Amplicons were pooled in equal amounts and then diluted to 10 pM for sequencing. Sequencing was performed on an Illumina MiSeq instrument using a 600-cycle V3 chemistry kit at the DeepSeq facility at the University of Nottingham. DNA sequence data for this experiment is available at the NCBI bio-project repository (ID PRJNA630964). The abundance matrix, metadata and taxonomy are available at https://github.com/isaisg/rootbarriersmicro.

h. 16S rRNA amplicon sequence data processing

For natural soil census analysis, sequences data were processed with MT-Toolbox (*29*). Briefly, sequence pairs were merged, quality-filtered and de-multiplexed according to their barcodes. The resulting sequences were then denoised and collapsed into amplicon sequence variants (ASVs), using DADA2 v.1.10.1 (*30*). Representative ASVs sequences were taxonomically classified with the mothur naive bayes classifier (*31*) trained on the SILVA 132 database (*32*). We filtered ASVs that were assigned to chloroplast, mitochondria, oomycete, archaea or did not have a known kingdom assignment. After the filtering, the remaining ASVs, with more than 1000 reads per

sample, were used to create the raw count abundance tables. The resulting abundance tables were processed and analyzed with functions from the ohchibi package (https://github.com/isaisg/ohchibi).

To compare alpha diversity across genotypes and fractions, we calculated the Shannon diversity index using the diversity function from the vegan package v2.5-5 (*33*). We used ANOVA to test for differences in alpha diversity between groups. Beta diversity analyses (Principal coordinate analysis, and canonical analysis of principal coordinates) were based on Bray-Curtis dissimilarity matrices calculated from the abundance table.

We used the capscale function from the vegan R package v.2.5-5 (*33*) to compute the canonical analysis of principal coordinates (CAP, fraction effect (soil, root and shoot)) with the following design:

BrayCurtis Dissimilarity ~ Fraction + Genotype + Condition (Rep)

To compute the variance explained by the Fraction effect, we performed PERMANOVA using the function adonis from the vegan R package v.2.5-5 (*33*).
For each of the 19 plant genotypes (except Col-0) we compared their beta-diversity versus Col-0 across each fraction independently. To compute the CAP projection of the 20 genotypes inside each of the three fractions (Root, Shoot and Soil) in the dataset, we used the following design:

BrayCurtis Dissimilarity ~ Genotype + Condition (Rep)

Next, we compared for each of the 19 genotypes (except Col-0) the position of all the samples belonging to that genotype in CAP1 and CAP2, independently in relationship to the position of all samples belonging to Col-0. For this analysis we used a leveneTest (car v.3.0.3 package (https://cran.r-project.org/web/packages/car/car.pdf), in R, followed by a *t*-test, controlling or not

for different variances between the two groups (1 of the 19 genotypes of interest and Col-0). We used the Bonferroni correction to adjust the *p*-values obtained for all the comparisons across the 3 sample fractions. Genotypes with a corrected *p*-value < 0.1, in either CAP1 or CAP2, were considered significantly different from Col-0. Additionally, to estimate the overall variance explained by all genotypes in the dataset for the three fractions independently, we performed a PERMANOVA test using the function adonis from the vegan R package v.2.5-5 (*33*). We used the R package DESeq2 v.1.24.0 (*34*) to compute the Genotype specific enrichment profiles across the three fractions, independently. For each taxonomic unit of the following taxonomic levels, Phylum, Class, Order, Family, Genus, and ASV, we estimated their abundance differences in each of the 19 genotypes against Col-0, using a generalized linear model (GLM) with the following design:

$$\text{Abundance} \sim \text{Rep} + \text{Genotype}$$

We adjusted the global (all three fractions with all 19 genotypes vs Col-0) *p*-value table using the False Discovery Rate (FDR) approach. In a given root diffusion barrier genotype, a taxonomic unit with a corrected *p*-value < 0.05 was considered differentially abundant against Col-0. We created a heatmap in which we visualized the enrichment patterns (log2 fold change) of all statistically significant taxonomic units in the different taxonomic levels, ASV, Family and Class, across the 19 Arabidopsis root diffusion barrier genotypes using ggplot2 v.3.2.1 package (*35*) in R.

i. Elemental analysis. Shoot

The shoot elemental content was measured using Inductively Coupled Plasma Mass Spectrometry (ICP-MS). The leaf material was collected in the following manner: leaf 5 to 9 of Arabidopsis rosette were harvested for the plants grown on the natural soil, and 4-9 rosettes of 14-day-old plants were

collected for the plants grown on agar plates (0.150 – 0.200 g fresh weight). Leaves/rosettes were washed three times with 18.2 MΩcm Milli-Q Direct water (Merck Millipore). Samples were placed in Pyrex digestion tubes and dried at 88˚C for 20h. After cooling, eight of approximately 108 samples from each sample set were weighed on Mettler five-decimal analytical balance. After weighing the appropriate number of samples, 1 mL of the concentrated trace metal grade nitric acid Primar Plus (Fisher Chemicals) was added to each tube. Prior to the digestion, 20 µg/L of Indium (In) was added to the nitric acid as an internal standard for assessing errors in dilution, variations in sample introduction and plasma stability in the ICP-MS instrument. The samples were then digested in DigiPREP MS dry block heaters (SCP Science; QMX Laboratories) for 4h at 115˚C. After cooling down, the digests were diluted to 10 mL with 18.2 MΩcm Milli-Q Direct water and elemental analysis was performed using an ICP-MS, PerkinElmer NexION 2000 equipped with Elemental Scientific Inc 4DXX FAST Dual Rinse autosampler, FAST valve and peristaltic pump. The instrument was fitted with PFA-ST3 MicroFlow nebulizer, baffled cyclonic C3 high sensitivity glass spray chamber cooled to 2ºC with PC3X Peltier heated/cooled inlet system, 2.0 mm i.d. quartz injector torch and a set of nickel cones. Twenty-four elements were monitored including following stable isotopes: ^{7}Li, ^{11}B, ^{23}Na, ^{24}Mg, ^{31}P, ^{34}S, ^{39}K, ^{43}Ca, ^{48}Ti, ^{52}Cr, ^{55}Mn, ^{56}Fe, ^{59}Co, ^{60}Ni, ^{63}Cu, ^{66}Zn, ^{75}As, ^{82}Se, ^{85}Rb, ^{88}Sr, ^{98}Mo, ^{111}Cd, ^{208}Pb and ^{115}In. Helium was used as a collision gas in Kinetic Energy Discrimination mode (KED) at a flow rate of 4.5 mL/min while measuring Na, Mg, P, S, K, Ca, Ti, Cr, Mn, Fe, Ni, Cu, Zn, As, Se and Pb to exclude possible polyatomic interferences. Remaining elements were measured in the standard mode. Any isobaric interferences were automatically corrected by the instrument Syngistix™ software for ICP-MS v.2.3 (Perkin Elmer). The ICP-MS measurements were performed in peak hopping scan mode with dwell times ranging from 25 to 50 ms depending of the element, 20 sweeps per reading and 3 replicates. The ICP-MS conditions were as follow: RF power – 1600 Watts, auxiliary gas flow rate 1.20 L/min. Torch alignment, nebulizer gas flow and quadrupole ion deflector (QID) voltages (in standard and KED mode) were optimized before analysis for highest intensities and lowest

interferences (oxides and doubly charged ions levels lower than 2.5%) with NexION Setup Solution containing 1 µg/L of Be, Ce, Fe, In, Li, Mg, Pb, and U in 1% nitric acid using a standard built-in software procedure. To correct for variation between and within ICP-MS analysis runs, liquid reference material was prepared using pooled digested samples, and run after the instrument calibration, and then after every nine samples in all ICP-MS sample sets. Equipment calibration was performed at the beginning of each analytical run using seven multi-element calibration standards (containing 2 µg/L In internal standard) prepared by diluting 1000 mg/L single element standards solutions (Inorganic Ventures; Essex Scientific Laboratory Supplies Ltd) with 10% nitric acid. As a calibration blank, 10% nitric acid containing 2 µg/L In internal standard was used and it was run throughout the course of the analysis.

Sample concentrations were calculated using external calibration method within the instrument software. Further data processing including calculation of final elements concentrations was performed in Microsoft Excel. First, samples set that have been run at different times were connected as an extension of the single-run drift correction. Linear interpolation between each pair of liquid reference material standards was used to generate a theoretical standard for each sample that was then used to correct the drift by simple proportion to the first liquid reference material standard analyzed in the first run. Liquid reference material composed of pooled samples was used instead of the CRM to match the chemical matrix of the samples as closely as possible, thereby emulating the sample drift. Second, the blank concentrations were subtracted from the sample concentrations and then each the final elements concentrations were obtained by multiplying by the dilution factor and normalizing the elements concentrations to the samples calculated dry weight. To increase the throughput through obviating the slow process of weighing each sample on a balance and reduce indeterminate error, for every 108 samples the dry weights of eight reference samples were measured and used to calculate the weights and then final elements concentration of the remaining samples based on a heuristic algorithm which uses the

best-measure elements in these samples, the weights of the eight weighed samples and the solution concentrations as described in Lahner et al. (*36*). Briefly, as a basis, eight samples were weighed, and their averaged, normalized to dry weight concentrations for multiple elements became the standard which was used to calculate all the other weights. Only the elements for which the relative standard deviation of the basis samples was below 25%, were used. The dry weight of the sample was determined by taking the average of the dry weights calculated from the concentration of each selected element (%RSD lower than 25%) quantified in that sample and the averaged, dry weight normalized concentration of the basis samples. Among all the dry weights that were averaged to obtain a final dry weight of the sample, the far outliers (dry weight greater than the twice of the dry weight average) and outliers (dry weight smaller than half of the dry weight average and greater than 1.5 times the dry weight average) were identified and removed.

j. Elemental analysis. Soil

The soil elemental content was also measured using ICP-MS. The soil samples were first dried using plastic weighing boats in the fume hood for approximately 72h at room temperature. Five grams of soil was then weighted in 50 mL Falcon tubes with a four-decimal balance, and digested with 20 mL of 1 M NH_4HCO_3, 5 mM diamine-triamine-penta-acetic acid (DTPA), and 5 mL 18.2 MΩcm Milli-Q Direct water (Merck Millipore), 1h at 150 rpm in a rotary shaker (adapted from (*37*)). Each sample was gravity filtered through a quantitative filter paper (Whatman 42- WHA1442070) until obtaining approximately 5 mL of filtrate. 0.5 mL of the filtrates were open-air digested in Pyrex tubes using 1 mL of concentrated trace metal grade nitric acid Primar Plus (Fisher Chemicals) spiked with 20 µg/L indium internal standard for 4h at 115ºC in a dry block heater (DigiPREP MS, SCP Science; QMX Laboratories, Essex, UK). Each sample was then diluted up to 10 mL with 18.2 MΩcm Milli-Q Direct water and the elemental analysis was performed using PerkinElmer NexION 2000 ICP-MS equipped with Elemental Scientific Inc. autosampler, in the collision mode

(He) as described above. To correct for variation between and within ICP-MS analysis runs, liquid reference material was prepared using pooled digested samples and run in exactly the same manner as for leaf samples. Sample concentrations were calculated using external calibration method within the instrument software. Further data processing, to obtain the final elements concentration, was performed in Microsoft Excel and included correction of the drift, subtraction of the blank concentration, multiplication by the dilution factor and normalization to the soil dry weight.

k. Elemental analysis. Statistics

In conjunction, for both shoot and soil elemental profiles we created a matrix (samples x ion) in which each cell was filled with the calculated element concentration in a given sample. Afterwards, we applied a z-score transformation of each individual ion across the samples in the matrix. Next, to compare the elemental profiles of shoot and soil we applied a canonical analysis of principal coordinates (CAP) using the Euclidean distance between samples, and the z-score matrix as input. We used the following formula in the design of the CAP analysis:

Euclidean Dissimilarity ~ Fraction + Genotype + Condition(Rep)

We compared, inside shoot and soil fractions independently, the total ionomic profile of each of the root diffusion barrier genotypes against Col-0 by projecting in CAP space all 20 genotypes in the dataset. Next, we compared for each of the 19 genotypes (except Col-0) the position, of all the samples belonging to that genotype, in CAP1 and CAP2 independently, in relationship to the position of all samples belonging to Col-0 using a leveneTest (car v.3.0.3 (https://cran.r-project.org/web/packages/car/car.pdf) package in R), followed by a *t*-test controlling or not for different variances between the two groups (1 of the 19 genotypes of interest and Col-0). To adjust the *p*-values obtained we used the Bonferroni correction. A genotype with a corrected *p*-value < 0.1, in either CAP1 or CAP2 was considered significantly different from Col-0.

We compared the concentration of each ion in the 19 root diffusion barrier genotypes against Col-0 in each fraction (Shoot and Soil) independently by fitting a linear model with the following design:

$$\text{Ion Concentration} \sim \text{Genotype} + \text{Rep}$$

After fitting the model, we applied the Dunnet test implemented in the multcomp v.1.4-12 R package. Further, we used the FDR approach to adjust the *p*-values obtained from the Dunnet tests. For a given root diffusion barrier genotype, an ion with a corrected *p*-value < 0.05 was considered differentially abundant against Col-0. The enrichment profiles of each ion across the shoot and soil fractions was visualized using a heatmap created by the ggplot2 v.3.2.1 (*35*), R package.

Finally, in order to compare the microbiome profiles against the elemental profiles we contrasted the dissimilarity matrices of each pair of datasets (e.g. Root Microbiome versus Shoot Ionome) using the Mantel test implementation of the vegan v2.5-5 (*33*), R package. We computed significance of the correlation between the matrices permuting the matrices 10,000 times (https://cran.r-project.org/web/packages/multcomp/multcomp.pdf).

2. Bacterial synthetic community (SynCom) study in Agar system.

a. Growth conditions for the bacterial strains and plant inoculation

The bacterial synthetic community was design using 41 bacteria chosen from two larger bacterial isolate collections: a root and a leaf collection. The root collection was prepared using only roots of Brassicaceae (mostly *Arabidopsis thaliana*) grown in two natural soils from North Carolina, US (*12*). For the leaf collection, bacterial strains were isolated from individual leaves of healthy Arabidopsis plants collected from six locations around Tübingen, Germany, or Zurich, Switzerland (*13*). Selected bacteria maximize synthetic community diversity and have enough sequence variability in their 16S *rRNA* gene to allow identification. To isolate single colonies from the

bacterial strains, −80°C glycerol stocks were grown on LB (root collection) and R2A [leaf collection; (Casein acid hydrolysate 0.5 g/L, Yeast extract 0.5 g/L, Protease peptone 0.5 g/L, Dextrose 0.5 g/L, Starch 0.5 g/L, Dipotassium phosphate 0.3 g/L, Magnesium sulfate 0.024 g/L, Sodium pyruvate 0.3 g/L, agar 15g/L, pH 7.2 supplemented with Methanol 0.5%)] plates at 28°C. A single colony was then inoculated in sterile test tubes containing 4 mL of LB medium (root collection) or R2A medium supplemented with methanol 0.5% (leaf collection) and grown in an incubator at 28°C with agitation at 250 r.p.m. All cultures were centrifuged in a benchtop centrifuge (Eppendorf 5810R), 3220 g at room temperature, and washed with 10 mM $MgCl_2$ to remove the media and cell debris. This step was repeated twice. Clean bacterial cells were resuspended in 1 mL of 10 mM $MgCl_2$, and the OD_{600nm} was then measured. Assuming that 1 OD_{600nm} unit is equal to 10^9 c.f.u/mL, individual bacteria were mixed at a final concentration of 10^5 c.f.u/mL in the synthetic community. The synthetic community inoculum (OD_{600nm}= 0.2; 100 µL) was spread using a L-shaped cell spreader (Fisher scientific) on the surface of 12X12cm square agar plates prior to transferring seedlings.

b. Seed sterilization

All seeds were sterilized with a mix of 70% bleach (commercial) and 0.2% Tween-20 (Sigma-Aldrich) with agitation for 8 minutes. Seeds were then rinsed with sterile distilled water at least three times to eliminate the bleach. This treatment efficiently removes the microbes from the seed surface. Before sowing, seeds were stratified in the dark at 4°C for at least 1 day.

c. *In vitro plant growth conditions. Root diffusion barrier genotypes*

To define the role of the plant microbiota in the regulation of the root diffusion barrier function, we analyzed a collection of plant mutants with a defective Casparian strip (*sgn3-3* and *sgn3-3 myb36-2*), a defective Casparian strip leading to an ectopic accumulation of suberin (*esb1-1* and *myb36-2*), and lines expressing the cuticle destructing factor 1 (*CDEF1*) that degrades suberin in Col-0

(*pCASP1::CDEF1 (wild-type)*) and two mutant backgrounds (*pCASP1::CDEF1 (esb1-1)* or *pELTP::CDEF1 (sgn3-3 myb36-2)*)**.** This selection represents different level of impairment in the root diffusion barriers.

Sterilized Col-0 and the different root diffusion barriers genotypes seeds were germinated on agar plate containing 0.5x MS (Murashige and Skoog) medium solidified with 1% bacto-agar for a week. Ten seedlings with the same developmental stage of the different genotypes were then transferred to 0.5x MS agar plates inoculated with the 41-member synthetic community. In parallel 10 seedlings were also transferred to no bacteria control (agar plates inoculated with only 10 mM $MgCl_2$). Plates were manually randomized and placed in a growth chambers and grown under a 16-h light/8-h dark regime at 21°C day/19°C night for another 7 days. We used 5 replicas of each treatment and this experiment was repeated twice.

d. DNA extraction

Three fractions, roots, shoots and agar were harvested separately from the individual plates. Roots and shoots from 5-7 plants were placed in 2 mL Eppendorf tubes with three sterile glass beads. These samples were then rinsed three times with sterile distilled water to remove weakly associated microbes and agar particles. Samples were stored at -80˚C until processing. For DNA extraction, root and shoot samples were lyophilized using an Alpha 2-4 LD freeze dry system for 3 days, and pulverized using a TissueLyser II (Qiagen), 2 cycles of 30 seconds, frequency 30 s^{-1}.

In parallel, agar from each plate was collected in 30 mL syringes with a square of sterilized Miracloth (Millipore) blocking the exit site. Agar samples were kept at -20°C for at least one week. Syringes were then thawed at room temperature and samples were squeezed gently through the Miracloth into 50 mL falcon tubes in a laminar flow cabinet. Falcon tubes containing the samples were centrifuged at max speed for 20 min and the supernatant was discarded. The pellet was

resuspended in 1 mL of sterile water and transferred into clean 1.5 mL Eppendorf tubes. Samples were centrifuged again, supernatant was decanted, and pellets were stored at -80°C until use. For the DNA extraction we used 96-well-format MoBio PowerSoil Kit (MOBIO Laboratories; Qiagen) following the manufacturer's instruction. Before starting the extraction, all samples were randomized by placing them in a plastic bag that was shaken several times. Samples were taken individually from the bag and loaded in the DNA extraction plates. This random distribution was maintained throughout library preparation and sequencing.

e. 16S rRNA amplicon sequence data processing

Bacterial 16S *rRNA* amplification and sequencing were performed as above (material and methods 1g). Synthetic community sequencing was processed with MT-Toolbox (*29*). Briefly, sequence pairs were merged, quality-filtered and de-multiplexed according to their barcodes. The resulting sequences were then denoised and collapsed into amplicon sequence variants (ASVs) using DADA2 v.1.10.1 (*30*). We mapped the representative ASVs sequences to a database containing the 16S *rRNA* sequences of the 41 bacterial isolates present in the synthetic community. For further analyses, we used only the ASVs that mapped with 100% identity to the reference 16S *rRNA*. These chosen ASVs accounted for >95% of the total reads in the sequencing runs. Finally, using the chosen ASVs we created raw count, rarefied (1000 reads per sample) and relative abundance tables. The resulting abundance tables were processed and analysed with functions from the ohchibi package (https://github.com/isaisg/ohchibi). DNA sequence data for this experiment is available at the NCBI bio-project repository (ID PRJNA630964).

For the experiments using root diffusion barrier mutants and lines, beta diversity analyses (canonical analysis of principal coordinates) were based on Bray-Curtis dissimilarity matrices calculated from the relative abundance tables.

For the same experiments, we computed the genotype effect on the microbiome assembly for the three fractions sampled (Agar, Root and Shoot), independently. To do so, we used the capscale function from the vegan R package v.2.5-5 (*33*) to compute the canonical analysis of principal coordinates (CAP) with the following design:

$$\text{BrayCurtis Dissimilarity} \sim \text{Genotype} + \text{Condition(Rep)}$$

Additionally, we estimated the variance explained by the genotype variable by performing PERMANOVA via the function adonis from the vegan v.2.5-5. R package (*33*).

We used the R package DESeq2 v.1.24.0 (*34*) to compute the genotype specific enrichment profiles across the three sample fractions independently. For each ASV in the abundance tables, we estimated its difference with the Col-0 by fitting a GLM with the following design:

$$\text{Abundance} \sim \text{Rep} + \text{Genotype}$$

We used the FDR approach to adjust *p*-value tables. An ASV was considered differentially abundant against its control treatments if it had a corrected *p*-value < 0.05.

For the genotypes dataset, for each member of the synthetic community, we visualized its enrichment (in relation to Col-0) trends across the three fractions sampled (Agar, Root and Shoot) using a heatmap created by the ggplot2 v.3.2.1 R package (*35*). Briefly, to construct the heatmap, we used the log2 fold change matrix derived from our fitted GLM described above. To better visualize the global trends, we took the Root derived log2 fold change matrix and applied hierarchical (R function hclust, complete method) clustering across the rows (strains) and genotypes (columns). Finally, we sorted the shoot and agar enrichment matrices using the root clustering and visualized the three fractions in a single plot.

f. Bacterial synthetic community tree

To build the phylogenetic tree of the bacterial synthetic community we used the supermatrix approach previously described in Levy *et al*. (*12*). Briefly, we scanned 31 previously defined marker genes across the genomes in our collection using the hmmsearch tool from the hmmer version 3.1b2 (*38*). Then, we aligned each individual marker using MAFFT (*39*) and filtered low quality columns in the alignment using trimAl (*40*). Next, we concatenated all filtered alignments into a super alignment. Finally, FastTree version 2.1 (*41*) was used to infer the phylogeny using the WAG model of evolution.

g. Comparison of the bacterial synthetic community composition with a natural Arabidopsis thaliana transect experiment (*42*)

To explore the representation of bacterial families found in Arabidopsis plants grown in natural conditions in our synthetic community (SynCom), we took the full genome taxonomic classification of the 41 isolates in the SynCom and we extracted the Family level classification of each one. Next, we took the previously published *Arabidopsis thaliana* transect experiment (*42*) and we sum the relative abundance (across the fraction samples) of all ASVs in the dataset that had an identical Family taxonomic classification as one of the isolates in our screening.

h. Primary root elongation

We quantified the primary root elongation in the different root diffusion barrier genotypes exposed or not to the bacterial synthetic community from pictures, using image J (*43*).

i. Determination of cortical cell volume in root diffusion barrier mutants and lines

Sterilized wild-type (Col-0), mutants *esb1-1*, *myb36-2*, *sgn3-3*, *sgn3-3 myb36-2*, and lines *pCASP1::CDEF1 (esb1-1)*, *pCASP1::CDEF1 (sgn3-3 myb36-2)* and *pCASP1::CDEF1 (Col-0)* seeds were germinated on agar plate containing 0.5x MS medium solidified with 1% bacto-agar

inoculated or not (no bacteria control, only 10 mM MgCl2) with the 41-member synthetic community for 5 days. Seedlings were incubated in a fresh solution of 10 µg/mL propidium iodide (prepared from a stock solution 1 mg/mL) for 5 min in the dark and then rinsed twice with water. Roots were carefully placed on a microscope slide with water and covered with a coverslip. We visualized the propidium iodide staining using a confocal microscope Leica SP8, 40X objective (NA = 0.8), with an excitation at 594 nm and an emission band-path of 610–650 nm. Longitudinal sections and transversal sections of roots were imaged at 15 cells after the onset of elongation. Longitudinal sections were acquired in a median section of the roots. Transversal sections were imaged using the real-time z sectioning with SuperZ Galvanometer. Using Fiji software, the longitudinal length and the surface of a transversal section of three to five cortical cells per plants were measured. For each plant, the average longitudinal cell length was multiplied by the average surface of a transversal section in order to obtain the cortical cell volume. Six plants per genotype and treatment were analyzed.

j. Developmental and physiological parameters. Statistical analysis

For the following developmental and physiological parameters: primary root elongation, shoot dry weight and cortical cell volume, we compared, for each one of the 7 Arabidopsis mutant lines, the distribution of the given parameter against Col-0. To do so, we fitted the following linear model for each parameter inside each bacterial treatment (NB and SynCom) independently:

$$\text{Parameter} \sim \text{Genotype}$$

Afterwards, we applied the Dunnet test implemented in the multcomp v.1.4-12 R package to compare each one of the 7 Arabidopsis mutant lines against Col-0. Finally, we corrected each *p*-value using the FDR method. A comparison was considered significant if it had an adjusted *p*-value < 0.1. To visualize the results, for each parameter, we plotted the estimated mean with 95% confidence interval of each genotype across the two bacterial treatments (NB and SynCom).

k. Shoot ionome in agar system. Statistical analysis

We created a matrix (samples x ion) in which each cell was filled with the calculated element concentration in a given sample. Afterwards, we applied a z-score transformation of each individual ion across the samples in the matrix. Next, to compare the elemental profiles across genotypes we applied a canonical analysis of principal coordinates (CAP) using the Euclidean distance between samples, and the z-score matrix as input. We used the following formula in the design of the CAP analysis.

Euclidean Dissimilarity ~ Genotype + Condition(Rep)

For the samples inoculated with the bacterial synthetic community, we compared the total ionomic profile of each of the root diffusion barrier genotypes against Col-0 by projecting in CAP space all 8 genotypes in the dataset. Next, we compared for each of the 7 genotypes (except Col-0) the position, of all the samples belonging to that genotype, in CAP1 and CAP2 independently, in relationship to the position of all samples belonging to Col-0 using a leveneTest (car v.3.0.3 (https://cran.r-project.org/web/packages/car/car.pdf) package in R), followed by a *t*-test controlling or not for different variances between the two groups (1 of the 7 genotypes of interest and Col-0). To adjust the *p*-values obtained we used the Bonferroni correction. A genotype with a corrected *p*-value < 0.1, in either CAP1 or CAP2 was considered significantly different from Col-0.

Then, we tested for each ion abundance the influence of both the genotype and the bacteria (NB vs SynCom) variables. To do so, we applied a linear model with the following design:

Ion Abundance ~ Bacteria + Genotype + Bacteria:Genotype

Afterwards, using the emmeans v.1.4 R package (https://cran.r-project.org/web/packages/emmeans/index.html), we extracted from the fitted linear model the inter genotype contrasts (e.g. *myb36.2* SynCom vs Col-0 SynCom, *myb36.2* NB vs Col-0 NB). We adjusted, the *p*-values of all the comparisons using the FDR method and considered significant a contrast that had an adjusted *p*-value < 0.05. We visualized the trends of the ionomic profiles by displaying in a heatmap the average z-score abundances per each ion across the 8 genotypes sampled.

I. Transcriptional analysis of the ABA and ethylene responsive genes. Statistical analysis

We evaluated the expression of genes related with the response to the phytohormones ABA and ethylene in a collection of root diffusion barriers mutants (*sgn3-3, myb36-2, esb1-1, sgn3-3 myb36-2, esb1-1 sgn3-3*). These hormones have been described as regulators of the endodermal suberization (*5*). To do the analysis we used a RNA-Seq count gene table from the literature (*44*) generated using the first 5 mm of root tips of 6-day-old plants grown on 0.5x MS (*44*). With this data we analyzed the expression of two literature-based cores of 370 and 375 ABA and ethylene response transcriptional markers, respectively (*26*, *27*) across the RNA-Seq experiment.

We used the R package DESeq2 v.1.24.0 (*34*) to identify differentially expressed genes between each genotype against wild-type Col-0. To do so we fitted the following generalized linear model to the count matrix described above.

$$\text{Gene abundance} \sim \text{Rep} + \text{Genotype}$$

A gene was considered statistically differentially expressed if it had a false discovery rate (FDR) adjusted *p*-value < 0.1.

For visualization purposes we created a standardized gene matrix. To do so, we applied a variance stabilizing transformation to the raw count gene matrix followed up by standardizing the expression of each gene along the samples.

We visualized the average expression of the ABA and ethylene markers genes in our data by subsetting the above described standardized gene matrix. We displayed the results of this analysis in boxplots using the package ggplot2 v.3.2.1, in R (*35*).

m. Plants growth conditions. Metabolite analysis

Sterilized Col-0 and the different root diffusion barriers genotypes (*esb1-1*, *myb36-2*, *sgn3-3*, *sgn3-3 myb36-2*, *pCASP1::CDEF1 (esb1-1)*, *pCASP1::CDEF1 (sgn3-3 myb36-2)* and *pCASP1::CDEF1 (Col-0)*) seeds were germinated on agar plate containing 0.5x MS (Murashige and Skoog) medium solidified with 1% bacto-agar for a week. Approximately 60 seedlings with the same developmental stage of the different genotypes were then transferred to 0.5x MS agar plates inoculated with the 41-members synthetic community. In parallel approximately 60 seedlings were also transferred to the no bacteria control (agar plates inoculated with only 10 mM $MgCl_2$). Plates were manually randomized and placed in a growth chambers and grown under a 16-h light/8-h dark regime at 21°C day/19°C night for another 7 days. We used 3 biological replicas of each treatment.

n. Root extraction. Metabolite analysis

Root samples from 14-day-old Col-0 and root diffusion barrier genotypes, inoculated or not with the bacterial synthetic community, were collected and rapidly placed at 4°C using ice. Before the untargeted metabolite analysis, between 25 mg and 166 mg of roots were extracted with 1 mL of chilled 80% methanol. Samples were disrupted in a TissueLyser II (Qiagen) using 1 cycle of 6 min, frequency 30 s^{-1}, and then shaken in an orbital shaker for 10 min at 4°C in the dark. Tubes

were centrifuged in a benchtop centrifuge (Eppendorf 5810R), 3220 g for 15 min at 4°C and the supernatants collected in new tubes. Afterward, the resulting pellets were re-extracted using 0.7 mL of chilled 80% methanol. Supernatants for each replicate were combined and stored at -20°C.

o. Sample analysis and data extraction. Metabolite analysis

Samples were evaporated to dryness *in vacuo*, using a centrifugal evaporator (SPD1140DDA Speedvac, Thermo Scientific, Waltham MA, USA), then reconstituted using a 10% methanol in water solution (100 µL). Samples were centrifuged at 13,000 r.c.f. at 4°C for 10 minutes, and the clarified supernatants transferred to amber vials for analysis. A QC sample was made by combining equal volume aliquots from each analytical sample.

Samples were analyzed using an Infinity 2 UHPLC, coupled to a 6546 QTOF (Agilent Technologies, Manchester, UK) via a method adapted from (*45*). Briefly, 2 µL of sample was separated using Kinetex C18 column (2.6u particle size, 150 x 2.1 mm; Phenomenex, Macclesfield, UK) fitted with a 0.2 µm stainless steel filter, held at 40°C. Solvents A and B comprised 5% versus 95% (LCMS grade) acetonitrile in water, respectively, both containing formic acid at 0.1% (v/v). Flow rate was set to 0.3 mL/minute, the gradient starting at 15% solvent B, moving to 25% at 2 minutes, 35% at 6 minutes, 45% at 8 minutes, 65% at 10 minutes, then 100% at 11 minutes. This was held for a further 3 minutes, then the gradient returned to starting conditions and the column re-equilibrated for another 3.5 minutes.

Untargeted MS (TOF) analysis was performed in negative mode, the dual AJS ESI source using N_2 drying gas at 8 L/min, 320°C, sheath gas at 11 L/min, 350°C (Genius NM32LA, Peak Scientific, Ichinnan UK), with the nebulizer set to 35 psi. The capillary, nozzle, and fragmentor voltages were set to 3500, 1000 and 110 volts respectively. The TOF captured spectra across a mass range of 100-1700 m/z, and m/z 112.9855 and 1033.9881 were used as refence ions throughout the run

(derived from Agilent solution G1969-85001). Sample injection order was randomized, with QC samples injected before every 6 runs. Following acquisition, chemical features and abundances were extracted using Agilent Mass Profiler software.

p. Metabolite analysis. Statistics

For the analysis of the data, we constructed a matrix consisting of 51,818 peaks across all 48 sampled analyzed. We standardized (z-score) the abundance of each peak across the 48 samples. We utilized the function prcomp from R to apply principal component analysis (PCA) over the standardized peak matrix. For visualization purposes, we estimated the mean position, with its corresponding 95% CI, of each treatment (Genotype+Bacteria) across the first two dimensions of the projection.

Additionally, we applied PERMANOVA using the adonis functions from the vegan package in R (*33*) with the following specification:

Euclidean Dissimilarity ~ Genotype + Bacteria + Genotype:Bacteria

Finally, we utilized the Mantel test coded in the Mantel function from the vegan package in R (*33*), to compare the metabolome PCA projection against the Root microbiome projection for the agar system. Significance of the correlation was obtained using 10,000 permutations.

3. Root diffusion barriers screening using plant-bacterium binary association assays.

a. Seed sterilization

All seeds were sterilized with a mix of 70% bleach (commercial) and 0.2% Tween-20 (Sigma-Aldrich) with agitation for 8 minutes. Seeds were then rinsed with sterile distilled water at least three times to eliminate the bleach. This treatment efficiently removes the microbes from the seed surface. Before sowing, seeds were stratified in the dark at 4°C for at least 1 day.

b. Growth conditions for the bacterial strain collections and plant inoculation

For the analysis of the plant microbiota effect on the root diffusion barriers, two bacterial collections were used: a root and a leaf collection. The root collection was prepared using only roots of Brassicaceae (mostly *Arabidopsis thaliana*) grown in two natural soils from North Carolina, US (*12*). For the leaf collection, bacterial strains were isolated from individual leaves of healthy Arabidopsis plants collected from six locations around Tübingen, Germany, or Zurich, Switzerland (*13*). To isolate single colonies from the bacterial strains, −80°C glycerol stocks were grown on LB (root collection) and R2A [leaf collection; (Casein acid hydrolysate 0.5 g/L, Yeast extract 0.5 g/L, Protease peptone 0.5 g/L, Dextrose 0.5 g/L, Starch 0.5 g/L, Dipotassium phosphate 0.3 g/L, Magnesium sulphate 0.024 g/L, Sodium pyruvate 0.3 g/L, agar 15g/L, pH 7.2 supplemented with Methanol 0.5%)] plates at 28°C. A single colony was then inoculated in sterile test tubes containing 4 mL of LB medium (root collection) or R2A medium supplemented with methanol 0.5% (leaf collection) and grown in an incubator at 28°C with agitation at 250 rpm. All cultures were centrifuged in a benchtop centrifuge (Eppendorf 5810R), 3220 g at room temperature, and washed with 10 mM $MgCl_2$ to remove the media and cell debris. This step was repeated twice. Clean bacterial cells were resuspended in 1 mL of 10 mM $MgCl_2$, and the OD_{600nm} was then measured. We equalized all individual strains to a final OD_{600nm} value equal to 0.01. The individual bacterial inoculum (200 µL) was spread using a L-shaped cell spreader (Fisher scientific) on the surface of 12X12cm square agar plates with 0.5x MS medium before sowing the seeds.

c. In vitro plant growth conditions

All seeds were direct germinated on plate containing 0.5x MS with salt mixture medium (Sigma-Aldrich) solidified with 1% bacto-agar (BD, Difco) and inoculated with individual bacteria as in Materials and Methods 3b. Plates were then manually randomized and grown in a growth

chambers under a 16-h light/8-h dark regime at 21°C day/19°C night for 6 days.

d. Propidium iodide penetration blockage screening using binary association assays

To determine the bacterial effect on the functionality of the root diffusion barriers we used the apoplastic tracer propidium iodide (PI, Invitrogen). PI is a fluorescent molecule which diffusion into the tissue layers of the root is blocked only after the dye reaches the differentiated endodermis (*14*). 6-day-old Col-0 seedlings directly germinated in contact with individual bacteria were incubated in a fresh solution of 10 µg/mL PI (prepared from a stock solution 1 mg/mL) for 10 min in the dark and then rinsed twice with water. Seedlings were carefully placed on a microscope slide with water and covered with a coverslip. Using a fluorescence microscope Leica CTR5000, 20X magnification, we quantified the number of cells from the onset of elongation until the endodermal cells blocked the PI penetration to the stele in response to the individual bacterial strains. In all cases we analyzed at least 3 plants per treatment.

e. Determination of root developmental parameters

For the determination of root developmental parameters, wild-type Col-0 seeds were direct germinated on plate containing 0.5x MS with salt mixture medium (Sigma-Aldrich) solidified with 1% bacto-agar (BD, Difco) and inoculated or not (no bacteria control) with the 41 representative individual bacteria as in materials and methods 3b. Plates were then manually randomized and grown in a growth chambers under a 16-h light/8-h dark regime at 21°C day/19°C night for 5 days. Root lengths were determined from pictures of the different plants exposed or not to the individual bacteria using ImageJ (*43*).

The distance/number of cells from the onset of elongation to the xylem, the distance/number of cells from the onset of elongation to the first root hair, the distance/number of cells from the onset of elongation to the Casparian strip, the root diameter, and the total number of cells were

determined on cleared root according to Ursache *et al.* (*46*). Six-day-old seedlings were fixed with 4% PFA for 60–120 min at 20°C. Seedlings were then washed twice with 1x PBS for 1 min and transferred to the Clearsee solution (10% xylitol, 15% Sodium deoxycholate, 25% urea) for 24h. Then, the seedlings were stained overnight in 0.2% Basic Fuchsin in ClearSee for lignin staining. Basic Fuchsin solution was removed and the seedlings were washed twice with ClearSee for 60 min with gentle shaking. Afterward, the seedlings were stained for 30 min in 0.1% Direct Yellow 96 (Sigma) prepared in ClearSee solution for cell wall visualization. The seedlings were washed twice in ClearSee for 30 min. Roots were carefully placed on a microscope slide with ClearSee and covered with a coverslip. We imaged the root tip using a confocal microscope Leica SP8, 10X objective (NA = 0.4) by performing a z-stack. We used an excitation at 440 nm and an emission band-path of 500–530 nm for Direct Yellow 96 and an excitation at 594 nm and an emission band-path of 600–650 nm for Basic Fuchsin. We measured the length of the meristematic zone using Fiji software. The meristematic zone was defined as the region from the quiescent center up to the onset of elongation. The onset of elongation was defined from epidermal cells that was twice the length of the immediately preceding cell. We measured the length and the number of epidermal cells from the onset of elongation to the first appearance of Casparian strip lignin, to the first appearance of protoxylem lignin and to the first root hair. For the distance and number of cells to protoxylem lignin, the measurement was performed for both protoxylem poles and then averaged. Root diameter was measured at the onset of elongation. In all cases we analyzed at least 5 plants per treatment.

f. Determination of root developmental parameters. Statistical analysis

To compare the magnitude of the bacterial effect between the root developmental parameters, we standardized (z-score) each one of the parameters. Afterwards, for each parameter, we used the standardized values to compare each one of the quantified 41 bacterial isolates against NB. To do so, we fitted for each parameter the following linear model:

Parameter ~ Strain

Afterwards, we applied the Dunnet test implemented in the multcomp v.1.4-12 R package to compare each one of the 41 bacterial isolates against NB. Finally, we corrected each *p*-value using the FDR method. A comparison was considered significant if it had an adjusted *p*-value < 0.1. To visualize the results, for each parameter, we plotted each one of the 41 estimates (in relation to NB) obtained from the fitted linear model.

g. Suberin synthesis screening using binary association assays

To determine the bacterial effect on suberin synthesis in the root, we used the suberization reporter line *pGPAT5::mCITRINE-SYP122.* This line expresses the plasma membrane localized mCITRINE-SYP122 marker driven by the suberin biosynthetic gene *GPAT5* promoter (*15*). 6-day-old *pGPAT5::mCITRINE-SYP122* seedlings, directly germinated in contact with individual bacteria, were placed on a microscope slide with water, covered with a coverslip and the expression pattern was quantified using a epifluorescence microscope Leica CTR5000, 20X magnification with a GFP filter. The expression pattern was quantified as the number of cells in the continuous, patchy and non-suberizing zones, in response to the individual bacterial strains. In all cases we analyzed at least 4 plants per treatment.

h. Statistical analyses for propidium iodide (PI) and suberin quantification

We normalized the PI (number of cells), and *GPAT5* expression (relative abundance of each zone) measurements using the no bacteria (NB) treatment present in all the batches for which the 416 distinct isolates were splitted into. To do so, we estimated a batch normalization factor (one per measurement) by dividing the average measurement across the NB samples of that batch over the computed average measurement in all the NB samples across all batches. Finally, we normalized all measurements in a given batch by multiplying each one of them by the

estimated normalization factor. Additionally, we calculated the relative abundance of the PI measurements of each individual treatment (e.g. Isolate 1 Batch 1) by dividing the normalized PI quantification to the normalized average total number of cells present (sum of all 3 suberin zones) in that given treatment. For each of the 416 isolates, we compared their PI quantification profile against the no bacteria (NB) one. Additionally, for the *GPAT5* expression, for each of the 416 isolates the sum of the no expression and patchy zones was compared against the same sum in the NB control. Both, the PI and *GPAT5* expression comparisons were performed using a leveneTest car v.3.0.3 package (https://cran.r-project.org/web/packages/car/car.pdf), in R, followed by a *t*-test controlling or not for different variances between the two groups (1 of the 416 isolates of interest and NB treatment). The *p*-values obtained for all comparisons were adjusted using the FDR correction. Isolates showing PI or *GPAT5* expression profiles with a corrected *p*-value < 0.1 were considered significantly different from the NB treatment. Finally, for each comparison performed we computed an estimate: difference between the mean of the isolate treatment and NB treatment.

We correlated the PI quantification against the sum of the No expression + Patchy zones of the suberin biosynthesis phenotype using the function cor.test with the pearson correlation method.

Additionally, we compared the distributions of the 416 estimates for the PI and suberin quantifications using the Kolmogorov-Smirnov test coded in the function ks.test from the stats package of R.

i. Total number of cells analysis

We defined the total number of cells as a proxy of primary root length by performing a correlation test (function cor.test) of the average value of the two variables across 41 bacterial isolates.

To evaluate the relationship between the total number of cells and the Propidium Iodide (PI) permeability, we took the average total number of cell and the average PI permeability measurement across the 416 isolates screened. Afterwards, we plotted each of the 416 pair of average values in a scatterplot. Additionally, we divided the total of cells in ranges of 10 units and estimated for each range the mean with its corresponding 95% confidence interval. For reach range, we overlayed its estimated mean with confidence interval over the scatterplot of values.

To evaluate the relationship between the total number of cells and the suberin biosynthesis, we took the average total number of cell and average suberin (sum of the relative abundance of the No suberization + Patchy zones) measurement across the 416 bacterial isolates screened. Afterwards, we plotted each of the 416 pair of average values in a scatterplot. Additionally, we divided the total of cells in ranges of 10 units and estimated for each range the mean with its corresponding 95% confidence interval. For reach range, we overlayed its estimated mean with confidence interval over the scatterplot of values.

j. Association between Casparian strip formation and root development

In order to estimate the association between the Casparian strip formation and root development, we fitted the following linear model for each of the 41 isolates:

Distance from onset of elongation to CS lignin~ Distance from onset of elongation to first root hair

We extracted the variance explained (R2) and the *p*-value for each of the 41 tested bacteria. Using the *p*-value, we classified bacteria into Developmental coupled ($p < 0.05$) and Developmental uncoupled ($p > 0.05$). We visualized the results of the model by projecting the Model *p*-value and Variance explained in a scatterplot.

k. Bacterial collection tree.

To build the phylogenetic tree of the screened bacterial isolates we used the supermatrix approach previously described in (*12*). Briefly, we scanned 31 previously defined marker genes across the genomes in our collection using the hmmsearch tool from the hmmer version 3.1b2 (*38*). Then, we aligned each individual marker using MAFFT (*39*), and filtered low quality columns in the alignment using trimAl (*40*). Next, we concatenated all filtered alignments into a superalignment. Finally, FastTree version 2.1 (*41*) was used to infer the phylogeny using the WAG model of evolution. Finally, we used the iTOL interface (*47*) to visualize the phylogenetic tree of the isolates screened. Additionally, over this tree, we overlaid for each isolate its corresponding propidium iodide and suberin biosynthesis estimates calculated against NB.

We used the phylogenetic tree to calculate, via the phytools v0.6-99 (*48*), R package, the phylogenetic signal (Pagel's Lambda) for the propidium iodide and suberin biosynthesis phenotypes using the average measurement (relative abundance and sum of no expression + patchy zones respectively) across all isolates in the dataset.

l. Comparison of the bacterial collection composition with a natural Arabidopsis thaliana transect experiment (*42*)

To explore the representation of bacterial families found in Arabidopsis plants grown under natural conditions, in our bacterial strains collection, we took the full genome taxonomic classification of all isolates screened and we extracted the Family level classification of each one. Next, we took the previously published Arabidopsis transect experiment (*42*) and we sum the relative abundance (across the fraction samples) of all ASVs in the dataset that had an identical Family taxonomic classification as one of the isolates in our screening.

m. Selection of the 41 representative bacterial strains.

To select a representative group of strains encompassing all the diversity of propidium iodide and suberin biosynthesis profiles observed in our screening, we splitted the distribution of estimates for both phenotypes in tertiles using the function ntile from the dplyr v.0.8.3 R package. After splitting the distributions, we selected 41 isolates making sure we sampled across all 9 combinations of groups. An additional criterion of selection was to maximize phylogenetic diversity by exploring the topology of the tree while selecting the strains.

4. Plant-bacterium binary association assays with the 41 selected bacteria

a. Growth conditions for the bacterial strains and plant inoculation

The 41 selected bacteria were inoculated from glycerol stocks into 4 mL LB medium in sterile test tubes, and grown at 28°C, with agitation at 250 rpm for 2 days. Cultures were centrifuged in a benchtop centrifuge (Eppendorf 5810R), 3220 g at room temperature, and washed twice with 10 mM $MgCl_2$ to remove the used medium and cell debris. Individual bacterial cultures were resuspended in 1 mL of 10 mM $MgCl_2$, and the OD_{600nm} was then measured. Assuming that 1 OD_{600nm} unit is equal to about 10^9 c.f.u/mL, we equalized individual strain concentrations to a final value of 10^5 c.f.u/mL. The individual bacterial inoculum (100 µL) was spread using a L-shaped cell spreader (Fisher scientific) on the surface of 12X12cm square agar plates with 0.5x MS medium prior to transferring seedlings.

In parallel, heat-killed controls from the 41 individual strains were obtained by heating 1.5 mL of individual culture at 10^7 c.f.u/mL at 95°C for 2 h in a heating block. 100 µL of the heat-killed solutions were also spread on the surface of 12X12cm square agar plates with 0.5x MS medium prior to transferring seedlings. As a no-bacteria control we used the same agar plates with 100 µL of sterile 10 mM $MgCl_2$ spread on its surface.

b. In vitro plant growth conditions

Sterilized Col-0 seeds were germinated on plate containing 0.5x MS medium solidified with 1% bacto-agar for a week. Ten seedlings were then transferred to each of the individual-strains-inoculated agar plates containing 0.5x MS, to the heat-killed-control inoculated plates, and to the no-bacteria control plates. Plates were manually randomized and placed in a growth chambers and grown under a 16-h light/8-h dark regime at 21°C day/19°C night for another 7 days. As a control we used Arabidopsis line *pCASP1::CDEF1(wild-type)* expressing the cuticle destructing factor 1 (CDEF1) under the control of an endodermis specific promoter *pCASP1* (At2g36100 promoter)(*16*). *CDEF1* (At4g30140) is a cutinase that degrade suberin, thus, this line has a significant less amount of suberin as compared with wild-type plants. We used 5 replicas of each treatment and this experiment was repeated twice.

c. Primary root elongation quantification

Plates were imaged seven days post-transferring, using a linear robot camera. Primary root length elongation was measured using ImageJ (*43*).

d. Suberin quantification

Suberin accumulation in response to the bacterial strains, the synthetic community or the natural microbial community was visualized using a specific staining with Fluorol Yellow 088 (*5*). To do this, plants were carefully collected from the plates or magenta jar and incubated in a freshly prepared solution of Fluorol Yellow 088 (0.01%w/v, in lactic acid) at 70°C for 30 mins, followed by two rinses with water. Then, samples were treated with aniline blue (0.5% w/v, in water) at room temperature for 30 mins in darkness. After two rinses with water, several roots were placed on microscope slides with water and suberin were visualized using an excitation at 488 nm and an emission band-path of 500–600 nm with a 10x objective (NA=0.4) on a Leica SP8 confocal microscope. Images were acquired using the “tile scanning” function with a tile size of 256x256 pixels and with a pinhole size of 9 airy units. The “focus map” function was used to adjust the

focus across the specimens. Tiles were assembled using the tiles stitching function of the Leica software.

Confocal microscope images were used to quantify the suberin deposition. We quantified the distance from the root tip to the continuous zone of suberization in response to individual bacterial strains using imageJ (*43*). This distance is inversely proportional to the suberin amount in the root. We used four plants per treatment and this experiment was repeated twice.

e. Analysis of the bacterial colonization

For the re-isolation and quantification of bacteria we used colony-forming unit (c.f.u). Three fractions roots, shoots, and agar were used in this analysis. Four roots and theirs respectively four shoots were harvested individually from 14-day-old plants grown in three individual plates. In parallel, a cube of agar (approximately of sides 0.5 cm) was also collected from the area where the roots were growing in the plate. All samples were weighted in previous weighted sterile 2-mL-Eppendorf tubes. Roots and shoots samples were then rinsed 3 times with 10 mM $MgCl_2$ to remove agar particles and then placed in a sterile tube containing 200 µL of 10 mM $MgCl_2$ and 3 glass beads. Agar samples were directly placed in a sterile tube containing 200 µL of 10 mM $MgCl_2$. All samples were homogenized in a TissueLyser II (Qiagen) using 2 cycles of 30 seconds, frequency 30 s^{-1}. 20 µL of these samples were then serially diluted in 96-wells plates using 10 mM $MgCl_2$. 5 µL of every single dilution was plated on LB and grown at 28°C. The number of c.f.u were counted using a stereo microscope Leica Wild M10. The c.f.u/mL of harvested samples were determined considering the dilution factors and normalized by the sample weight. We used three replicas per treatment and this experiment was repeated twice.

f. Statistical analyses concerning the suberin content, primary root elongation and dry weight quantifications

We normalized the suberin content (distance from the root tip to the continuous zone of suberization), primary root elongation (length cm), and dry weight (mg/plant) measurements using the no bacterial (NB) treatment present in all the batches for which the 41 distinct isolates were splitted into. To do so, we estimated a batch normalization factor (one per measurement) by dividing the average measurement across the NB samples of each batch over the computed average measurement in all the NB samples across all batches. Finally, we normalized all measurements in a given batch by multiplying each one of them by the estimated normalization factor.

For each of the 41 bacterial isolates chosen, we compared each of the three phenotypes described above against the NB treatment using a leveneTest car v.3.0.3 package (https://cran.r-project.org/web/packages/car/car.pdf), in R, followed by a *t*-test controlling or not for different variances between the two groups (1 of the 41 isolates of interest and NB treatment). We used the Bonferroni correction to adjust the *p*-values obtained for all comparisons. Phenotypes with a corrected *p*-value < 0.1 were considered significantly different from those found in the NB treatment. Finally, for each comparison performed we computed an estimate (difference between the mean of the bacterial isolate and NB treatments). To compare the magnitude of change (against NB) between the three phenotypes, we plotted the distribution (41 estimates) of the absolute value of the estimates for each phenotype.

For the 41 isolates chosen, we correlated the suberin deposition (distance to continuous zone) with the suberin biosynthesis measurement (Proportion of cells to continuous zone) using the average values of both measurements across the 41 isolates with the function cor.test in R. We visualized the correlation using a scatterplot created with the package ggplot2 v.3.2.1 in R (*35*). Finally, we splitted the positive side (larger than NB) of the suberin profiles distribution using quantiles via the ntile function in the dplyr v.0.8.3 R package.

We correlated the suberin deposition profiles and the bacterial colonization in the roots (c.f.u) across the 41 isolates using the cor.test function in R. This correlation was visualized using a scatterplot constructed via the package ggplot2 v.3.2.1 in R (*35*).

A *t*-test was used to compare the primary root elongation and dry weight distributions between the NB and the heat-killed controls.

g. Statistical analyses concerning the ionome quantification across the 41 bacterial isolates.

For each elemental profile, we constructed an abundance matrix (isolate samples x ion). Next, we normalized the abundance of each ion across the 82 different treatments (41 live bacteria + 41 heat-killed controls) by using the ion abundance measured in no bacteria (NB) treatment present across all the batches for which the 82 distinct bacterial treatments were splitted into. To do so, we estimated a batch normalization factor (one per ion) by dividing the average ion abundance in the NB samples of that batch over the computed average ion abundance in all the NB samples across all batches. Finally, we normalized all measurements of that ion in that given batch by multiplying each measurement by the estimated normalization factor.

We compared the abundance of each of ion measured in each of the 82 treatments (41 bacterial isolates + 41 heat-killed controls) against the abundance of that ion in the NB treatment by using a leveneTest (car v.3.0.3 package (https://cran.r-project.org/web/packages/car/car.pdf) in R), followed by a *t*-test controlling or not for different variances between the two groups (1 of the 82 treatments of interest and NB treatment). We used the FDR correction to adjust the *p*-values obtained for all comparisons. An isolate was considered to have an elemental profile significantly different from the NB treatment if it had a corrected *p*-value < 0.05.

To estimate the global ionome profile differences across the 41 distinct bacterial isolates and its corresponding heat-killed controls we took the normalized ionome matrix and applied a z-score transformation to each ion across all samples. Afterwards, we applied principal component analysis (PCA) using the function prcomp in R. To facilitate the visualization of the analysis, for each of the 83 treatments (41 bacterial isolates + 41 heat-killed controls + NB), we computed the average (plus 95% C.I) placement of each treatment in the component 1 and 2 of the PCA projection. Additionally, we visualized the z-score ionome matrix using a heatmap generated with the ggplot2 package in R (*35*). We overlaid on the heatmap the results of the comparisons between each ion in each of the 82 treatments against NB.

Finally, we used the cor.test R function to correlate the z-score measurement of each ion abundance against the z-score of the suberin deposition (distance to continuous zone) quantification across the 41 chosen bacterial isolates. We adjusted the estimated *p*-values using the Bonferroni method. We consider that there was a significant correlation between a given ion and the suberin deposition if the adjusted *p*-value was < 0.05.

5. Effect of a bacterial synthetic community (SynCom) on suberin deposition

a. Growth conditions for the bacterial strains and plant inoculation

The bacterial synthetic community was design using the 41 selected bacteria in materials and methods 2a and 2g. Briefly, cultures from each strain were grown individually in sterile test tubes containing 4 mL of LB, at 28°C and agitation at 250 rpm. Cultures were then centrifuge in a benchtop centrifuge (Eppendorf 5810R), 3220 g at room temperature and washed separately twice with 10 mM $MgCl_2$ to remove the media and cell debris. Individual bacterial cultures were resuspended in 1 mL of 10 mM $MgCl_2$, and the OD_{600nm} was then measured. Assuming that 1 OD_{600nm} unit is equal to 10^9 c.f.u/mL, individual bacteria were mixed at a final concentration of 10^5

c.f.u/mL in the synthetic community. The synthetic community inoculum ($0D_{600nm}$ = 0.2, 100 µL) was spread using a L-shaped cell spreader (Fisher scientific) on the surface of 12X12cm square agar plates prior to transferring seedlings.

In parallel, heat-killed controls from the 41-members synthetic community were obtained by heating 2 mL of the synthetic community prepared at 10^7 c.f.u/mL at 95°C for 2h in a heating block. 100 µL of the heat-killed solutions were also spread on the surface of 12X12cm square agar plates prior to transferring seedlings. As a no-bacteria control we spread 100 µL of sterile 10 mM $MgCl_2$ on the surface of agar plates. For all treatments, agar plates with no plants, inoculated with the synthetic community, were used to control the effect of the different media on bacteria growth.

b. In vitro plant growth conditions. Nutritional stresses

To determine the role of the plant microbiota controlling the deposition of suberin in response to nutritional stresses, we analyzed seven different stress conditions known to induce changes in the suberin concentration in the root (*5*). Sterilized Col-0 seeds were germinated for a week on agar plates containing 0.5x MS medium solidified with 1% bacto-agar. Ten seedlings were transferred to agar plates inoculated with the 41-members synthetic community and exposed to different nutritional stresses. To impose the stresses, the composition of the 0.5 x MS medium (***macro-elements***: NH_4NO_3 (825 mg L^{-1}), $CaCl_2$ (166.1 mg L^{-1}), $MgSO_4$ (90.345 mg L^{-1}), KNO_3 (950 mg L^{-1}), KH_2PO_4 (85 mg L^{-1}), ***micro-elements***: H_3BO_3 (3.1 mg L^{-1}), $CoCl_2 \cdot 6H_2O$ (0.0125 mg L^{-1}), $CuSO_4 \cdot 5H_2O$ (0.0125 mg L^{-1}), $Na_2EDTA \cdot 2H_2O$ (18.65 mg L^{-1}), $FeSO_4 \cdot 7H_2O$ (13.9 mg L^{-1}), $MnSO_4 \cdot H_2O$ (8.45 mg L^{-1}), $Na_2MoO_4 \cdot 2H_2O$ (0.1065 mg L^{-1}), KI (0.415 mg L^{-1}), $ZnSO_4 \cdot 7H_2O$ (4.3 mg L^{-1}), ***vitamins:*** myo-Inositol (50 mg L^{-1}), Nicotinic acid (free acid) (0.25 mg L^{-1}), Pyridoxine-HCl (0.25 mg L^{-1}), Thiamine hydrochloride (0.05 mg L^{-1}), ***amino acids***: Glycine (1 mg L^{-1}, pH 5.6-5.7)) in the agar plates was amended. These amendments included Zn-free medium (without

$ZnSO_4 \cdot 7H_2O$), Fe-free medium (without FeSO4·7H2O), Mn-free medium (without MnSO4·H2O), K-free medium (KNO_3 was substituted by NH_4NO_3, KH_2PO_4 was substituted by NaH_2PO_4, and KI was substituted by NaI), P-free medium (without KH_2PO_4), and 0.5x MS medium supplemented with 100 mM NaCl.

In parallel, 10 seedlings were also transferred to agar plates (all treatments) containing the bacterial heat-killed control and the no bacteria control (only 10 mM $MgCl_2$). Plates were manually randomized and placed in a growth chambers and grown under a 16-h light/8-h dark regime at 21°C day/19°C night for another 7 days. We used 5 replicas of each treatment and this experiment was repeated twice.

c. In vitro plant growth conditions. Root diffusion barrier genotypes

To define the role of the plant microbiota in the regulation of the root diffusion barriers function, we analyzed a collection of plant mutants with a defective Casparian strip (*sgn3-3* and *sgn3-3 myb36-2*), a defective Casparian strip leading to an ectopic accumulation of suberin (*esb1-1* and *myb36-2*), and lines expressing the cuticle destructing factor 1 (*CDEF1*) that degrades suberin in Col-0 (*pCASP1::CDEF1 (wild-type)*) and two mutant backgrounds (*pCASP1::CDEF1 (esb1-1)* or *pELTP::CDEF1 (sgn3-3 myb36-2)*)**.** This selection represents different level of impairment in the root diffusion barriers.

Sterilized Col-0 seeds were germinated on agar plate containing 0.5x MS medium solidified with 1% bacto-agar for a week. Ten seedlings of the different genotypes were then transferred to 0.5x MS agar plates inoculated with the 41-member synthetic community. In parallel 10 seedlings were also transferred to no bacteria control (agar plates inoculated with only 10 mM $MgCl_2$). Plates were manually randomized and placed in a growth chambers and grown under a 16-h light/8-h

dark regime at 21°C day/19°C night for another 7 days. We used 5 replicas of each treatment and this experiment was repeated twice.

d. In vitro plant growth conditions. Hormone mutants and lines

To define the mechanism of the microbiome suberization pathway, we analyzed the following mutants: *aba2-1* (NASC156) (*20*), an ABA biosynthetic mutant with a reduced level of endogenous ABA; *abi4-1* (NASC8104) (*21*), involved in ABA signal transduction with a reduced sensitive to ABA, and the line *pCASP1::abi1-1*, impaired in endodermal ABA signaling (*5*). In parallel, we analyzed the ethylene receptor mutant *etr1-1* (NASC237) (*49*), and the ethylene insensitive mutant *ein3-1* (NASC8052) (*50*). All seeds were sterilized, germinated and grown as above. We used 5 replicas of each treatment and this experiment was repeated twice. In the case of the line *pCASP1::abi1-1,* we also analyzed the suberin accumulation in 5-day-old seedlings directly germinated on 0.5x MS plates inoculated with the bacterial synthetic community.

We also analyzed the *6xABRE_A::erGFP* and *6xABRE_R::erGFP* reporter lines (*22*). Sterilized seeds of both reporter lines were germinated on agar plate containing 0.5x MS medium solidified with 1% bacto-agar for a week. Five seedlings of each line were transferred to 0.5x MS agar plates inoculated with the 41-member synthetic community or with no bacteria control (10 mM $MgCl_2$). In parallel, five seedlings of each line were transferred to 0.5x MS agar plates supplemented with 100 mM NaCl or 1 µM ABA. Plates were manually randomized and placed in a growth chambers and grown under a 16-h light/8-h dark regime at 21°C day/19°C night for another 7 days. We analyzed 3 to 5 plants for each line and each treatment. For the analysis, plants were incubated in a fresh solution of 10 µg/mL propidium iodide (prepared from a stock solution 1 mg/mL) for 5 min in the dark and then rinsed twice with water. Roots were carefully placed on a microscope slide with water and covered with a coverslip. Using a confocal microscope Leica SP8, 20X objective (NA=0.7), we imaged median section of the root tip in the

case *of 6xABRE_A::erGFP* and *6xABRE_R::erGFP*, and median section of the root mature zone at 35 cells after the onset of elongation for the line *6xABRE_R::erGFP*.

For GFP visualization, we used an excitation at 488 nm and an emission band-path of 500–550 nm, and for propidium iodide visualization we used an excitation at 594 nm and an emission band-path of 610–650 nm. Using Fiji software, we quantified the average pixel intensity in the quiescent center, the columella, and the lateral root cap for the root tip and in the epidermis, the cortex, and vascular tissues for the root mature zone. The different tissues were identified using propidium iodide staining.

e. Hormone mutants and lines. Statistical analysis

For the *pCASP::abi1* experiments, we compared independently, at 5 days and 14 days, the suberin accumulation between the Genotype-Bacterial treatments (NB-Col-0,NB-SynCom, *pCASP::abi1*-NB *and pCASP::abi1*-SynCom) applying and ANOVA model with the following specification:

Suberin Measurement~ Treatment

At 5 days we used as suberin measurement the relative abundance of the following zones (No suberization + Patchy). At 14 days we used as suberin measurement the distance to continuous suberization zone. We visualized the results using an averaged stacked bar-graph representation for the measurements at 5 days and boxplots at 14 days, respectively. Differences between treatments were indicated using the confidence letter display derived from the Tukey's post hoc test implemented in the package emmeans.

For the *6xABRE_A::erGFP* and *6xABRE_R::erGFP* reporter lines we displayed the pixel intensity in the quiescent center, the columella, and the lateral root cap for the root tip and in the epidermis, the cortex, and vascular tissues for the root mature zone using boxplots.

f. In vitro plant growth conditions. Different concentration of the synthetic community inoculum

To analyze the effect of different bacterial synthetic community concentrations on endodermal suberization, wild-type Col-0 seeds were direct germinated on plate containing 0.5x MS with salt mixture medium (Sigma-Aldrich) solidified with 1% bacto-agar (BD, Difco), and inoculated or not (no bacteria control, only 10 mM $MgCl_2$) with different concentrations of the 41-member bacterial synthetic community as in materials and methods 5a. We used 4 dilutions 10E-4x, 10E-3x, 10E-2x, 10E-1x, the standard concentration 1x (OD_{600nm} = 0.2), and two concentrated synthetic communities, 2x and 3.2x. Plates were then manually randomized and grown in a growth chambers under a 16-h light/8-h dark regime at 21°C day/19°C night for 5 days.

Suberin were stained using Fluorol Yellow 088 (*5*), visualized and quantified according to materials and methods 4d.

g. Visualization of root-associated bacteria

For the bacterial colonization visualization, wild-type Col-0 seeds were direct germinated on plate containing 0.5x MS with salt mixture medium (Sigma-Aldrich) solidified with 1% bacto-agar (BD, Difco) and inoculated or not (no bacteria control, only 10 mM $MgCl_2$) with the 41-members bacterial synthetic community as in Materials and Methods 5a. Plates were then manually randomized and grown in a growth chambers under a 16-h light/8-h dark regime at 21°C day/19°C night for 6 days.

g.1. Bacteria visualization on the rhizoplane.

For bacteria visualization on the surface of the root, seedlings were incubated in a fresh solution containing 10 µg/mL propidium iodide (prepared from a stock solution 1 mg/mL) and 5 µg/mL

Wheat Germ Agglutinin-Alexa Fluor 488 (WGA-488, Thermo Fisher, prepared from a stock solution 1 mg/mL) for 10 min in the dark, and then rinsed twice with water. Propidium iodide allows the visualization of plant cell wall and bacteria. WGA-488 allows the visualization of gram-positive bacteria. Seedlings were placed on a microscope slide with water and covered with a coverslip. Using a confocal microscope Leica SP8, 40X objective (NA=0.85), we imaged the surface of the root tip, the elongation zone and mature zone (20 cells after the onset of elongation) by performing a z-stack. We used an excitation at 488 nm and an emission band-path of 510–540 nm for WGA-488 and an excitation at 594 nm and an emission band-path of 610–650 nm for propidium iodide.

g.2. Endophytic bacteria visualization

For the visualization of the endophytes, 6-day-old seedlings were fixed with 4% PFA at 20°C for 60 min. Seedlings were then washed twice in 1x PBS for 1 min. Seedling were then cleared in 10% KOH at 70°C for 3h, and washed five times in phosphate buffer saline (pH 7.4). Subsequently, the seedlings were incubated in a solution containing 1 mg/mL Direct Yellow 96 (cell wall staining, Sigma) in the dark for 1 h, then washed twice in water. Seedlings were then incubated in a solution containing 5 µg/mL Wheat Germ Agglutinin-Alexa Fluor 594 (WGA-594, Thermo Fisher, prepared from a stock solution 1 mg/mL), then washed twice in water. Seedlings were placed on a microscope slide with water and covered with a coverslip. Imaging was performed using a confocal microscope Leica SP8, 63X objective (NA=1.2). We used an excitation at 594 nm and an emission band-path of 610–650 nm for WGA-594, and an excitation at 440 nm and an emission band-path of 500–530 for Direct Yellow 96.

h. RNA extraction

RNA was extracted from Arabidopsis roots according to Logemann *et al*. (*51*). We used three independent biological replicas per treatment and we repeated this experiment twice. Briefly, approximately 10 roots from 14-day-old seedlings were harvested from each sample and flash

frozen using liquid N_2. Frozen roots were pulverized using a TissueLyzer II (Qiagen), 2 cycles of 30 seconds, frequency 30 s^{-1}, and 400 µL of Z6-buffer; 8 M guanidine HCl, 20 mM MES, 20 mM EDTA at pH 7.0 was added to the samples. Following the addition of 400 µL phenol:chloroform:isoamylalcohol; 25:24:1, samples were vortexed and centrifuged (20,000 *g*, 10 min) for phase separation. The aqueous phase was then transferred to a new 1.5 mL tube and 0.05 volumes of 1 N acetic acid and 0.7 volumes 96% ethanol were added. The RNA was precipitated at −20°C overnight. Following centrifugation, (20,000 *g*, 10 min, 4°C) the pellet was washed with 200 µL sodium-acetate (pH 5.2) and 70% ethanol. The RNA was dried and dissolved in 30 µL of ultrapure water and stored at −80°C until use.

i. Plant RNA sequencing

Before sequencing, RNA samples were quantified using the Qubit RNA BR Assay Kit (Invitrogen; Q10210) and quality was assessed using RNA Screen Tape (Agilent; 5067-5576) on the Agilent 4200 TapeStation System (Agilent; G2991A). Although TapeStation results showed RNA with high RNA integrity numbers (RINs > 8), indicative of good quality RNA, we detected the presence of high molecular weight nucleic acids typical of genomic DNA, therefore DNase treatment was carried out on the samples. TURBO DNase (Ambion; AM2238) was used to remove DNA from RNA samples. Briefly, 22.5 µL of RNA was combined with 2.5 µL of 10x TURBO DNase Buffer and 1 µL (2 Units) of TURBO DNase and incubated at 37°C for 30 min. The RNA was then dissolved with 75 µL of nuclease free water and purified using the Qiagen RNeasy MinElute Cleanup Kit (Qiagen; 74204). The final elution was carried out with 15 µL of nuclease free water. For library construction, 200 ng of high-quality RNA was used as input into Lexogen Quant Seq 3' mRNA Seq (FWD) Library Prep Kit (Lexogen; 015) and the standard protocol was followed. At the PCR stage 13 cycles of PCR were used. Library yield was measured by Qubit dsDNA HS (Invitrogen; Q32851) and library size was assessed using the High Sensitivity D1000 ScreenTape (Agilent; 5067- 5584) on the Agilent 4200 TapeStation System (Agilent; G2991A). Libraries were

normalized to each other based on size and Qubit dsDNA HS concentration and pooled together. The pool was quantified by qPCR using the KAPA Library Quantification Kit for Illumina Platforms (KAPA Biosystems; KK4873). The library pool was denatured and diluted according to the Illumina NextSeq System protocol (Illumina Document #15048776v09) and then sequenced on the Illumina NextSeq 500 on a NextSeq 500/550 High Output Kit v2.5 (75 Cycles) (Illumina; 20024906), to generate ~5 million 75bp single-end reads per sample.

j. RNA-Seq reads processing

Initial quality assessment of the Illumina RNA-Seq reads was performed using FastQC v0.11.8. (Babraham Bioinformatics, Cambridge, UK). Trimmomatic v0.36 (*52*) was used to identify and discard reads containing the Illumina adaptor sequence. The resulting high-quality reads were then mapped against the TAIR10 Arabidopsis reference genome using HISAT2 v2.1.0 (*53*) with default parameters. The featureCounts function from the Subread package (*54*) was then used to count reads that mapped to each one of the 27,206 nuclear protein-coding genes. Raw sequence data and read counts are available at the NCBI Gene Expression Omnibus, accession number GSE151376.

We dissected the genes responsible for the microbiota branch controlling endodermal suberization using an approach that contrast sets of differentially expressed genes across the distinct treatments/variables, [Col-0 axenic (microbiota pathway OFF, *Schengen* pathway OFF), Col-0 inoculated with the SynCom (microbiota pathway ON, *Schengen* pathway OFF), *myb36-2* axenic (microbiota pathway OFF, *Schengen* pathway ON), and *myb36-2* inoculated with the SynCom (microbiota pathway ON, *Schengen* pathway ON)]. The inoculation of *myb36-2* with the microbiota permits visualization of the effect of both suberin regulatory branches, the microbiota and the *Schengen* pathways, on the plant transcriptional response at the same time.

We used the R package DESeq2 v.1.24.0 (*34*) to identify a set of differentially expressed genes across the bacterial (NB, SynCom) treatments interacting along the two genotypes (Col-0, *myb36-*

2) assayed. To do so, we grouped both of the design variables (bacterial treatment and genotype) into a new grouping variable (e.g. Col-0_NB or *myb36.2*_SynCom) and fitted the following generalized linear model (GLM):

Gene Abundance ~ Rep + group

Next, we set up the following two contrasts to identify genes that shown the bacterial main effect (Contrast I) and the genotype main effect (Contrast II).

I. *(myb36.2*_SynCom and Col-0_SynCom) / (*myb36.2*_NB and Col-0_NB)

II. (*myb36.2*_SynCom and *myb36.2*_NB) / (Col-0_SynCom and Col-0_NB)

Then, using the contrasts described above, we defined the following differentially expressed gene sets. A gene was considered significantly differentially expressed if it had an FDR adjusted *p*-value < 0.05.

For the definition of the following differentially expressed gene sets, positive log2 fold changes imply higher expression in the numerator groups of the contrast formula while negative log2 fold changes imply higher expression in the denominator groups of the contrast formulas:

bacteria_up = Contrast 1 log2FoldChange > 0

bacteria_down = Contrast 1 log2FoldChange < 0

genotype_up = Contrast 2 log2FoldChange > 0

genotype_down = Contrast 2 log2FoldChange < 0

Finally, we performed the following set of operations to define the clusters of genes (C1, C2, C3, C4, C5, C6, C7, and C8) presented in Figure 4 and Supplemental Figure S10.

C1 = bacteria_up – (genotype_up ∪ genotype_down)

C2 = bcteria_down - (genotype_up ∪ genotype_down)

C3 = genotype_ up - (bacteria_up ∪ bacteria_down)

C4 = genotype_down - (bacteria_up ∪ bacteria_down)

C5 = bacteria_up ∩ genotype_up

C6 = bacteria_up ∩ genotype_down

C7 = bacteria_down ∩ genotype_up

C8 = bacteria_down ∩ genotype_down

To visualize the expression of the different differentially expressed gene sets we applied a variance stabilizing transformation to the raw count gene matrix. We then standardized each gene along the samples to generate a standardized matrix. Using the standardized matrix, we subset the differentially expressed gene sets into clusters (C1, C2, C3, C4, C5, C6, C7, and C8), and for each gene we calculated the mean expression value in a particular level of the grouping variable (e.g. Col-0_SynCom). The resulted matrix of differentially expressed gene across the 4 levels in our design (Col-0_SynCom, *myb36.2*_SynCom, Col-0_NB and *myb36.2*_NB) was used in Figure 4 and Supplemental Figure S10. Gene Ontology (GO) enrichment was performed for each cluster of differentially expressed genes using the R package clusterProfiler v.3.12.0 (*55*).

To define reference sets of ethylene and ABA genes, we downloaded the lists of 375 genes (*27*) and 3,061 genes (*26*) classified as ethylene and ABA responsive genes, respectively. In the case of ABA, we only used for the analysis the genes that exhibited an absolute log2 fold changes > 2 in 6 out of 7 timepoints described in (*27*). With these filtering conditions, we identified 284 and 86 upregulated and downregulated ABA core genes, respectively. We visualized the average

expression of the ABA and ethylene reference genes in our data by subsetting the above described matrix of differentially expressed genes across the 4 levels defined in our design (Col-0_SynCom, *myb36.2*_SynCom, Col-0_NB and *myb36.2*_NB). We displayed the results of this analysis in boxplots using the package ggplot2 v.3.2.1(*35*), in R. To examine the enrichment of the ABA and ethylene core sets across the 8 clusters of differentially expressed genes, we applied a hypergeometric test. The *p*-values of each test were adjusted using the FDR method. We considered an enrichment as significant if it had an adjusted *p*-value < 0.05.

We also analyzed the expression of genes controlling the phenylpropanoid pathway and their transcriptional regulator (*19*, *56*) in our data set by subsetting the above described matrix of differentially expressed genes across the 4 levels defined in our design (Col-0_SynCom, *myb36.2*_SynCom, Col-0_NB and *myb36.2*_NB). We visualized the result of this analysis as a heatmap using the package ggplot2 v.3.2.1(*35*), in R.

We also analyzed the expression of 19 *3-Ketoacyl-Coenzyme A Synthases* (*KCS*), coding key enzymes in fatty acid elongation, in our data set by subsetting the above described matrix of differentially expressed genes across the 4 levels defined in our design (Col-0_SynCom, *myb36.2*_SynCom, Col-0_NB and *myb36.2*_NB). We visualized the result of this analysis as a heatmap using the package ggplot2 v.3.2.1(*35*), in R.

To identify the 48 genes repressed by the microbiome pathway and recovered by the *Schengen* pathway activation in the *myb36-2* mutant, we took all genes belonging to C7 and applied hierarchical clustering over them (method ward.D2) using their expression profiles across the 4 levels in our design. Afterwards, we cut the dendrogram of the genes using the R function cutree and subset the group of 48 genes from the sub clusters defined. To perform the GO ontology enrichment, we used the R package clusterProfiler v.3.12.0 (*55*).

k. Sample preparation for suberin composition analysis

Root samples from 14-day-old Col-0 Arabidopsis plants were collected for suberin quantification. Samples were submerged quickly (around 3 seconds) in distilled H_2O, followed by another "dipwash" in a second container with pure distilled H_2O to remove any agar particles attached to the root. Then, washed roots were placed on a paper towel to remove the excess of water and the sample fresh weight was determined using an analytical balance.

Before suberin quantification, 200 mg of root samples were delipidated (removal of soluble, not covalently linked lipids) at room temperature. Roots were cut in small pieces (1-1.5 cm) with a scalpel, and transfer to a glass vial with Teflon-lined screw caps containing an excess of chloroform:methanol (2:1, v/v) (e.g. 4-10 mL). Samples were extracted with chloroform:methanol (2:1, v/v) with agitation for 2 h. Solvent was then discarded and fresh chloroform:methanol (2:1, v/v) solution was added to the samples and the extraction process was repeated again. This cycle of extraction was repeated twice. Subsequently, solvent was discarded, and the extraction process with fresh chloroform/methanol (1:2, v/v) was performed overnight. The overnight extraction step was repeated once. Used solvent was discarded and samples were extracted with methanol with agitation for 2 h. In the last step, the solvent was removed, and the samples were air dried in the fume hood for two days and then in an oven at 40°C for another two days.

l. Root suberin depolymerization and compositional analysis

The remaining cell wall material was depolymerized by transesterification in 2 mL of 10% methanolic BF_3 solution for 16 h at 70°C. After cooling down 10 µg of internal standard dotriacontane was added from a stock solution (10mg/50ml). The samples were mixed by vortexing and transferred to a precleaned 9-mL vial containing 4 mL of saturated aqueous solution of $NaHCO_3$. Suberin constituents in this methanolysate were subsequently extracted with 3x 2mL

Chloroform. Combined Chloroform phases were washed twice with H_2O, dried with Na_2SO_4 and then concentrated to a volume of approximately 50 µL in a N_2-stream at 50°C. Finally, 20 µL of pyridine was added and extracted monomers were derivatized with 20 µL bis-(*N,N*-trimethylsilyl)-tri-fluoractetamide (BSTFA) at 70°C for 40 min to convert hydroxyl and carboxyl groups into their corresponding trimethysilyl (TMS) ethers and esters prior to GC analysis.

GC and GC-MS analysis of depolymerization products was performed as described in (*57*). Monomers were identified from their EI-MS spectra (70 eV, *m/z* 50-700) after capillary GC (DB-1 column, 30 m x 0.32 mm, 0.1 µm (J&W), on-column-injection at 50°C, 2 min at 50°C, 10°C min^{-1} to 150°C, 1 min at 150°C, 3°C min^{-1} to 310°C, 30 min at 310°C and Helium carrier gas with 2mL min^{-1}) on an Agilent 6890N gas chromatograph combined with a 5973N Mass Selective Detector [(MSD) Agilent Technologies, Germany)] equipped with a quadrupole mass filter. Quantification of suberin monomers was performed with and identical GC system, combined with a Flame Ionization Detector (FID) based on the internal standard. All analyses were performed with three to five replicates from two independent experiments.

m. Statistical analyses concerning the bacterial synthetic community experiments

For both experimental designs (stresses and mutants), we normalized the suberin (distance to continuous zone), primary root elongation (length cm), and dry weight (mg/plant) measurements by using the no bacteria (NB) treatment present in all the batches for which all stresses and mutants were splitted into. To do so, we estimated a batch normalization factor (one per measurement) by dividing the average measurement across the NB samples of that batch over the computed average measurement in all the NB samples across all batches. Finally, we normalized all measurements in a given batch by multiplying each one of them by the estimated normalization factor.

For the nutrient stress experiments, we compared the effect of the bacterial synthetic community (bacteria effect) on the suberin and dry weight across all nutrient stresses tested by fitting a linear model with the following design:

Phenotype ~Stress + Bacteria + Stress:Bacteria

Afterwards, using the emmeans v.1.4 R package (https://cran.r-project.org/web/packages/emmeans/index.html), we extracted from the linear model the intra stresses contrasts between NB and SynCom (e.g. -Fe SynCom vs -Fe NB, Full SynCom vs Full NB). We adjusted the *p*-values of all comparisons using the FDR method, and considered a significant contrast when it had an adjusted *p*-value < 0.05.

For the nutrient stress experiments, we correlated the suberin content (distance to continuous zone) and the dry weight measurements across all the treatments (stresses) computed using the cor.test R function.

In the chemical quantification of suberin, the amount of each monomer was compared between the NB and the SynCom treatments using a leveneTest (car v.3.0.3 package (https://cran.r-project.org/web/packages/car/car.pdf), in R), followed by a *t*-test controlling or not for different variances between the two groups. We used the FDR correction to adjust the *p*-values obtained for all comparisons. A monomer was considered to have a significantly different amount between the NB and SynCom treatments if it had a corrected *p*-value < 0.05.

For the root diffusion barrier mutants and lines experiments, we compared for each genotype independently the effect of the SynCom (bacteria effect) on the suberin, primary root elongation and dry weight using a leveneTest (car v.3.0.3 package (https://cran.r-project.org/web/packages/car/car.pdf), in R), followed by a *t*-test controlling or not for different

variances between the two groups. We used the FDR method to adjust the *p*-values of all the comparisons. The results were visualized using boxplots generated with the ggplot2 v.3.2.1 R package (*35*).

To compare the effect of the different synthetic community concentrations over the suberin accumulation, we fitted the following ANOVA model:

Relative abundance (No suberization + Patchy) zones~ Inoculation treatment

We visualized the results of the suberization profiles across the inoculation treatments using an averaged stacked bar-graph representation. Differences between treatments were indicated using the confidence letter display derived from the Tukey's post hoc test implemented in the package emmeans.

n. Statistical analyses of the elemental profiles

For both experimental designs (mutants and stresses), we constructed matrices with the ion quantifications across samples. Afterwards, we normalized the abundance of each ion using the ion abundance measured in the no bacteria (NB) treatment that is present across all the batches, for which the nutrient stresses and genotypes treatments were splitted into. To do so, we estimated a batch normalization factor (one per ion) by dividing the average ion abundance in the NB samples of that batch over the computed average ion abundance in all the NB samples across all batches. Finally, we normalized all measurements by multiplying each measurement by the estimated normalization factor.

For the nutrient stress experiments, we explored the global ionomic differences across the stress treatments and the bacterial treatments (no bacteria, live bacteria, and heat-killed control) via dimensionality reduction approaches (principal component analysis and canonical analysis of

principal coordinates). Briefly, we took the normalized ionome matrix and applied a z-score transformation to each ion across all samples. Then, we applied principal component analysis (PCA) using the function prcomp in R. Additionally, to explore specifically the differences between the bacterial treatments, we applied CAP using the following formula:

Euclidean Dissimilarity ~ Bacterial treatment + Condition(Stress)

Then, we tested for each ion abundance the influence of both the stress and the bacteria (NB vs SynCom) variables. To do so, we applied a linear model with the following design:

Ion Abundance ~ Bacteria + Stress + Bacteria:Stress

Afterwards, using the emmeans v.1.4 R package (https://cran.r-project.org/web/packages/emmeans/index.html), we extracted from the fitted linear model the intra stress contrasts between NB and SynCom (e.g. -Fe SynCom vs -Fe NB, Full SynCom vs Full NB) and the inter stress contrasts as well (e.g. -Fe SynCom vs Full SynCom, +NaCl NB vs Full NB). The *p*-values of all the comparisons were adjusted using the FDR method and we considered significant a contrast that had an adjusted *p*-value < 0.05. We visualized the mentioned contrasts using a heatmap where we displayed the z-score ion matrix.

Finally, we correlated the z-score measurement of each ion against the z-score of the suberin content (distance to continuous zone) across all the stresses applying the cor.test R function. We adjusted the estimated *p*-values using the FDR method and determined that there was a significant correlation between a given ion and the suberin content if the adjusted *p*-value was < 0.05.

To identify the sector of the ionome tightly controlled by suberin, we took the normalized ionome matrix computed for the 8 genotypes analyzed in the SynCom agar experiment and applied a z-

score transformation to each ion across all samples. Afterwards, we subset the following genotype treatments from it: Col-0, *pCASP1::CDEF*, *pCASP1::CDEF (esb1.1)* and *pELTP::CDEF(myb36-2 sgn3-3)*. Afterwards, we created a combined variable joining the bacterial (NB and Syncom) and genotype variables. Subsequently, for each ion we fitted the following linear model:

$$\text{Abundance ion} \sim \text{Combined variable}$$

Then, for each ion we applied a Dunnett test comparing each level in the Combined variable (e.g. Col-0 SynCom, *pCASP1::CDEF* NB, *pCASP1::CDEF* SynCom) to Col-0 NB (reference level in the model). Afterwards, from the Dunnett contrasts we obtained the estimates of each comparison across all ions and constructed an estimate matrix. Finally, we classified each ion based on the directionality of the estimates. We visualized this directionality via a heatmap created using ggplot2 v.3.2.1 package (*35*) in R.

6- Experiment with natural microbial communities

a. Microbial isolation from soil

Soil microbial populations were extracted from a soil from Sutton-Bonington Campus (University of Nottingham, UK; +52° 49′ 59.75″N, −1° 14′ 56.62″W). 500 mL of dry soil were mix vigorously with 500 mL of autoclaved RO water to bring microbes into suspension. We let the solution rest for 20 minutes to let the big soil particles settle. The supernatants were then filtered using a funnel lined with miracloth in sterile conditions. The filtrated soil solutions were incubated for an additional 20 min. The supernatants were spin in a centrifuge (Eppendorf 5810R) 3220 g at room temperature for 30 min. Pellets were resuspended in 50 mL of MES pH 6. Soil solutions were centrifuged again at 3220 g at room temperature for 30 min. Pellets were resuspended in 100 mL MES pH 6.0 with vigorous shaking and/or vortexing. We repeat this centrifugation and resuspension step once. We finally centrifuged the soil solutions at 3220 g at room temperature

for 30 min and the pellets were resuspended in 50 mL MES pH 6.0. The soil solutions contained the microbes were incubated on ice until use.

b. Plant growth conditions

To demonstrate that the buffering effect on suberin is conserved in more complex natural microbial communities, we used wild-type Col-0 plants and the mutant *aba2-1*. Sterilized seeds of both genotypes were germinated on agar plates containing 0.5x MS medium solidified with 1% bacto-agar for 4 days. At least nine seedlings of the different genotypes were transferred to magenta jars containing 30 g of perlite, amorphous volcanic glass that is nutritional inert. Magenta jars filled with perlites were previously sterilized in two cycles with 24 h of separation between them. Before transferring, the jars were supplemented with 70 mL of liquid 0.5x MS medium or the same medium modified to imposed high salinity (70 mM NaCl) stress. Magenta jars were inoculated with 200 µL of the synthetic community, and the natural microbial community resuspended in the media at a final concentration of 10^5 c.f.u/mL. In parallel nine seedlings were also transferred to no bacteria control (magenta jars inoculated with only 200 µL 10 mM $MgCl_2$). Magenta jars were covered, manually randomized and placed in a growth chambers under a 16-h light/8-h dark regime at 21°C day/19°C night for another 10 days. We used 4 replicas of each treatment.

c. Shoot area quantification

The area of the plant shoots was quantified from pictures showing a high contrast between the green of the leaves and the homogenous white background obtained by using perlite as a substrate. The quantification was performed using the tool Measurement Log on Photoshop. We used a customize scale to transform pixels into mm.

d. Statistical analyses of experiments in the perlite system

Given the three variables design in this dataset, Condition (Full and + NaCl), Genotype (Col-0 and *aba2.1*), and Community (No bacteria (NB), SynCom and Natural community), we tested the effect of the community on a particular combination of Condition and Genotype independently (e.g. Full Col-0, + NaCl *aba2.1*, etc). To do so, we fitted inside each combination the following linear model:

$$\text{Phenotype} \sim \text{Community}$$

Afterwards, we applied the Dunnet test implemented in the multcomp v.1.4-12 R package to compare the SynCom and natural community treatments against the NB treatment. Finally, we corrected each *p*-value using the FDR method. A comparison was considered significant if it had an adjusted *p*-value < 0.05.

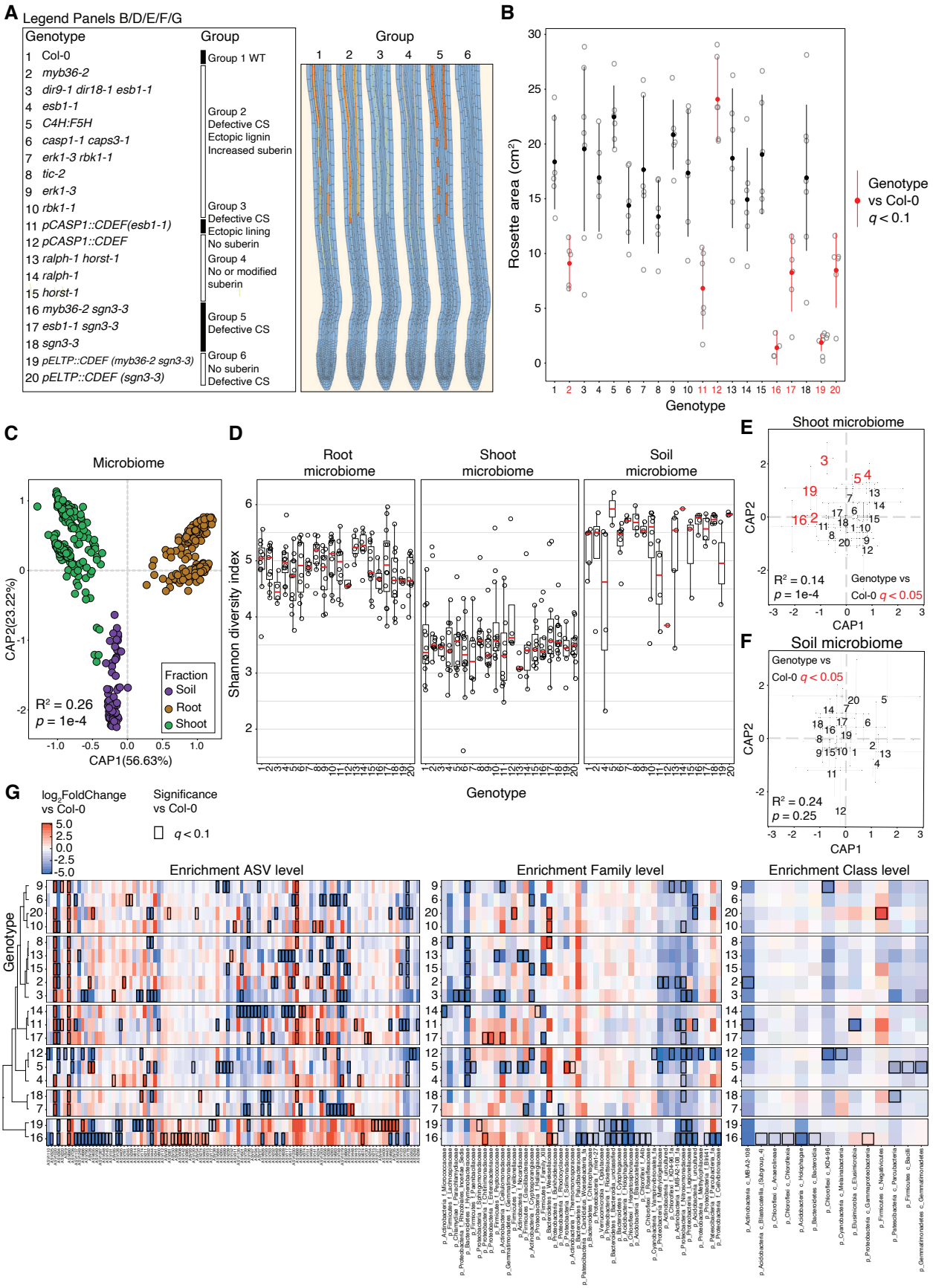
A
Legend Panels B/D/E/F/G
Genotype
Group
1 Col-0
2 myb36-2
3 dir9-1 dir18-1 esb1-1
4 esb1-1
5 C4H:F5H
6 casp1-1 caps3-1
7 erk1-3 rbk1-1
8 tic-2
9 erk1-3
10 rbk1-1
11 pCASP1::CDEF(esb1-1)
12 pCASP1::CDEF
13 ralph-1 horst-1
14 ralph-1
15 horst-1
16 myb36-2 sgn3-3
17 esb1-1 sgn3-3
18 sgn3-3
19 pELTP::CDEF (myb36-2 sgn3-3)
20 pELTP::CDEF (sgn3-3)
Group 1 WT
Group 2 Defective CS Ectopic lignin Increased suberin
Group 3 Defective CS Ectopic lining No suberin
Group 4 No or modified suberin
Group 5 Defective CS
Group 6 No suberin Defective CS
Group
1 2 3 4 5 6
B
Rosette area (cm²)
Genotype
Genotype vs Col-0 q < 0.1
C
Microbiome
CAP2(23.22%)
CAP1(56.63%)
R² = 0.26
p = 1e-4
Fraction
Soil
Root
Shoot
D
Root microbiome
Shoot microbiome
Soil microbiome
Shannon diversity index
Genotype
E
Shoot microbiome
CAP2
CAP1
R² = 0.14
p = 1e-4
Genotype vs Col-0 q < 0.05
F
Soil microbiome
Genotype vs Col-0 q < 0.05
CAP2
CAP1
R² = 0.24
p = 0.25
G
log2FoldChange vs Col-0
5.0
2.5
0.0
-2.5
-5.0
Significance vs Col-0
q < 0.1
Enrichment ASV level
Enrichment Family level
Enrichment Class level
Genotype

fig. S1. Root diffusion barrier regulatory network influences plant microbiome composition in a natural soil.

A. Scheme of the root diffusion barrier phenotypes found in the collection of mutants and lines used. This collection of genotypes represents combinatorial impairments in the different sectors of the root diffusion barrier network such as the Casparian strip and suberin synthesis or the activation of the *Schengen* pathway (see also table S1)**.** The synthesis of suberin monomers is catalyzed by several cytochrome P450 oxygenases (CYP), such as CYP86A1/HORST and CYP86B1/RALPH located in the endodermis (*58*). The transcription factor MYB36 controls the expression of the genes involved in the synthesis of the Casparian strip (*18*, *59*, *60*) such as *CASPARIAN STRIP MEMBRANE DOMAIN PROTEINS (CASPs)* (*4*, *61*), the dirigent-like protein *ESB1* needed for the proper polymerization of lignin (*62*), and the receptor-like kinase *SCHENGEN3 (SNG3)* that acts as part of a surveillance system to check the integrity of Casparian strip (*6*, *24*, *63*). In the figure, lignin is in yellow and suberin in orange. **B.** Rosette area of the different root diffusion barrier genotypes grown in a natural soil. Genotypes are ordered according to the legend on panel A. The central dots represent the estimated mean and the vertical lines the 95% confidence interval. Genotypes in red are significantly different from Col-0 wild-type (pairwise FDR adjusted *t*-test, $q < 0.1$). **C.** Canonical analysis of principal coordinates (CAP) showing the projected microbiome assembly between each fraction sampled: soil, root and shoot. Plants were grown in a natural soil from the University of Nottingham, Sutton Bonington campus, and we determined the bacterial root, shoot and soil community profiles using 16S *rRNA* amplicon sequencing. In general, our results reproduced previous findings (*10*, *11*); sample fraction (soil, root, shoot) explained most (26%) of the variance. **D.** Graphs showing the alpha diversity across sample fractions (root, shoot and soil) and plant genotypes (numbers, (see also Fig. 1A) estimated using the Shannon Diversity index. Genotypes are ordered according to the legend on panel A. **E, F**. Canonical analysis of principal coordinates (CAP) of microbiome composition showing the projected microbiome assembly of plant genotypes (numbers) within **E.** shoot and **F.** soil fractions. Numbers in red are genotypes with a distinct microbial composition as compared with Col-0 ($q < 0.05$). PERMANOVA R^2 and *p*-values are shown within each plot. **G.** Heatmaps showing the root enrichment patterns (in relation to Col-0) of different taxonomic units (ASVs, Family and Class) across the collection of root diffusion barrier genotypes. The tiles of the heatmaps are colored based on the $\log_2$ fold change estimated from a generalized linear model contrasting the abundance of each taxonomic unit (x-axis) in a given root diffusion barrier genotype (y-axis) against Col-0. The root diffusion barrier genotypes (y-axis) are clustered. Squares outlined in black represent taxonomic units at each taxonomic level (ASV, Family and Class) significantly enriched (red) and depleted (blue) with respect to Col-0 ($q < 0.1$).

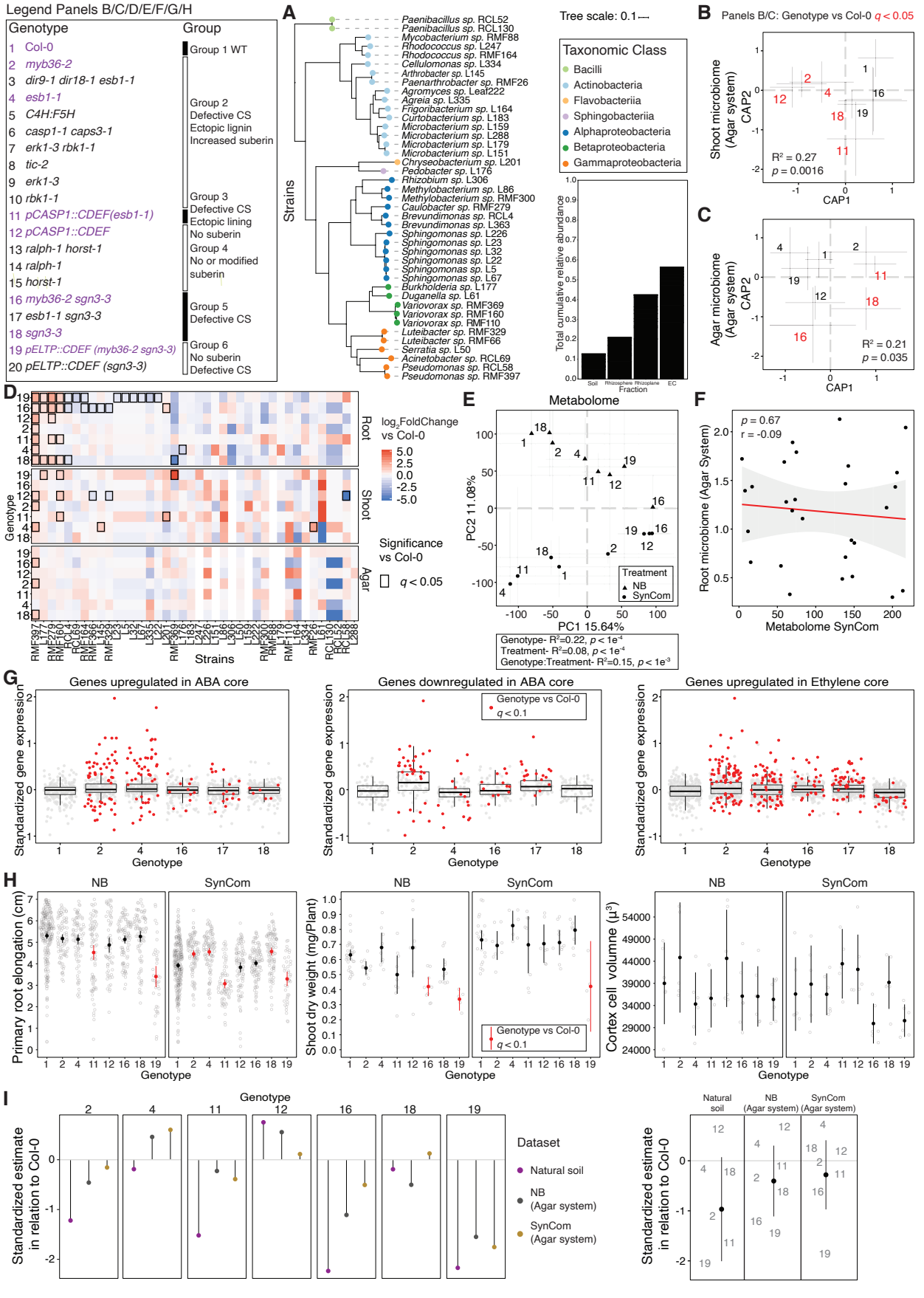
Legend Panels B/C/D/E/F/G/H
Genotype
Group
1 Col-0
2 myb36-2
3 dir9-1 dir18-1 esb1-1
4 esb1-1
5 C4H:F5H
6 casp1-1 caps3-1
7 erk1-3 rbk1-1
8 tic-2
9 erk1-3
10 rbk1-1
11 pCASP1::CDEF(esb1-1)
12 pCASP1::CDEF
13 ralph-1 horst-1
14 ralph-1
15 horst-1
16 myb36-2 sgn3-3
17 esb1-1 sgn3-3
18 sgn3-3
19 pELTP::CDEF (myb36-2 sgn3-3)
20 pELTP::CDEF (sgn3-3)
Group 1 WT
Group 2 Defective CS Ectopic lignin Increased suberin
Group 3 Defective CS Ectopic lining No suberin
Group 4 No or modified suberin
Group 5 Defective CS
Group 6 No suberin Defective CS
A
Strains
Tree scale: 0.1
Taxonomic Class
Bacilli
Actinobacteria
Flavobacteriia
Sphingobacteriia
Alphaproteobacteria
Betaproteobacteria
Gammaproteobacteria
Total cumulative relative abundance
Soil
Rhizosphere
Rhizoplane
EC
Fraction
B
Panels B/C: Genotype vs Col-0 q < 0.05
Shoot microbiome (Agar system) CAP2
CAP1
R² = 0.27
p = 0.0016
C
Agar microbiome (Agar system) CAP2
CAP1
R² = 0.21
p = 0.035
D
Genotype
Root
Shoot
Agar
log2FoldChange vs Col-0
5.0
2.5
0.0
-2.5
-5.0
Significance vs Col-0
q < 0.05
Strains
E
Metabolome
PC2 11.08%
PC1 15.64%
Treatment
NB
SynCom
Genotype- R²=0.22, p < 1e-4
Treatment- R²=0.08, p < 1e-4
Genotype:Treatment- R²=0.15, p < 1e-3
F
p = 0.67
r = -0.09
Root microbiome (Agar System)
Metabolome SynCom
G
Genes upregulated in ABA core
Genes downregulated in ABA core
Genes upregulated in Ethylene core
Standardized gene expression
Genotype vs Col-0
q < 0.1
Genotype
H
NB
SynCom
Primary root elongation (cm)
Shoot dry weight (mg/Plant)
Cortex cell volumne (µ³)
Genotype vs Col-0
q < 0.1
Genotype
I
Genotype
Standardized estimate in relation to Col-0
Dataset
Natural soil
NB (Agar system)
SynCom (Agar system)
Natural soil
NB (Agar system)
SynCom (Agar system)

fig. S2. Plants with atypical root diffusion barrier function assemble an altered microbiota in an agar plate system.

A. (left) Phylogenetic tree of 41 bacterial strains isolated from Arabidopsis plants, used in the synthetic community (SynCom). Tree tips are colored according to the taxonomic class. (right) The bar graph shows the total cumulative relative abundance at the family level of the bacterial synthetic community members present across the different sample fractions (soil, rhizosphere, rhizoplane and endophytic compartment (EC)) defined in an ecological survey of natural Arabidopsis populations (*42*). Notice that the bacterial synthetic community contains bacterial strains that belong to families that sum ~60% of the total relative abundance of all the endophytic compartment samples obtained across natural Arabidopsis populations (*42*) **B, C.** Canonical analysis of principal component (CAP) of microbiome composition showing the projected microbiome assembly of the different plant genotypes selected within the **B.** shoot and **C.** agar fractions. Plants genotypes were grown on agar plates inoculated with the bacterial synthetic community. Genotypes are represented by numbers following the legend at the top of the figure. Genotypes in red are significantly different from Col-0 ($p < 0.05$). Variance explained (R^2) and *p*-values were obtained using PERMANOVA. **D.** Heatmaps showing the enrichment ($\log_2$ fold change) of the different bacterial isolates from the synthetic community across the different plant genotypes (numbers) and sample fractions (root, shoot, and agar). Squares outlined in black are bacterial strains significant enriched (red) and depleted (blue) with respect to Col-0 ($q < 0.05$). **E.** Untargeted metabolite analysis using roots of the different root diffusion barrier genotypes grown axenically or with the synthetic community. Principal component analysis of metabolic composition showing the projected metabolome of the different plant genotypes grown in axenic conditions or with the bacterial synthetic community. Notice that genotypes, bacterial treatments, and their interaction explain 45% of the variance observed. PERMANOVA R^2 and *p*-values are shown. **F.** Pairwise correlation analysis between the root metabolome and the root microbiome composition of root diffusion barrier genotypes grown on agar plates (agar system). Mantel r statistic, and the *p*-value obtained from 10,000 permutations are shown. Notice that the root metabolome and the root microbiome composition dissimilarities do not correlate, supporting the conclusion that these metabolite differences do not explain the atypical microbiomes of these mutants and lines. **G.** We

checked if the transcriptional response to ABA and ethylene, phytohormones controlling the deposition of suberin at the endodermis (*5*), is altered in a representative selection of root diffusion barrier mutants *sgn3-3*, *esb1-1*, *myb36-2*, *esb1-1 sgn3-3*, and *sgn3-3 myb36-2* grown axenically on agar plates. Boxplots showing the standardized expression of two literature-based cores of 370 and 375 ABA and ethylene response transcriptional markers, respectively (*26*, *27*) across a RNA-Seq experiment from the literature (*44*). Values in red represent genes statistically different from wild type Col-0 plants ($q < 0.1$). **H.** The growth impairment observed in the root diffusion barrier genotypes grown in a natural soil is reduced in the agar plate system. (left) Primary root elongation, (middle) shoot dry weight, and (right) the cortical cell volume used as a proxy for the water status (*64*) of the selected root diffusion barrier genotypes grown in axenic agar plates (NB) or inoculated with the 41-members bacterial synthetic community (SynCom). Genotypes are represented by numbers according to the legend at the beginning of the figure. The central dots represent the estimated mean and the vertical lines the 95% confidence interval. Genotypes in red are significantly different from Col-0 wild-type (linear model followed by a Dunnett test against Col-0, $q < 0.1$). In this system, the presence of the bacterial synthetic community has a positive effect on shoot dry weight for all root diffusion barrier genotypes used. **I.** (left) Standardized shoot growth of the root diffusion barrier genotypes (numbers on the top) across the different growing systems used: natural soil, axenic agar system (NB), and agar system inoculated with the bacterial synthetic community (SynCom). The effect of the system used on the shoot growth in the genotypes was determined in relation to wild-type plants Col-0. Vertical bars represent the magnitude of the standardized estimates for each genotype in relation to Col-0, and theirs tips are colored according to the growing system used. (right) Standardized effect of the different growing systems used on plant shoot growth. The central dots represent the estimated mean and the vertical lines the 95% confidence interval.

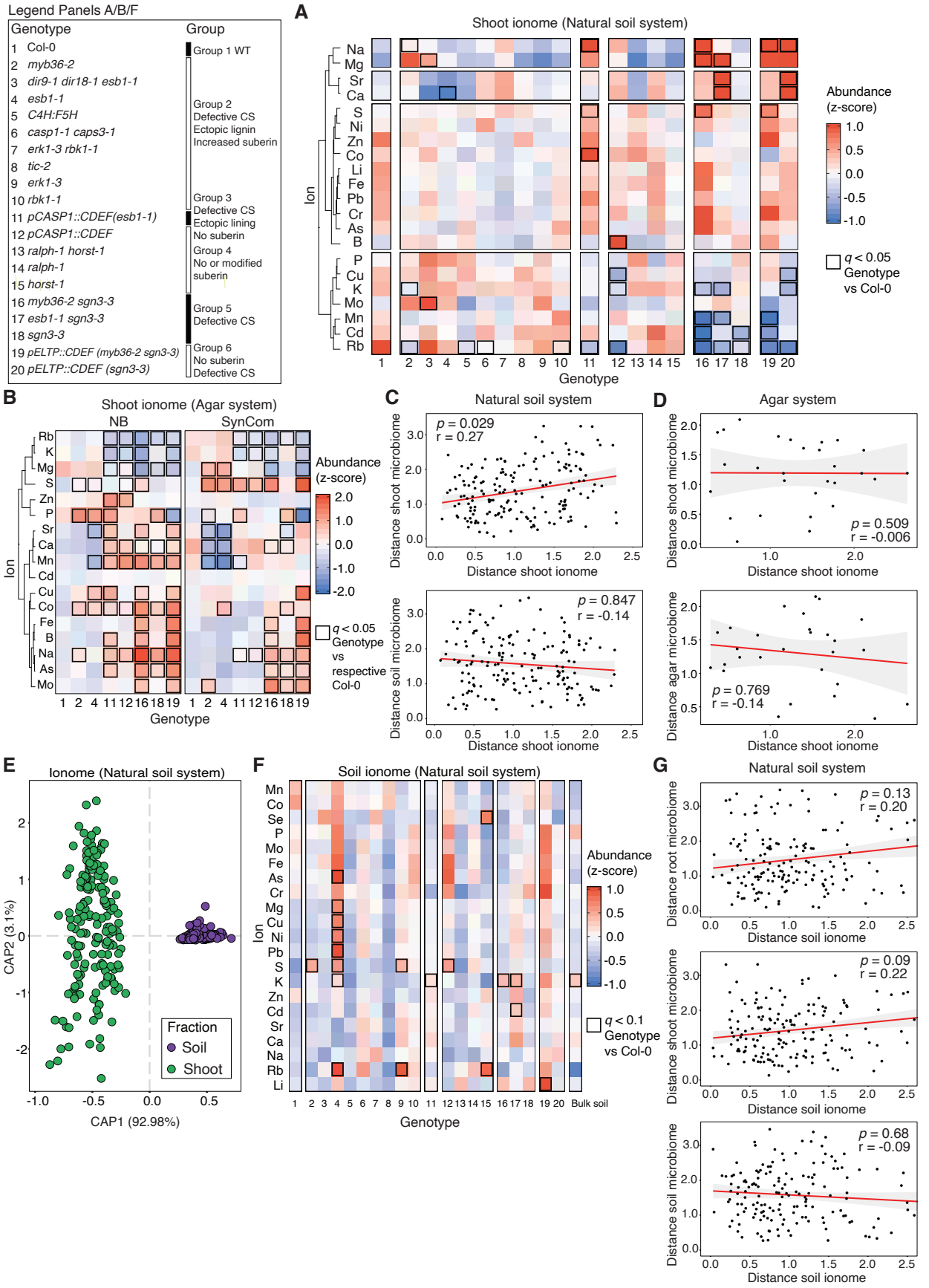
Legend Panels A/B/F
Genotype
Group
1 Col-0
2 myb36-2
3 dir9-1 dir18-1 esb1-1
4 esb1-1
5 C4H:F5H
6 casp1-1 caps3-1
7 erk1-3 rbk1-1
8 tic-2
9 erk1-3
10 rbk1-1
11 pCASP1::CDEF(esb1-1)
12 pCASP1::CDEF
13 ralph-1 horst-1
14 ralph-1
15 horst-1
16 myb36-2 sgn3-3
17 esb1-1 sgn3-3
18 sgn3-3
19 pELTP::CDEF (myb36-2 sgn3-3)
20 pELTP::CDEF (sgn3-3)
Group 1 WT
Group 2 Defective CS Ectopic lignin Increased suberin
Group 3 Defective CS Ectopic lining No suberin
Group 4 No or modified suberin
Group 5 Defective CS
Group 6 No suberin Defective CS
A
Shoot ionome (Natural soil system)
Ion
Genotype
Abundance (z-score)
q < 0.05 Genotype vs Col-0
B
Shoot ionome (Agar system)
NB
SynCom
Genotype
Abundance (z-score)
q < 0.05 Genotype vs respective Col-0
C
Natural soil system
Distance shoot microbiome
Distance shoot ionome
p = 0.029
r = 0.27
Distance soil microbiome
p = 0.847
r = -0.14
D
Agar system
p = 0.509
r = -0.006
Distance agar microbiome
p = 0.769
r = -0.14
E
Ionome (Natural soil system)
CAP1 (92.98%)
CAP2 (3.1%)
Fraction
Soil
Shoot
F
Soil ionome (Natural soil system)
Bulk soil
Genotype
Abundance (z-score)
q < 0.1 Genotype vs Col-0
G
Natural soil system
Distance root microbiome
Distance soil ionome
p = 0.13
r = 0.20
p = 0.09
r = 0.22
p = 0.68
r = -0.09

fig. S3. Root diffusion barrier regulatory network maintains mineral nutrients homeostasis in plant colonized by microbes.

A, B. Heatmap showing the standardized concentration (z-score) of each mineral nutrient in the plant shoot across the root diffusion barrier genotypes **A.** grown in a natural soil (Natural soil system), and **B.** on the agar plate system (Agar system). Genotypes are represented by numbers according to the legend at the beginning of the figure. Statistically significant enriched (red) and depleted (blue) mineral nutrient with respect to Col-0 are outlined in black ($q < 0.05$). **C.** Pairwise correlation analysis between the shoot ionome and the shoot and soil microbiome composition of root diffusion barrier genotypes grown in a natural soil (Natural soil system). **D.** Pairwise correlation analysis between the shoot ionome and the shoot and agar microbiome composition of root diffusion barrier genotypes grown on agar plates (Agar system). Panels C and D show the Mantel r statistic, and the *p*-value obtained from 10,000 permutations. **E.** Canonical analysis of principal coordinates (CAP) showing the projected ionomic profiles between the shoot and soil fractions from root diffusion barrier genotypes grown in a natural soil. **F.** Heatmap showing the standardized concentration (z-score) of each mineral nutrient (rows) in the soil across all plants genotypes (columns) grown in a natural soil. Genotypes are represented by numbers according to the legend at the beginning of the figure. Values that are statistically significant enriched (red) and depleted (blue) with respect to Col-0 are outlined in black ($q < 0.1$). **G**. Individual correlation analysis between the microbiome composition of the plant root, plant shoot and soil, and the soil elemental profiles in root diffusion barrier genotypes grown in a natural soil. Each panel shows the Mantel r statistic, and the corresponding *p*-value, obtained from 10,000 permutations.

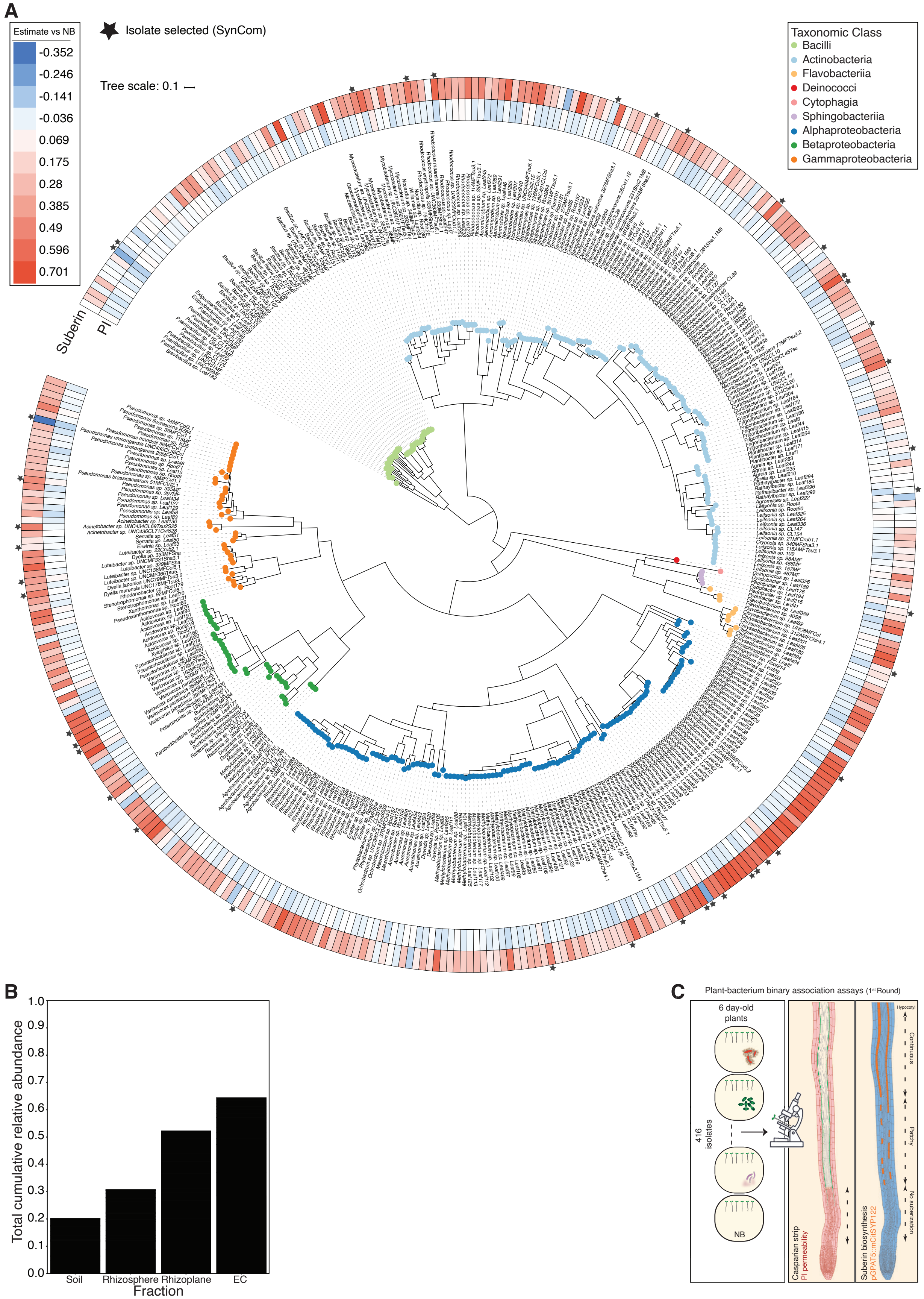
A
Estimate vs NB
-0.352
-0.246
-0.141
-0.036
0.069
0.175
0.28
0.385
0.49
0.596
0.701
Isolate selected (SynCom)
Tree scale: 0.1
Suberin
PI
Taxonomic Class
Bacilli
Actinobacteria
Flavobacteriia
Deinococci
Cytophagia
Sphingobacteriia
Alphaproteobacteria
Betaproteobacteria
Gammaproteobacteria
B
Total cumulative relative abundance
1.0
0.9
0.8
0.7
0.6
0.5
0.4
0.3
0.2
0.1
0.0
Soil
Rhizosphere
Rhizoplane
EC
Fraction
C
Plant-bacterium binary association assays (1st Round)
6 day-old plants
416 isolates
NB
Casparian strip
PI permeability
Suberin biosynthesis
pGPAT5::mCitSYP122
Hypocotyl
Continuous
Patchy
No suberization

fig. S4. Bacterial isolates collection approximates the taxonomy of natural communities and influences root barriers deposition.

A. Phylogenetic tree using the 397 bacterial genome sequences available for the 416-members bacteria collection used in this work. The tips of the tree are colored according to the bacterial taxonomic class. The inner and the outer rings shows the effect of each isolate on the Casparian strip function in a propidium iodide diffusion assay, and on the endodermal suberization (Sum of No suberization + Patchy zones) using the reporter line *pGPAT5::mCITRINE-SYP122*, respectively. The star represents the isolates that have been selected for further experiments either in binary association assays or in the synthetic community. **B.** The bar graph shows the total cumulative relative abundance at the family level of our isolates present in the different sample fractions (soil, rhizosphere, rhizoplane and endophytic compartment (EC)) defined in an ecological survey of natural Arabidopsis populations (*42*). Thus, the collection of 416 individual bacterial strains isolated from the roots and shoots of Arabidopsis grown in natural soils and use in this work (*12*, *13*), encompasses members of bacterial families that sum ~65% of the total relative abundance of all endophytic compartment samples obtained in this ecological survey of natural Arabidopsis populations across Europe (*42*). **C.** Schematic representation of the screening pipeline used to evaluate the effect of the bacterial isolates collection on the root diffusion barriers. See material and methods section for details.

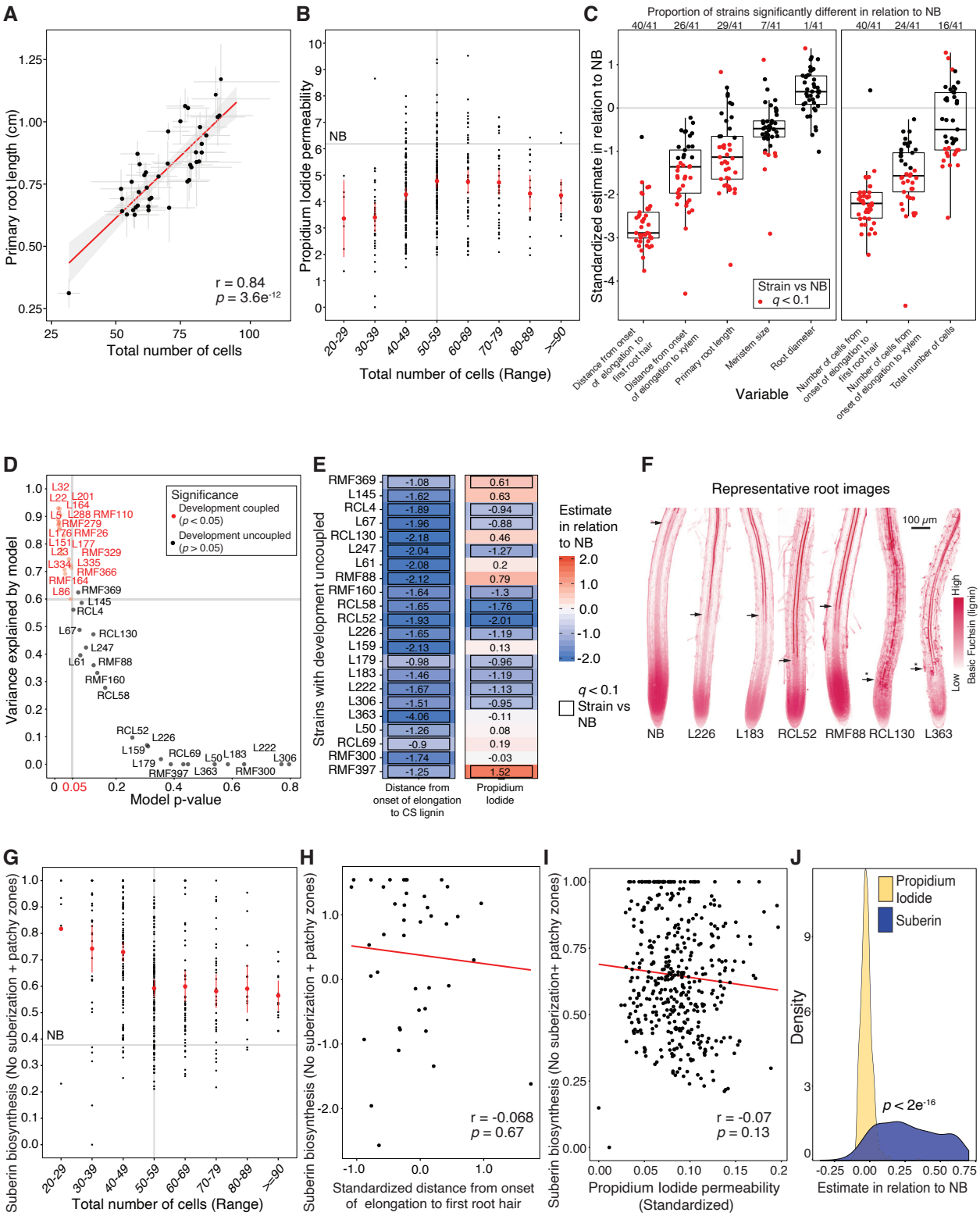
A
Primary root length (cm)
Total number of cells
r = 0.84
p = 3.6e-12
B
Propidium Iodide permeability
NB
Total number of cells (Range)
20-29
30-39
40-49
50-59
60-69
70-79
80-89
>=90
C
Proportion of strains significantly different in relation to NB
40/41
26/41
29/41
7/41
1/41
40/41
24/41
16/41
Standardized estimate in relation to NB
Strain vs NB
q < 0.1
Distance from onset of elongation to first root hair
Distance from onset of elongation to xylem
Primary root length
Meristem size
Root diameter
Number of cells from onset of elongation to first root hair
Number of cells from onset of elongation to xylem
Total number of cells
Variable
D
Variance explained by model
Model p-value
Significance
Development coupled (p < 0.05)
Development uncoupled (p > 0.05)
L32
L22
L201
L164
L5
L288
RMF110
RMF279
L176
RMF26
L151
L177
L23
RMF329
L334
L335
RMF366
RMF164
L86
RMF369
L145
RCL4
L67
RCL130
L247
L61
RMF88
RMF160
RCL58
RCL52
L226
L159
RCL69
L50
L183
L222
L306
L179
RMF397
L363
RMF300
E
Strains with development uncoupled
Distance from onset of elongation to CS lignin
Propidium Iodide
RMF369 -1.08 0.61
L145 -1.62 0.63
RCL4 -1.89 -0.94
L67 -1.96 -0.88
RCL130 -2.18 0.46
L247 -2.04 -1.27
L61 -2.08 0.2
RMF88 -2.12 0.79
RMF160 -1.64 -1.3
RCL58 -1.65 -1.76
RCL52 -1.93 -2.01
L226 -1.65 -1.19
L159 -2.13 0.13
L179 -0.98 -0.96
L183 -1.46 -1.19
L222 -1.67 -1.13
L306 -1.51 -0.95
L363 -4.06 -0.11
L50 -1.26 0.08
RCL69 -0.9 0.19
RMF300 -1.74 -0.03
RMF397 -1.25 1.52
F
Representative root images
Estimate in relation to NB
2.0
1.0
0.0
-1.0
-2.0
q < 0.1 Strain vs NB
100 μm
High
Low
Basic Fuchsin (lignin)
NB
L226
L183
RCL52
RMF88
RCL130
L363
G
Suberin biosynthesis (No suberization + patchy zones)
NB
Total number of cells (Range)
H
Suberin biosynthesis (No suberization + patchy zones)
r = -0.068
p = 0.67
Standardized distance from onset of elongation to first root hair
I
Suberin biosynthesis (No suberization+ patchy zones)
r = -0.07
p = 0.13
Propidium Iodide permeability (Standardized)
J
Propidium Iodide
Suberin
Density
p < 2e-16
Estimate in relation to NB

fig. S5. Members of the root microbiome modify the root diffusion barriers formation. **A.** The total number of cells in the root highly correlates with the root length. Pearson correlation analysis between the root length and the total number of cells in the root of plants exposed to a representative selection of 41 individual bacterial isolates. The correlation coefficient r and its *p*-value are shown. In plants colonized by individual bacteria, the total number of cells in the root is a proxy for the root length. **B.** Individual bacteria effect on propidium iodide (PI) diffusion is not a mere consequence of an altered root growth. Analysis of the distribution of the PI diffusion values across the total number of cells in the root of plants exposed to a collection of 416 individual bacterial isolates. For the analysis, the total number of cells values were divided in ranges. In the graph, the central dots represent the estimated mean and the red vertical lines the 95% confidence interval. Grey horizontal and vertical lines are the no bacteria (NB) control average values. Notice that the PI diffusion follows a normal distribution across the root total number of cells. **C.** Analysis of root developmental parameters in plants exposed to a representative selection of 41 individual bacterial strains. Boxplots show the standardized effect of the different bacterial isolates in relation to plants grown axenically (NB) on root development. We analyzed markers of root development such as: distance from the onset of elongation to the first root hair, distance from the onset of elongation to the xylem, primary root length, meristem size, root diameter, number of cells from the onset of elongation to the first root hair, number of cells from the onset of elongation to the xylem, and the total number of cells in the root. Values in red are significantly different from the no bacteria control ($q < 0.1$). The number of bacteria that significantly change the individual parameters are at the top of the figure. Notice that the formation of the first root hair is the most responsive developmental marker to the presence of individual bacterial strains, showing the most cohesive behavior with the highest magnitude, thus it best integrates the bacterial effect on root development. **D.** Members of the root microbiome have the capacity to modify Casparian strips formation independently of the root development. To evaluate association between the Casparian strip formation and the root developmental program, we fitted a linear model. The linear model predicts if changes observed in the distance from the onset of elongation to the Casparian strip (dependent variable) are explained by the changes detected in the distance from the onset of elongation to the first root hair (independent variable) in plants colonized by the representative 41 individual bacteria. The scatterplot shows the relationship between the variance explained

(R2) and the *p*-value extracted from each fitted model for the individual bacterial isolates. Bacterial strains that showed a significant association ($p < 0.05$) between the two parameters analyzed were considered as development coupled (in red). Notice that 22 bacterial isolates (in black in the figure) have a specific effect on the Casparian strip formation that is uncoupled from the formation of the first root hair. **E.** Selection of the 22 individual bacterial isolates with a specific effect on Casparian strip formation (Development uncoupled from D.). The heatmap shows the standardized estimate distance from the onset of elongation to the formation of the Casparian strip, and the propidium iodide diffusion in plants exposed to these isolates in relation to plants grown axenically. **F.** Exemplary pictures of changes in Casparian strip formation induced by individual bacteria. Lignin was stained using Basic Fuchsin and visualized in a confocal microscopy. Arrows point the deposition of lignin in the Casparian strip at the endodermis. Stars means ectopic deposition of lignin in the root. **G**. Individual bacteria effect on endodermal suberization is not just a consequence of an altered root growth. Analysis of the distribution of the standardized expression of the suberization reporter *pGPAT5::mCITRINE-SYP122* across the total number of cells in the root in plant exposed to 416 individual bacterial isolates. For the analysis, we used the sum of the number of cells in the no suberization zone and the patchy zone, and the root total number of cells values were divided in ranges. In the graph, the central dots represent the estimated mean and the vertical lines the 95% confidence interval of it. Grey horizontal and vertical lines are the no bacteria (NB) control average values. Notice that the mean of the number of cells to the continuous suberization zone (sum of no suberized + patchy) decreases with the increase of the total number of cells in the root. This result demonstrates that premature suberization in plants colonized by individual bacteria is not always a consequence of root growth arrest. **H.** Suberin deposition is uncoupled from other bacterial effect on root development. Graph shows the Pearson correlation between the standardized distance from the onset of elongation to the first root hair, used as a marker of root development, and the expression of suberin marker line *pGPAT5::mCITRINE-SYP122* in the no suberization zone and the patchy zone (Suberin biosynthesis (No suberization+ Patchy Zones). The correlation coefficient r and its *p*-value are shown. Notice that the expression of the suberin reporter *pGPAT5::mCITRINE-SYP122* did not correlate with the standardized distance from the onset of elongation to the first root hair, used as a root development marker. **I.** Pearson correlation analysis between the bacterial effect on suberin biosynthesis and propidium iodide permeability. The correlation coefficient r and its *p*-value are shown. **J.** Quantification of the bacterial magnitude effect on propidium iodide diffusion and suberin synthesis. The graph shows the distribution of the calculated effect sizes for all strains versus no-bacteria control across the two variables analyzed. The difference (*p*-value) between the distributions was calculated using a Kolmogorov-Smirnov test.

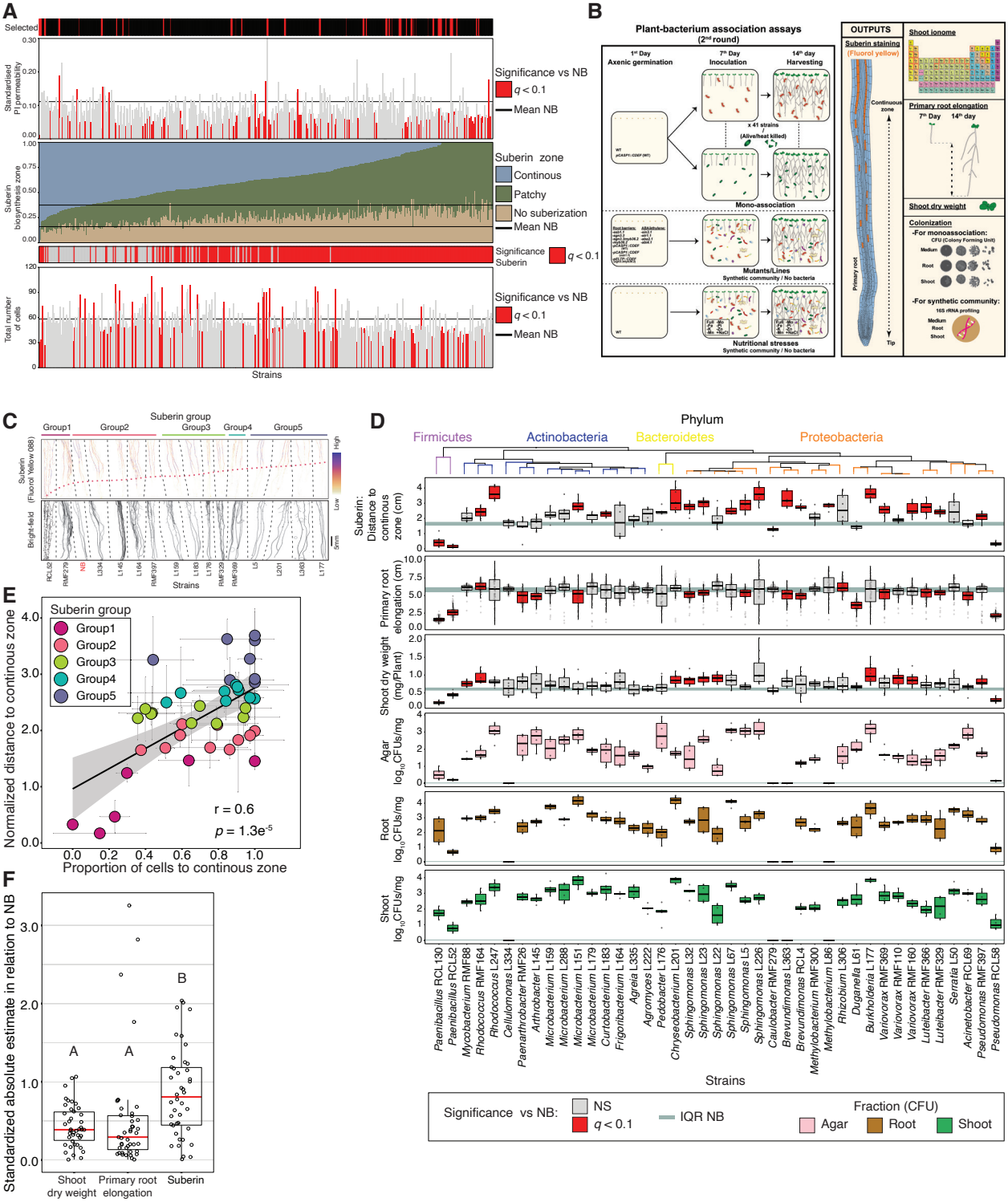
A
Selected
Standardised pairwise relatedness
Significance vs NB
q < 0.1
Mean NB
Suberin zone
Continous
Patchy
No suberization
Mean NB
Suberin biosynthesis zone
Significance Suberin
q < 0.1
Total number of cells
Significance vs NB
q < 0.1
Mean NB
Strains
B
Plant-bacterium association assays
(2nd round)
1st Day
Axenic germination
7th Day
Inoculation
14th day
Harvesting
x 41 strains
(Alive/heat killed)
Mono-association
Mutants/Lines
Synthetic community / No bacteria
Nutritional stresses
Synthetic community / No bacteria
OUTPUTS
Suberin staining
(Fluorol yellow)
Continuous zone
Primary root
Tip
Shoot ionome
Primary root elongation
7th Day
14th day
Shoot dry weight
Colonization
-For monoassociation:
CFU (Colony Forming Unit)
Medium
Root
Shoot
-For synthetic community:
16S rRNA profiling
Medium
Root
Shoot
C
Suberin group
Group1
Group2
Group3
Group4
Group5
Suberin (Fluorol Yellow 088)
High
Low
Bright-field
3mm
RCL58
RMF270
NB
L334
L145
L194
RMF397
L159
L180
L176
RMF329
RMF369
L5
L201
L363
L177
Strains
D
Phylum
Firmicutes
Actinobacteria
Bacteroidetes
Proteobacteria
Suberin: Distance to continous zone (cm)
Primary root elongation (cm)
Shoot dry weight (mg/Plant)
Agar log10CFUs/mg
Root log10CFUs/mg
Shoot log10CFUs/mg
Paenibacillus RCL130
Paenibacillus RCL52
Mycobacterium RMF88
Rhodococcus RMF164
Rhodococcus L247
Cellulomonas L334
Paenarthrobacter RMF26
Arthrobacter L145
Microbacterium L159
Microbacterium L288
Microbacterium L151
Microbacterium L179
Curtobacterium L183
Frigoribacterium L164
Agreia L335
Agromyces L222
Pedobacter L176
Chryseobacterium L201
Sphingomonas L32
Sphingomonas L23
Sphingomonas L22
Sphingomonas L67
Sphingomonas L5
Sphingomonas L226
Caulobacter RMF279
Brevundimonas L363
Brevundimonas RCL4
Methylobacterium RMF300
Methylobacterium L86
Rhizobium L306
Duganella L61
Burkholderia L177
Variovorax RMF369
Variovorax RMF110
Variovorax RMF160
Luteibacter RMF366
Luteibacter RMF329
Serratia L50
Acinetobacter RCL89
Pseudomonas RMF397
Pseudomonas RCL58
Strains
Significance vs NB:
NS
q < 0.1
IQR NB
Fraction (CFU)
Agar
Root
Shoot
E
Suberin group
Group1
Group2
Group3
Group4
Group5
Normalized distance to continous zone
Proportion of cells to continous zone
r = 0.6
p = 1.3e-5
F
Standardized absolute estimate in relation to NB
A
A
B
Shoot dry weight
Primary root elongation
Suberin

fig. S6. Bacterial isolates influence the suberin deposition in the endodermis.

A. Bar graphs representing bacterial isolates average effect on propidium iodide (PI) permeability, suberin biosynthesis, and the total number of cells in the root. (See Fig. 2A). The data is sorted according to the number of cells in the zone of continuous expression (in blue in the figure) from high to low values. The isolates that significantly modified ($q < 0.1$) the propidium iodide diffusion (PI permeability) are highlighted in red. The different zones of suberin deposition in the root are colored: No suberization in brown, patchy in green and the continuous zone in blue. For the suberin biosynthesis this information is in the bottom bar (Significance Suberin). A selection of 41 bacterial isolates, that covers the variability found in the root diffusion barrier phenotypes, and the taxonomy diversity found in the strain collection (fig. S4A), is shown in red in the bar on the top of the panel (Selected, see Fig. 2A and 2B). **B.** Schematic representation of the pipeline used to define the bacterial mechanism controlling the coordination between endodermal suberization and mineral nutrient accumulation in the plant. See material and methods section. **C**. The panel shows the effect of bacterial strains on suberin accumulation. The red dotted line highlights the initiation of the continuous zone of suberization. Notice that the distance from the root tip to the continuously suberized zone is inversely proportional to the amount of suberin in the endodermis. The panel on the bottom shows the root systems from the same plants (Bright-field). Groups match Fig. 2C. **D.** Boxplots representing the plant phenotypes analyzed in response to the individual 41 bacterial strains (3 top panels), and bacterial colonization (3 bottom panels). Each plant phenotype, endodermal suberization (suberin (distance to continuous zone)), the elongation of the primary root (primary root elongation), and shoot dry weight (shoot dry weight) was compared with its corresponding phenotype in plants grown axenically. Values in red are statistically different ($q < 0.1$) from the axenic control while values in grey are not. The horizontal grey strips represent the phenotypic values in axenic plants. The colonization capacity of the individual isolates was determined in three fractions, agar (CFU agar), root (CFU root) and plant shoot (CFU shoot) using log-transformed-colony forming units. All data are sorted in the figure according to the bacterial phylogenetic tree on the top. **E.** Pearson correlation analysis between the quantification of endodermal suberization using Fluorol Yellow in 14-day-old plants (normalized distance to continuous zone), and the suberin estimation using the suberin biosynthetic marker *GPAT5* (Proportion of cells to continuous zone) in 6-day-old plants, which have no secondary growth in the root,

exposed to the 41 bacterial strains. The strong correlation observed between both quantifications excludes the impact of suberin from the periderm in our experiment. The correlation coefficient r and its associated *p*-value are also in the figure. Different colors represent the groups of bacteria defined in Fig. 2C. **F.** We analyzed whether the bacterial effect on suberization could be explained by an indirect effect on plant development (*65*). We determined the elongation of the primary root and the shoot dry weight of plants inoculated with the selected bacteria (Panel D), and we quantified the magnitude of the bacterial effect on these phenotypes, as compared with the effect on suberin deposition. Boxplots show the standardized absolute values of the effect sizes distribution (Absolute estimate against NB) for each plant phenotype analyzed in D. We found a large effect size for suberization, which was different from the effect size found in these developmental parameters. Therefore, we conclude that effects on plant development are not sufficient to explain the extensive effect of individual bacteria on endodermal suberization. We compared the distribution of estimates among the three developmental parameters using an ANOVA model, compact letters display of a post-hoc Tukey test are displayed over each boxplot.

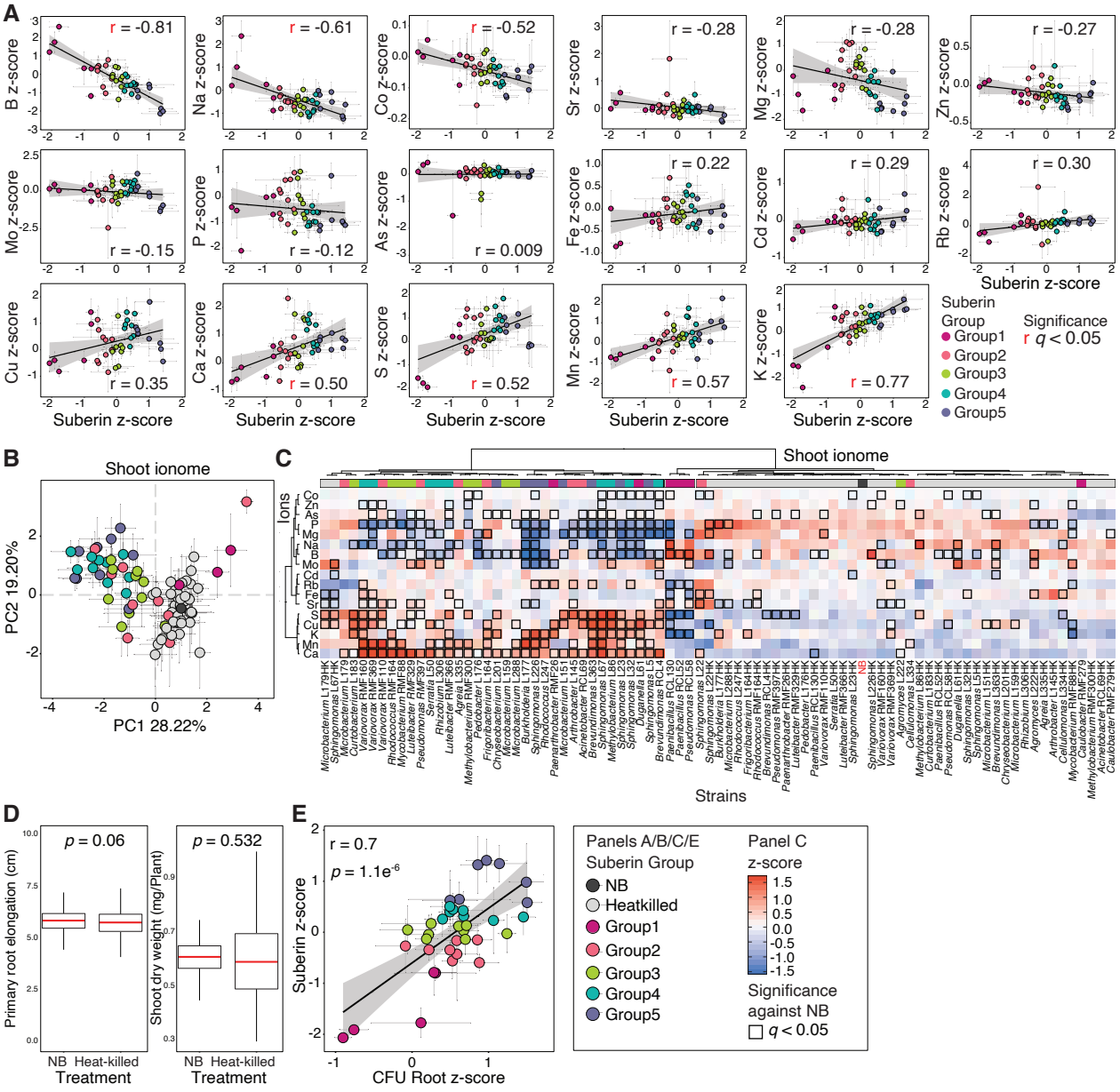

fig. S7. Bacterial isolates influence the shoot ionome.

A. Pearson correlation analysis between the individual mineral nutrient concentrations and the endodermal suberization. The correlation coefficient r is colored according to *q*-value. Colors in the figure match bacterial groups defined in Fig. 2C. **B.** Principal component analysis (PCA) of mineral nutrient composition showing the ionomic projection of individual bacterial isolates, heat-killed controls and no bacteria control (NB). Each bacterium or control (points) in the scatter-plot represents the average distribution of values across the two axes. Colors represent the groups of bacteria defined in Fig. 2C. **C.** Heatmap analysis showing the standardized mineral nutrient concentrations in shoots of plant inoculated with the 41 individual bacterial strains

with the heat-killed controls or grown axenically (NB). The values have been clustered according to the bacterial treatment and mineral nutrient concentration. Values that are statistically significant different from the no bacteria control (q-value < 0.05) are outlined in black. Colors in the bar on the top match the groups in the PCA analysis and correspond to the suberin groups defined in Fig. 2C. Notice that we use the heat-killed controls in B and C to exclude that the differences observed in the shoot ionome in response to our bacterial selection were an indirect effect caused by the presence of the bacterial-derived ionome in the leaves. Plants were grown in the presence of a 100x time more concentrated heat-killed bacterial cultures and the elemental profiles of these plants were determined. Panels B and C show that the ionome of the heat-killed bacterial controls were similar to the no bacteria control, and that both were significantly different from the ionomic profiles of plants inoculated with individual live bacterial strains. **D.** Boxplots showing the values distribution within the two plant phenotypes analyzed, primary root elongation (Primary root elongation (cm)), and shoot dry weight (Shoot dry weight (mg/Plant)), between the no bacterial control (NB) and the heat-killed control (Heatkilled). The differences between the two distributions was calculated using a *t*-test, the *p*-value is shown in the figure. This panel shows that the heat-killed strains have no significant effect on primary root elongation or plant shoot dry weight. Therefore, these results rule out the possibility that the differences found in the ionomic phenotypes were caused by an indirect fertilization effect of addition of the bacterial cultures (panels B and C), or that some heat-resistant Microbe-Associated Molecular Patterns (MAMPs) detected by the plant immune system influenced plant development (Panel D). **E.** Pearson correlation analysis between the suberin deposition (Suberin) and bacterial colonization of the root (CFU Root). The correlation coefficient r and its associated *p*-value are also in the figure. Different colors represent the groups of bacteria defined in Fig. 2C.

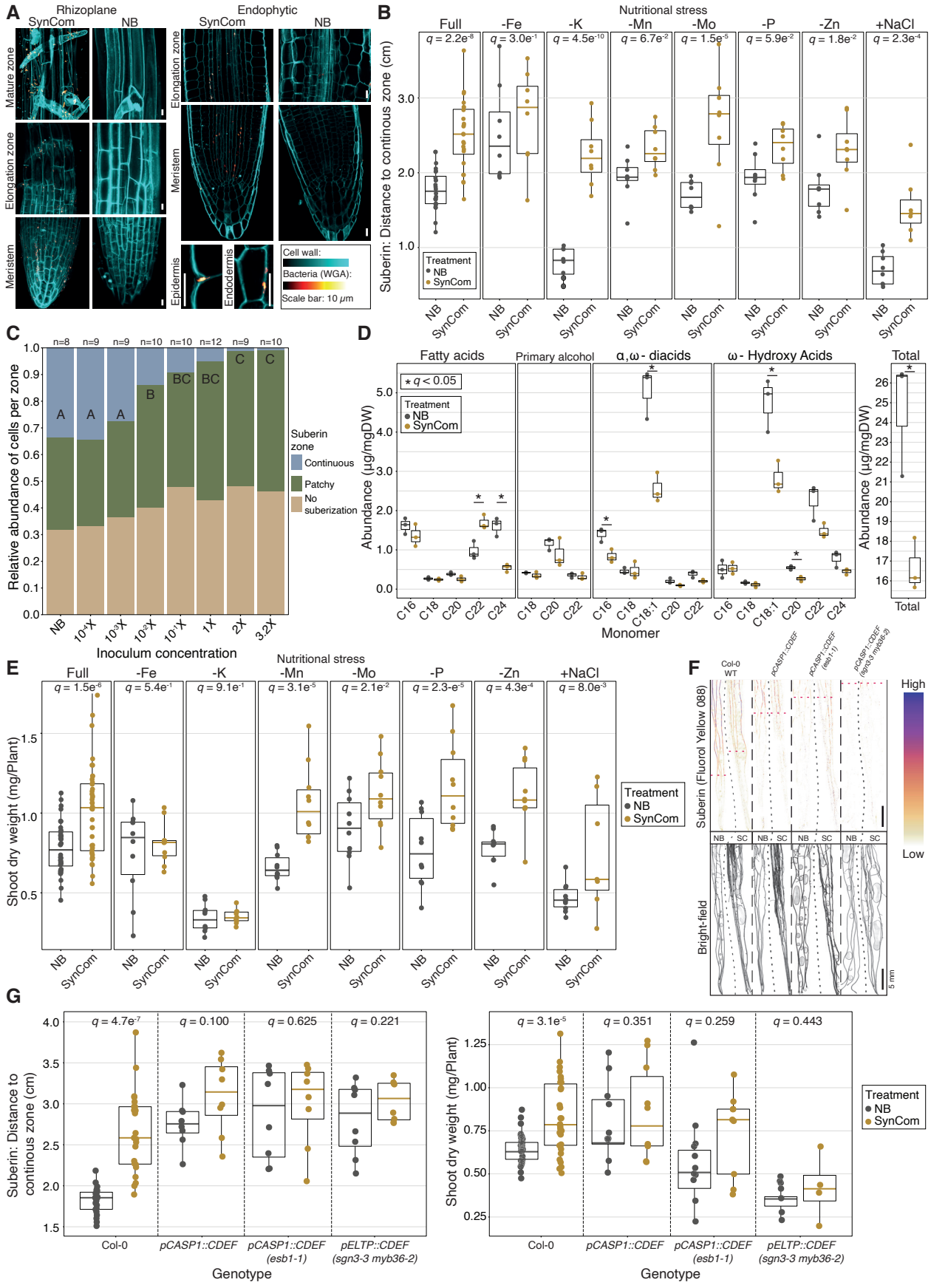
A
Rhizoplane
SynCom
NB
Endophytic
SynCom
NB
Mature zone
Elongation zone
Meristem
Epidermis
Endodermis
Cell wall:
Bacteria (WGA):
Scale bar: 10 μm
B
Nutritional stress
Full
-Fe
-K
-Mn
-Mo
-P
-Zn
+NaCl
Suberin: Distance to continous zone (cm)
Treatment
NB
SynCom
C
Relative abundance of cells per zone
Suberin zone
Continuous
Patchy
No suberization
Inoculum concentration
D
Fatty acids
Primary alcohol
α,ω - diacids
ω - Hydroxy Acids
Total
Abundance (μg/mgDW)
Monomer
E
Nutritional stress
Shoot dry weight (mg/Plant)
F
Col-0 WT
pCASP1::CDEF
pCASP1::CDEF (esb1-1)
pCASP1::CDEF (sgn3-3 myb36-2)
Suberin (Fluorol Yellow 088)
Bright-field
High
Low
5 mm
G
Suberin: Distance to continous zone (cm)
Shoot dry weight (mg/Plant)
Col-0
pCASP1::CDEF
pCASP1::CDEF (esb1-1)
pELTP::CDEF (sgn3-3 myb36-2)
Genotype

fig. S8. Bacterial buffering effect on endodermal suberization benefits plant adaptation to nutrient stresses.

A. The bacterial synthetic community colonized the rhizoplane and the endophytic compartment of the root. (left) Pictures showing the colonization of the rhizoplane by the bacterial synthetic community across the different root zones: meristematic (meristem), elongation and differentiation zone (mature zone). (Right) Pictures showing the presence of bacteria in the endophytic compartment across the different tissue layers in the meristematic and elongation zones of the root. (right, bottom) Details of bacteria colonization in the root epidermis and endodermis. Bacteria were detected using Wheat Germ Agglutinin-Alexa Fluor (WGA). **B.** Boxplots representing the distances from the root tip to the continuous zone of suberization (Suberin: distance to the continuous zone (cm)) in plants inoculated (SC) or not (NB) with the bacterial synthetic community and grown across the different nutrient stresses (identified on the top of the panel). Within stresses the synthetic community treatment was compared against plants grown axenically, the *q*-value of this comparison is in each panel. **C.** Bar-graphs showing the averaged suberization patterns in wild-type Col-0 plants inoculated with different concentrations of the 41-members bacterial synthetic community. The no suberization, patchy and continuous suberization zones are colored in brown, green, and blue respectively. The number of plants analyzed per treatment is on the top of the figure. Letters correspond to a Tukey post-hoc test. **D.** Boxplots showing the normalized amount (mg/mgDW) of suberin constitutive monomers (Fatty acids, Primary alcohol, a,ω-diacids, ω-Hydroxy acids) and the total suberin (Total, far right) found in wild-type plants exposed (SynCom, in brown in the figure) or not (NB, in grey in the figure) to the bacterial synthetic community and grown in full nutrient conditions. Star represent values that are significantly different between SynCom and NB treatments in each case ($q < 0.05$). This panel shows that bacterial-inoculated plants grown in full nutrient conditions showed a strong reduction in predominant suberin monomers and in the total amount of suberin when compared to plants grown axenically. **E.** Boxplots representing the normalized rosette dry weight (Shoot dry weight (mg/Plant)) of plants inoculated (SC) or not (NB) with the bacterial synthetic community and grown across the different nutrient stresses (identified on the top of the figure). Within stresses each synthetic community treatment was compared against plants grown axenically, the *q*-value of this comparison is in each panel. **F.** Figure shows the suberin deposition in the endodermis of plants grown in axenic conditions (NB)

or inoculated with the bacterial synthetic community (SC). Endodermal suberization pattern was analyzed in wild-type and in lines (*pCASP1::CDEF1*, *pCASP1::CDEF1(esb1-1)* and *pELTP::CDEF1(myb36-2 sgn3-3*)) which lack the ability to accumulate endodermal suberin due to the expression of cuticle destructing factor1 (CDEF1) (*16*) in the endodermis of wild-type plants and two different genetic backgrounds, *esb1-1*, and the double mutant *myb36-2 sgn3-3* with defective Casparian strip (*3*, *7*). Suberin was stained using Fluorol Yellow 088. The red line represents the initiation point of the continuous zone of suberization. The bottom panel shows images of the root systems from the same plants (Bright-field). Plants were grown under sufficient nutrient conditions to avoid any interference from nutrient starvation responses. **G.** (left) Results from the quantification of the distance from the root tip to the continuous zone of suberization (Suberin: Distance to continuous zone (cm)), and (right) the normalized rosette dry weight (Shoot dry weight (mg/Plant)) in the lines described in E exposed (SynCom) or not (NB) to the bacterial synthetic community. Within genotypes each synthetic community treatment value was compared against the plants grown axenically, the *q*-value of this comparison is in each panel. Notice that the suberin-deficient line (expressing CDEF) abolished the synthetic community effect on suberin deposition together with the beneficial effect on plant growth (Panels E and F). These results revealed that suberin is an important factor for the beneficial bacterial effect in response to nutrient stresses.

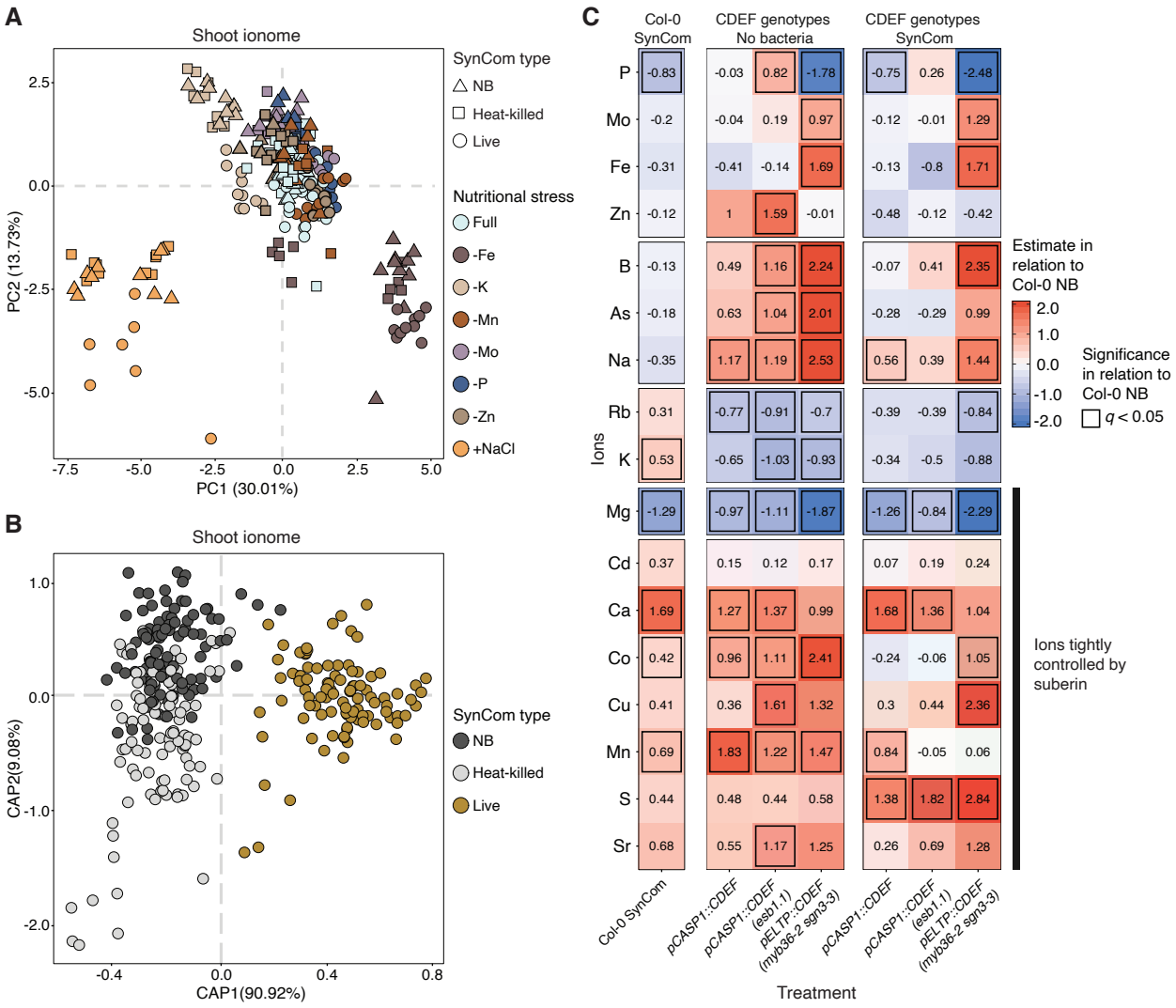

fig. S9. Microbial effect on endodermal suberization regulates mineral nutrient homeostasis in the plant in response to nutrient scarcities.

A. Principal component analysis (PCA) of the shoot ionomic projection of wild-type plants inoculated with the bacterial synthetic community (SynCom) (Live, circle), the heat-killed (HK, square) synthetic community or the no bacteria control (NB, triangle), and grown across different nutrient stresses (designated with different colors in the figure). **B.** Canonical analysis of principal coordinates (CAP) showing the shoot ionomic projection of each bacterial treatment: bacterial synthetic community (SynCom), Heat-killed bacterial synthetic community (Heat-killed) and no bacteria control (NB) of wild-type plants grown on different nutrient stresses. **C.** A sector of the shoot ionome is controlled by endodermal suberization. Heatmap showing the standardized mineral nutrient concentrations in wild-type plant inoculated with the bacterial synthetic community

(Col-0 SynCom), in Arabidopsis lines (*pCASP1::CDEF1*, *pCASP1::CDEF1(esb1-1)* and *pELTP::CDEF1(myb36-2 sgn3-3*)) which lack the ability to accumulate endodermal suberin due to the expression of cuticle destructing factor1 (CDEF1) (*16*) grown in axenic conditions (CDEF genotypes No bacteria) or inoculated with the bacterial synthetic community (CDEF genotypes SynCom). Significant ($q < 0.05$) values in relation to Col-0 NB treatment are outlined in black. Mineral nutrients controlled by endodermal suberization are named in the figure as “Ions tightly controlled by suberin”.

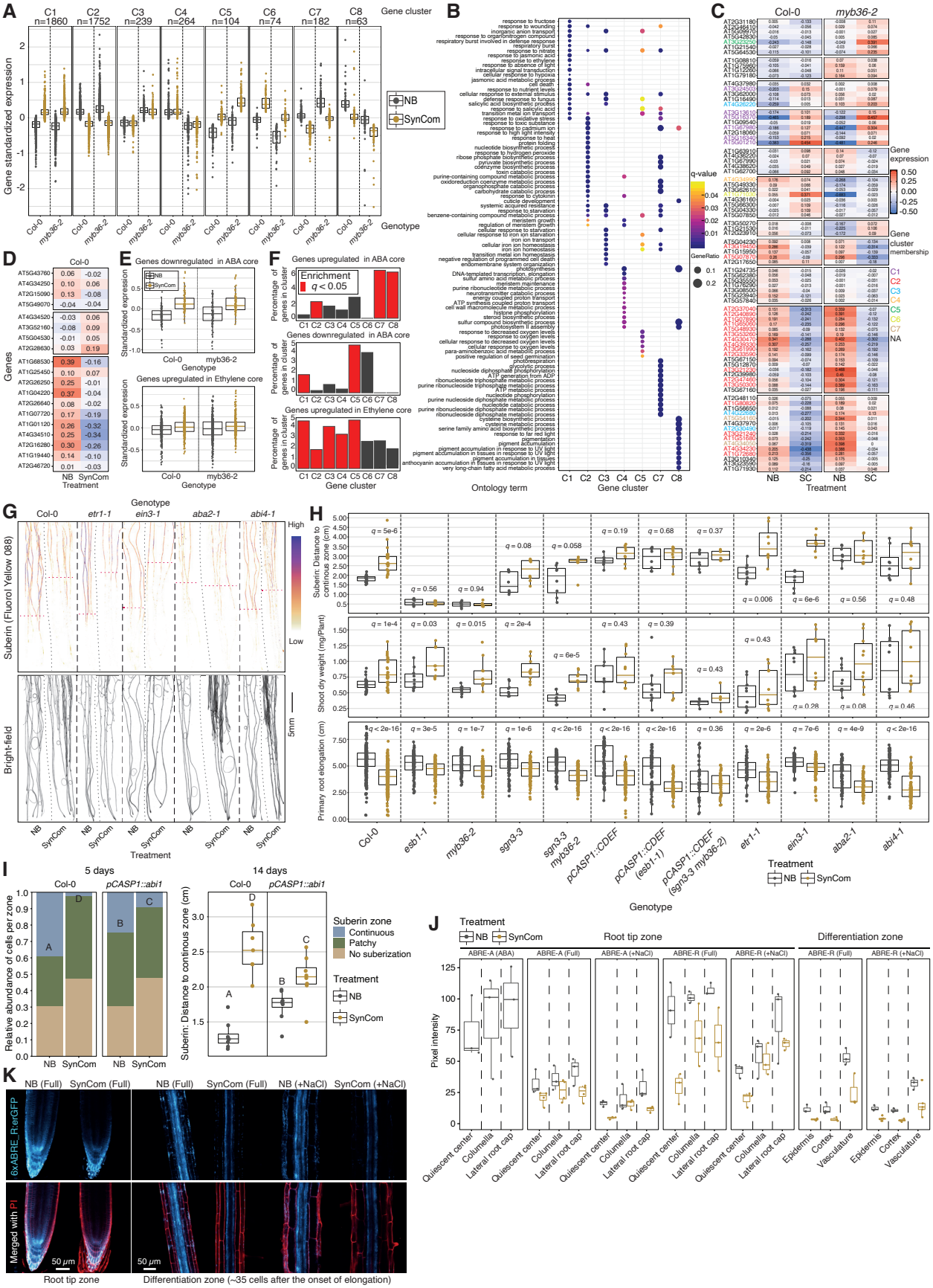
A
C1 n=1860
C2 n=1752
C3 n=239
C4 n=264
C5 n=104
C6 n=74
C7 n=182
C8 n=63
Gene cluster
Gene standardized expression
NB
SynCom
Col-0
myb36-2
Genotype
B
Ontology term
q-value
GeneRatio
Gene cluster
C
Col-0
myb36-2
Gene expression
Gene cluster membership
NB
SC
Treatment
D
Col-0
Genes
NB
SynCom
Treatment
E
Genes downregulated in ABA core
Genes upregulated in Ethylene core
Standardized expression
Genotype
F
Genes upregulated in ABA core
Enrichment
q < 0.05
Genes downregulated in ABA core
Genes upregulated in Ethylene core
Percentage of genes in cluster
Gene cluster
G
Genotype
Col-0
etr1-1
ein3-1
aba2-1
abi4-1
Suberin (Fluorol Yellow 088)
Bright-field
High
Low
5mm
Treatment
H
Suberin: Distance to continous zone (cm)
Shoot dry weight (mg/Plant)
Primary root elongation (cm)
Col-0
esb1-1
myb36-2
sgn3-3
sgn3-3 myb36-2
pCASP1::CDEF
pCASP1::CDEF (esb1-1)
pCASP1::CDEF (sgn3-3 myb36-2)
etr1-1
ein3-1
aba2-1
abi4-1
Genotype
Treatment
NB
SynCom
I
5 days
14 days
Col-0
pCASP1::abi1
Relative abundance of cells per zone
Suberin: Distance to continous zone (cm)
Suberin zone
Continuous
Patchy
No suberization
Treatment
NB
SynCom
J
Treatment
NB
SynCom
Root tip zone
Differentiation zone
ABRE-A (ABA)
ABRE-A (Full)
ABRE-A (+NaCl)
ABRE-R (Full)
ABRE-R (+NaCl)
Pixel intensity
Quiescent center
Columella
Lateral root cap
Epidermis
Cortex
Vasculature
K
NB (Full)
SynCom (Full)
NB (+NaCl)
SynCom (+NaCl)
6xABRE_R:erGFP
Merged with PI
50 μm
Root tip zone
Differentiation zone (~35 cells after the onset of elongation)

fig. S10. Microbiome effect on suberization is a new branch of the endodermal suberization regulatory network.

A. Boxplots showing the standardized expression of the genes identified in the RNA-Seq experiment across the clusters defined in this study. The number of genes per cluster (n) is at the top of each panel. **B.** The top 15 ranked gene ontology terms according to gene count contained in the different gene clusters (Fig. 4A). The color of each point represents the *p*-value adjusted using the Benjamin-Hochberg procedure, and the size of each point denotes the percentage of total differential expressed genes in the given gene ontology term (Gene Ratio). **C.** Heatmap showing the expression of genes and transcription factors involved in the phenylpropanoid synthesis, across the different genotypes (Col-0 and *myb36-2*) and treatments (uninoculated (NB) or inoculated (SC) plants) used in the RNA-Seq experiments. Different names colors represent clusters membership. **D.** Heatmap showing the expression of 19 *3-Ketoacyl-Coenzyme A Synthases (KCS)* genes involved in the fatty acid elongation, in wild-type Col-0 plants grown in axenic conditions (NB) or inoculated with the bacterial synthetic community (SC). **E.** Due to the fact that plant hormones ABA (positively) and ethylene (negatively) affect endodermal suberization (*5*), we explored the expression of two literature-based cores of 370 and 375 ABA and ethylene response transcriptional markers, respectively (*26*, *27*) across the RNA-Seq gene clusters. Boxplots displaying the standardized expression of the literature-based core genes related with ABA and ethylene (*26*, *27*) in the RNA-Seq. **F.** Bar graphs showing the percentage of the literature-based ABA- and ethylene-core genes (*26*, *27*) present in the different clusters defined in Figure 4A. Red bars mean that the cores genes are enriched in this cluster (Hypergeometric test $q < 0.05$). **G.** Endodermal suberization in Col-0, the ethylene mutants *etr1-1* and *ein3-1*, and the ABA mutants *aba2-1* and *abi4-1*, exposed (SC) or not (NB) to the synthetic community. The red line represents the initiation of the continuous zone of suberization. The bottom panel shows the root systems from the same plants (Bright-field). **H.** Boxplots representing the distances from the root tip to the continuous zone of suberization (Suberin: Distance to the continuous zone (cm)), dry weight (Shoot dry weight (mg/Plant)), and primary root elongation (Primary root elongation (cm)), in wild-type plants (Col-0), a collection of root diffusion barrier mutants and lines, and ABA and ethylene mutants inoculated (SynCom) or not (NB) with the bacterial synthetic community. Within genotypes each synthetic community treatment was compared against plants grown axenically,

the *q*-value of this comparison is in each panel. **I.** Bar-graph showing the suberization pattern in wild-type plants Col-0 or the line *pCASP1::abi1-1*, impaired in endodermal ABA signaling (*5*) grown in axenic conditions (NB) or with the bacterial synthetic community (SynCom). Plants were either direct germinated in the presence of the bacterial synthetic community for 5 days (left panel; 5 days) or germinated in axenic conditions for a week and then transferred to agar plates inoculated with the synthetic community for another 7 days (right panel; 14 days). In both cases suberin was stained using Fluorol Yellow 088. **J.** The bacterial synthetic community interferes with the ABA signaling. Quantification of pixel intensity as a proxy for GFP expression in pictures of the *6xABRE_A::erGFP* and *6xABRE_R::erGFP* reporter lines (*22*) grown in standard MS plates (Full) or MS plates supplemented with 1 μM ABA (ABA) or 100 mM NaCl (+NaCl) in axenic conditions (NB) or in the presence of the bacterial synthetic community (SynCom). The boxplots show the pixel intensity (GFP signal) in two root zones, the root tip and the differentiation zone (~35 cells after the onset of elongation). In the root tip the analysis included the quiescent center, the columella, and the lateral root cap. In the differentiated zone pixels were quantified in the epidermis, the cortex and the vascular tissue. The different tissues were identified using propidium iodide staining. **K.** Exemplary pictures of the GFP expression in the *6xABRE_R::erGFP* reporter line grown in standard MS plates (Full) or MS plates supplemented with 100 mM NaCl (+NaCl) in axenic conditions (NB) or in the presence of the bacterial synthetic community (SynCom). Left panel shows the root tip and the right panel the differentiation zone.

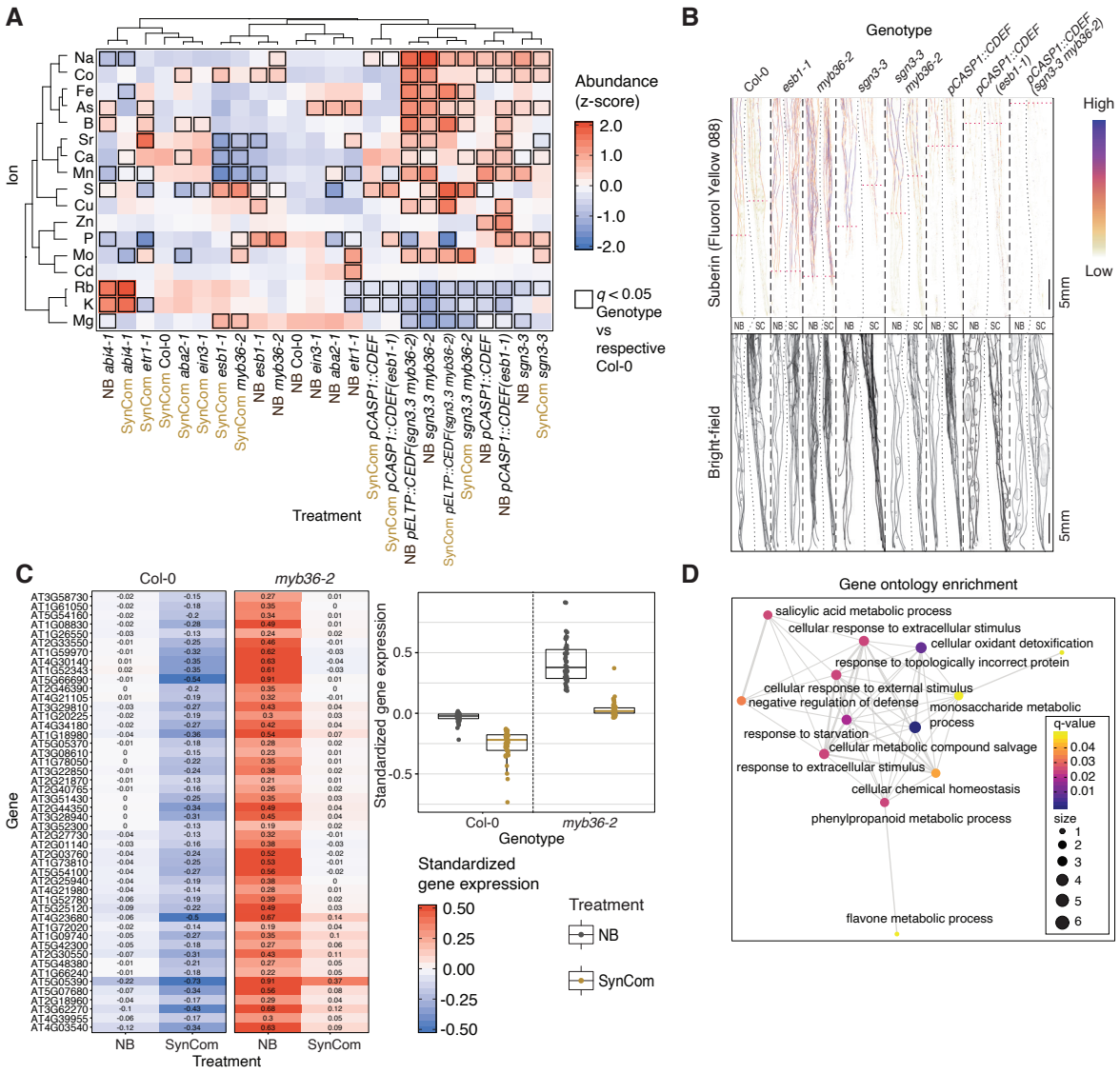

fig. S11. The Schengen pathway exerts an epistatic effect on the microbiome branch of suberization.

A. Heatmap showing the average standardized mineral nutrient concentrations in shoots of wild-type plants, a collection of root diffusion barrier mutants and lines, and ABA and ethylene mutants inoculated with the bacterial synthetic community (SynCom), or grown axenically (NB). The values have been clustered according to the bacterial treatment and mineral nutrient concentrations. Values that are statistically significant different from its respective Col-0 control (NB Col-0 for NB samples and SynCom Col-0 for SynCom samples) (q-value < 0.05) are outlined in black.

B. Figure shows the endodermal suberization in wild-type plants (Col-0), root diffusion barrier

mutants (*esb1-1*, *myb36-2*, *sgn3-3*, *sgn3-3 myb36-2*), and the lines (*pCASP1::CDEF1*, *pCASP1::CDEF1(esb1-1)* and *pELTP::CDEF1(myb36-2 sgn3-3)* inoculated (SC) or not (NB) with the synthetic community (SC). Suberin was stained using Fluorol Yellow 088. The red line highlights the initiation point of the continuous zone of suberization. The bottom panel shows images of the root systems from the same plants (Bright-field). **C.** (left) Heatmap showing the expression of the 48 genes repressed by the microbiome pathway and recovered after the *Schengen* pathway activation in *myb36-2*. (right) Boxplots showing the standardized expression of the 48 genes repressed by the microbiome pathway and recovered after the *Schengen* pathway activation in *myb36-2*. **D.** Network of statistically significant gene ontology terms contained in the 48 genes repressed by the microbiome pathway and recovered after the *Schengen* pathway activation in *myb36-2*. The network was computed using the emapplot function from the package clusterProfiler in R. The color of each point represents the *p*-value adjusted using the Benjamin-Hochberg procedure, and the size of each point denotes the number of genes mapped in that particular term (Size).

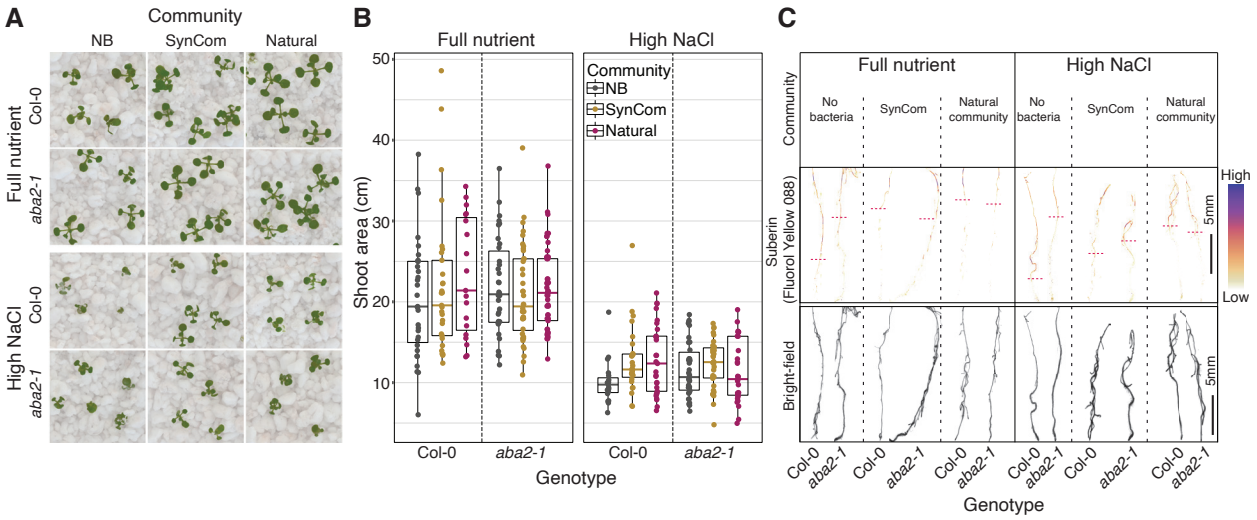

fig. S12. Bacterial synthetic community effect on suberization is robust to the larger compositional variation observed in natural microbial communities.

A. Wild-type plants (Col-0), and the ABA mutant *aba2-1*, inoculated with the bacterial synthetic community (SynCom), a natural community or grown in axenic conditions (NB) with full nutrient or 70 mM NaCl in the perlite system. **B.** Boxplots representing the shoot area determined in plants from A. Plants were inoculated with the bacterial synthetic community (SynCom), a natural community or grown in axenic conditions (NB). **C.** Endodermal suberization in Col-0, and *aba2-1*, inoculated with the synthetic community, a natural community, or grown axenically (NB) in the perlite system under full nutrient conditions or 70 mM NaCl. Suberin was stained using Fluorol Yellow 088. The red line represents the initiation of the continuous zone of suberization. The bottom panel shows the root systems from the same plants (Bright-field).

Tables

table S1. Root diffusion barrier mutants and lines used in this work. See also Materials and Methods section.

Order	Mutants	Mutant ID	Provider	Reference
1	*esb1-1*		1	(*62*)
2	*myb36-2*	GK-543B11	1	(*18*)
3	*sgn3-3*	SALK_043282	2	(*63*)
4	*myb36-2 sgn3-3*		1	(*44*)
5	*casp1-1 casp3-1*	SAIL_265_H05/SALK_011092	2	(*61*)
6	*erk1-3*	SALK_060966	3	(*66*)
7	*rbk1-1*	SALK_043441	3	(*66*)
8	*erk1-3 rbk1-1*		3	(*66*)
9	*tic-2*	SAIL_753_E03	3	(*67*)
10	*dir9-1 dir18-1 esb1-1*	GABI_323A02/SALK_115430	1	
11	*esb1-1 sgn3-3*		1	(*25*)
12	*ralph-1*	SM.37066	4	(*68*)
13	*horst-1*	SALK_107454	4	(*68*)
14	*ralph-1 horst-1*		4	(*68*)
Order	**Lines**	**ID**	**Provider**	**Reference**
1	*C4H::F5H*		4	(*69*)
2	*pCASP1::CDEF1(wild-type)*		2	(*16*)
3	*pCASP1::CDEF1(esb1-1)*		2	(*25*)
4	*pELTP::CDEF1(sgn3-3)*		1	
5	*pELTP::CDEF1(myb36-2 sgn3-3)*		1	(*44*)

Providers Legend:

1- Prof David Salt (University of Nottingham, UK)

2- Prof Niko Geldner (University of Lausanne, Switzerland)

3- Dr Jose Gutierrez-Marcos (University of Warwick, UK)

4- Dr Rochus Benni Franke (University of Bonn, Germany)

table S2. Table showing the minimum and maximum number of biological replicas per individual treatment (Min. # of biol. Replicas, Max. # of biol. Replicas), mean of biological replicas (Mean of biol. Replicas used), and the number of independent experiments performed to generate the different figure panels in this work. See also Materials and Methods section.

Figure Panel	Min. # of biol. replicas	Max. # of biol. replicas	Mean of biol. replicas used	Independent experiments	Figure Panel	Min. # of biol. replicas	Max. # of biol. replicas	Mean of biol. replicas used	Independent experiments
1A	4	12	10	2	S2H_Cortex	5	6	6	1
1B	7	20	11	2	S2H_DW	4	30	12	2
1C	5	12	10	2	S2H_PR	40	298	100	2
1D	4	30	11	2	S2I	4	30	9	2
2A_PI	3	12	5	1	S3A	5	12	10	2
2A_Suberin	9	27	16	1	S3B	4	30	12	2
2A_Cells	9	27	16	1	S3E	188	207	198	2
2C	6	72	10	2	S3F	1	13	10	2
2D	10	10	10	2	S4A	3	27	10	1
3B	8	24	10	2	S5A	8	34	16	1
3C	7	40	14	2	S5B	3	12	5	1
3D	7	30	13	2	S5C	5	14	6	1
4A	3	6	5	2	S5D	5	7	6	1
4B	3	6	5	2	S5E	5	7	6	1
4C	8	24	12	2	S5G	9	27	16	1
4E	5	10	8	2	S6A_PI	3	12	5	1
S10A	3	6	5	2	S6A_Sub	9	27	16	1
S10C	3	6	5	2	S6A_Cells	9	27	16	1
S10D	3	6	5	2	S6D_CFUAgar	6	6	6	2
S10E	3	6	5	2	S6D_CFURoot	6	6	6	2
S10H_DW	4	30	12	2	S6D_CFUShoot	6	6	6	2
S10H_PR	40	298	100	2	S6D_DW	10	10	10	2
S10H_Sub	8	24	10	2	S6D_PR	44	91	79	2
S10I_14days	7	8	8	2	S6D_Suberin	6	8	8	2
S10I_5days	11	12	12	1	S6E	6	8	8	1
S10J	3	5	4	1	S7B	9	10	10	2
S11A	4	30	12	2	S7C	9	10	10	2
S11C	3	6	5	2	S7D_DW	110	406	258	2
S12B	19	49	32	1	S7D_PR	858	3241	2050	2
S1B	4	8	6	2	S7E	6	8	7	2
S1C	73	189	148	2	S8B	8	24	10	2
S1D	1	12	8	2	S8C	8	12	10	1
S1E	4	12	10	2	S8D	3	3	3	1
S1F	1	8	4	2	S8E	7	40	14	2
S1G	4	12	10	2	S8G_DW	4	30	12	2
S2B	7	19	11	2	S8G_Suberin	8	24	10	2
S2C	9	19	11	2	S9A	7	30	13	2
S2D	7	20	11	2	S9B	7	30	13	2
S2E	3	3	3	1	S9C	4	30	14	2
S2G	6	6	6	2					

References

1. M. Barberon, N. Geldner, Radial transport of nutrients: the plant root as a polarized epithelium. *Plant Physiol.* **166**, 528–37 (2014).
2. J. M. Allaire, S. M. Crowley, H. T. Law, S. Y. Chang, H. J. Ko, B. A. Vallance, The Intestinal Epithelium: Central Coordinator of Mucosal Immunity. *Trends Immunol.* **39** (2018), pp. 677–696.
3. M. Coskun, Intestinal Epithelium in Inflammatory Bowel Disease. *Front. Med.* **1**, 24 (2014).
4. I. C. R. Barbosa, N. Rojas-Murcia, N. Geldner, The Casparian strip—one ring to bring cell biology to lignification? *Curr. Opin. Biotechnol.* **56** (2019), pp. 121–129.
5. M. Barberon, J. E. M. Vermeer, D. De Bellis, P. Wang, S. Naseer, T. G. Andersen, B. M. Humbel, C. Nawrath, J. Takano, D. E. Salt, N. Geldner, Adaptation of Root Function by Nutrient-Induced Plasticity of Endodermal Differentiation. *Cell*. **164**, 447–459 (2016).
6. V. G. Doblas, E. Smakowska-Luzan, S. Fujita, J. Alassimone, M. Barberon, M. Madalinski, Y. Belkhadir, N. Geldner, Root diffusion barrier control by a vasculature-derived peptide binding to the SGN3 receptor. *Science (80-.).* **355**, 280–284 (2017).
7. A. Feng Zhou, P. Marhavy, D. Wu, T. Lahaye, N. Geldner Correspondence, F. Zhou, A. lia Emonet, V. rie Dé nervaud Tendon, N. Geldner, Co-incidence of Damage and Microbial Patterns Controls Localized Immune Responses in Roots Article Co-incidence of Damage and Microbial Patterns Controls Localized Immune Responses in Roots. *Cell*. **180**, 440-453.e18 (2020).
8. K. Yu, Y. Liu, R. Tichelaar, N. Savant, E. Lagendijk, S. J. L. van Kuijk, I. A. Stringlis, A. J. H. van Dijken, C. M. J. Pieterse, P. A. H. M. Bakker, C. H. Haney, R. L. Berendsen, Rhizosphere-Associated Pseudomonas Suppress Local Root Immune Responses by Gluconic Acid-Mediated Lowering of Environmental pH. *Curr. Biol.* **29**, 3913-3920.e4 (2019).

9. D. E. Salt, I. Baxter, B. Lahner, Ionomics and the Study of the Plant Ionome. *Annu. Rev. Plant Biol.* **59**, 709–733 (2008).

10. G. Castrillo, P. J. P. L. Teixeira, S. H. Paredes, T. F. Law, L. de Lorenzo, M. E. Feltcher, O. M. Finkel, N. W. Breakfield, P. Mieczkowski, C. D. Jones, J. Paz-Ares, J. L. Dangl, Root microbiota drive direct integration of phosphate stress and immunity. *Nature*. **543**, 513–518 (2017).

11. O. M. Finkel, I. Salas-González, G. Castrillo, S. Spaepen, T. F. Law, P. J. P. L. Teixeira, C. D. Jones, J. L. Dangl, The effects of soil phosphorus content on plant microbiota are driven by the plant phosphate starvation response. *PLoS Biol.* **17**, e3000534 (2019).

12. A. Levy, I. Salas Gonzalez, M. Mittelviefhaus, S. Clingenpeel, S. Herrera Paredes, J. Miao, K. Wang, G. Devescovi, K. Stillman, F. Monteiro, B. Rangel Alvarez, D. S. Lundberg, T. Y. Lu, S. Lebeis, Z. Jin, M. McDonald, A. P. Klein, M. E. Feltcher, T. G. Rio, S. R. Grant, S. L. Doty, R. E. Ley, B. Zhao, V. Venturi, D. A. Pelletier, J. A. Vorholt, S. G. Tringe, T. Woyke, J. L. Dangl, Genomic features of bacterial adaptation to plants. *Nat. Genet.* **50**, 138–150 (2018).

13. Y. Bai, D. B. Müller, G. Srinivas, R. Garrido-Oter, E. Potthoff, M. Rott, N. Dombrowski, P. C. Münch, S. Spaepen, M. Remus-Emsermann, B. Hüttel, A. C. McHardy, J. A. Vorholt, P. Schulze-Lefert, Functional overlap of the Arabidopsis leaf and root microbiota. *Nature*. **528**, 364–369 (2015).

14. J. Alassimone, S. Naseer, N. Geldner, A developmental framework for endodermal differentiation and polarity. *Proc. Natl. Acad. Sci. U. S. A.* **107**, 5214–5219 (2010).

15. T. G. Andersen, S. Naseer, R. Ursache, B. Wybouw, W. Smet, B. De Rybel, J. E. M. Vermeer, N. Geldner, Diffusible repression of cytokinin signalling produces endodermal symmetry and passage cells. *Nature*. **555**, 529–533 (2018).

16. S. Naseer, Y. Lee, C. Lapierre, R. Franke, C. Nawrath, N. Geldner, Casparian strip diffusion barrier in Arabidopsis is made of a lignin polymer without suberin. *Proc. Natl.*

Acad. Sci. U. S. A. **109**, 10101–10106 (2012).

17. A. Emonet, F. Zhou, J. Vacheron, C. M. Heiman, V. D. Tendon, K.-W. Ma, P. Schulze-Lefert, C. Keel, N. Geldner, *bioRxiv*, in press, doi:10.1101/2020.08.03.233817.
18. T. Kamiya, M. Borghi, P. Wang, J. M. C. Danku, L. Kalmbach, P. S. Hosmani, S. Naseer, T. Fujiwara, N. Geldner, D. E. Salt, The MYB36 transcription factor orchestrates Casparian strip formation. *Proc. Natl. Acad. Sci. U. S. A.* **112**, 10533–8 (2015).
19. J. Liu, A. Osbourn, P. Ma, MYB transcription factors as regulators of phenylpropanoid metabolism in plants. *Mol. Plant*. **8** (2015), pp. 689–708.
20. M. González-Guzmán, N. Apostolova, J. M. Bellés, J. M. Barrero, P. Piqueras, M. R. Ponce, J. L. Micol, R. Serrano, P. L. Rodríguez, The short-chain alcohol dehydrogenase ABA2 catalyzes the conversion of xanthoxin to abscisic aldehyde. *Plant Cell*. **14**, 1833–1846 (2002).
21. E. M. Söderman, I. M. Brocard, T. J. Lynch, R. R. Finkelstein, Regulation and function of the arabidopsis ABA-insensitive4 gene in seed and abscisic acid response signaling networks. *Plant Physiol.* **124**, 1752–1765 (2000).
22. R. Wu, L. Duan, J. L. Pruneda-Paz, D. H. Oh, M. Pound, S. Kay, J. R. Dinneny, The 6xABRE synthetic promoter enables the spatiotemporal analysis of ABA-mediated transcriptional regulation. *Plant Physiol.* **177**, 1650–1665 (2018).
23. K. Hiruma, N. Gerlach, S. Sacristán, R. T. Nakano, S. Hacquard, B. Kracher, U. Neumann, D. Ramírez, M. Bucher, R. J. O'Connell, P. Schulze-Lefert, Root Endophyte Colletotrichum tofieldiae Confers Plant Fitness Benefits that Are Phosphate Status Dependent. *Cell*. **165**, 464–74 (2016).
24. S. Fujita, D. De Bellis, K. H. Edel, P. Köster, T. G. Andersen, E. Schmid-siegert, V. D. Tendon, A. Pfister, P. Marhavý, R. Ursache, V. G. Doblas, M. Barberon, J. Daraspe, A. Creff, G. Ingram, J. Kudla, N. Geldner, SCHENGEN receptor module drives localized ROS production and lignification in plant roots. *EMBO J.*, 1–18 (2020).

25. P. Wang, M. Calvo-Polanco, G. Reyt, M. Barberon, C. Champeyroux, V. Santoni, C. Maurel, R. B. Franke, K. Ljung, O. Novak, N. Geldner, Y. Boursiac, D. E. Salt, Surveillance of cell wall diffusion barrier integrity modulates water and solute transport in plants. *Sci. Rep.* **9**, 4227 (2019).

26. L. Song, S. S. C. Huang, A. Wise, R. Castanoz, J. R. Nery, H. Chen, M. Watanabe, J. Thomas, Z. Bar-Joseph, J. R. Ecker, A transcription factor hierarchy defines an environmental stress response network. *Science (80-.).* **354** (2016), doi:10.1126/science.aag1550.

27. K. N. Chang, S. Zhong, M. T. Weirauch, G. Hon, M. Pelizzola, H. Li, S. S. Carol Huang, R. J. Schmitz, M. A. Urich, D. Kuo, J. R. Nery, H. Qiao, A. Yang, A. Jamali, H. Chen, T. Ideker, B. Ren, Z. Bar-Joseph, T. R. Hughes, J. R. Ecker, Temporal transcriptional response to ethylene gas drives growth hormone cross-regulation in Arabidopsis. *Elife*. **2013** (2013), doi:10.7554/eLife.00675.

28. D. S. Lundberg, S. Yourstone, P. Mieczkowski, C. D. Jones, J. L. Dangl, Practical innovations for high-throughput amplicon sequencing. *Nat. Methods*. **10**, 999–1002 (2013).

29. S. M. Yourstone, D. S. Lundberg, J. L. Dangl, C. D. Jones, MT-Toolbox: Improved amplicon sequencing using molecule tags. *BMC Bioinformatics*. **15**, 284 (2014).

30. B. J. Callahan, P. J. McMurdie, M. J. Rosen, A. W. Han, A. J. A. Johnson, S. P. Holmes, DADA2: High-resolution sample inference from Illumina amplicon data. *Nat. Methods*. **13**, 581–583 (2016).

31. P. D. Schloss, S. L. Westcott, T. Ryabin, J. R. Hall, M. Hartmann, E. B. Hollister, R. A. Lesniewski, B. B. Oakley, D. H. Parks, C. J. Robinson, J. W. Sahl, B. Stres, G. G. Thallinger, D. J. Van Horn, C. F. Weber, Introducing mothur: Open-Source, Platform-Independent, Community-Supported Software for Describing and Comparing Microbial Communities. *Appl. Environ. Microbiol.* **75**, 7537–7541 (2009).

32. C. Quast, E. Pruesse, P. Yilmaz, J. Gerken, T. Schweer, P. Yarza, J. Peplies, F. O. Glöckner, The SILVA ribosomal RNA gene database project: Improved data processing and web-based tools. *Nucleic Acids Res.* **41** (2013), doi:10.1093/nar/gks1219.

33. J. Oksanen, vegan : Community Ecology Package. R package version 1.8-5 (2007).

34. M. I. Love, W. Huber, S. Anders, Moderated estimation of fold change and dispersion for RNA-seq data with DESeq2. *Genome Biol.* **15**, 550 (2014).

35. H. Wickham, *ggplot2: elegant graphics for data analysis* (Springer International Publishing, 2016; http://link.springer.com/10.1007/978-3-319-24277-4), vol. 174 of *Use R!*

36. B. Lahner, J. Gong, M. Mahmoudian, E. L. Smith, K. B. Abid, E. E. Rogers, M. L. Guerinot, J. F. Harper, J. M. Ward, L. McIntyre, J. I. Schroeder, D. E. Salt, Genomic scale profiling of nutrient and trace elements in Arabidopsis thaliana. *Nat. Biotechnol.* **21**, 1215–1221 (2003).

37. P. N. Soltanpour, A. P. Schwab, A new soil test for simultaneous extraction of macro and micro-nutrients in alkaline soils. *Commun. Soil Sci. Plant Anal.* **8**, 195–207 (1977).

38. M. Wu, J. A. Eisen, A simple, fast, and accurate method of phylogenomic inference. *Genome Biol.* **9**, R151 (2008).

39. K. Katoh, K. Misawa, K.-I. Kuma, T. Miyata, “MAFFT: a novel method for rapid multiple sequence alignment based on fast Fourier transform.”

40. S. Capella-Gutiérrez, J. M. Silla-Martínez, T. Gabaldón, trimAl: a tool for automated alignment trimming in large-scale phylogenetic analyses. *Bioinforma. Appl. NOTE*. **25**, 1972–1973 (2009).

41. M. N. Price, P. S. Dehal, A. P. Arkin, FastTree 2 - Approximately maximum-likelihood trees for large alignments. *PLoS One*. **5**, e9490 (2010).

42. T. Thiergart, P. Durán, T. Ellis, N. Vannier, R. Garrido-Oter, E. Kemen, F. Roux, C. Alonso-Blanco, J. Ågren, P. Schulze-Lefert, S. Hacquard, Root microbiota assembly and adaptive differentiation among European Arabidopsis populations. *Nat. Ecol. Evol.* **4**,

122–131 (2020).

43. J. Schindelin, I. Arganda-Carreras, E. Frise, V. Kaynig, M. Longair, T. Pietzsch, S. Preibisch, C. Rueden, S. Saalfeld, B. Schmid, J. Y. Tinevez, D. J. White, V. Hartenstein, K. Eliceiri, P. Tomancak, A. Cardona, Fiji: An open-source platform for biological-image analysis. *Nat. Methods*. **9** (2012), pp. 676–682.

44. G. Reyt, P. Ramakrishna, I. Salas-González, S. Fujita, D. Tiemessen, C. Lapierre, K. Morreel, M. Calvo, P. Flis, N. Geldner, Y. Boursiac, W. Boerjan, G. Castrillo, D. E. Salt, Schengen-pathway controls spatially separated and chemically distinct lignin deposition in the endodermis. *bioRxiv*, in press, doi:10.1101/2020.10.07.329664.

45. E. C. Perin, R. L. Crizel, V. Galli, R. da Silva Messias, C. V. Rombaldi, F. C. Chaves, Extraction and Quantification of Abscisic Acid and Derivatives in Strawberry by LC-MS. *Food Anal. Methods*. **11**, 2547–2552 (2018).

46. R. Ursache, T. G. Andersen, P. Marhavý, N. Geldner, A protocol for combining fluorescent proteins with histological stains for diverse cell wall components. *Plant J.* **93**, 399–412 (2018).

47. I. Letunic, P. Bork, Interactive Tree Of Life (iTOL) v4: recent updates and new developments. *Web Serv. issue Publ. online*. **47** (2019), doi:10.1093/nar/gkz239.

48. L. J. Revell, phytools: an R package for phylogenetic comparative biology (and other things). *Methods Ecol. Evol.* **3**, 217–223 (2012).

49. J. Hua, E. M. Meyerowitz, Ethylene responses are negatively regulated by a receptor gene family in Arabidopsis thaliana. *Cell*. **94**, 261–271 (1998).

50. T. Potuschak, E. Lechner, Y. Parmentier, S. Yanagisawa, S. Grava, C. Koncz, P. Genschik, “EIN3-Dependent Regulation of Plant Ethylene Hormone Signaling by Two Arabidopsis F Box Proteins: EBF1 and EBF2 romyces cerevisiae are composed of four primary sub-units: CDC53 (cullin1), RBX1, SKP1, and an F box pro-tein. The F box proteins contain a degenerated protein domain of approximately 50-60 amino acid

residues, identified first in the N-terminal region of cyclin F (Bai" (2003).

51. J. Logemann, J. Schell, L. Willmitzer, Improved method for the isolation of RNA from plant tissues. *Anal. Biochem.* **163**, 16–20 (1987).

52. A. M. Bolger, M. Lohse, B. Usadel, Trimmomatic: A flexible trimmer for Illumina sequence data. *Bioinformatics*. **30**, 2114–2120 (2014).

53. D. Kim, B. Langmead, S. L. Salzberg, HISAT: A fast spliced aligner with low memory requirements. *Nat. Methods*. **12**, 357–360 (2015).

54. Y. Liao, G. K. Smyth, W. Shi, The Subread aligner: fast, accurate and scalable read mapping by seed-and-vote, doi:10.1093/nar/gkt214.

55. G. Yu, L. G. Wang, Y. Han, Q. Y. He, ClusterProfiler: An R package for comparing biological themes among gene clusters. *Omi. A J. Integr. Biol.* **16**, 284–287 (2012).

56. C. M. Fraser, C. Chapple, The Phenylpropanoid Pathway in Arabidopsis. *Arab. B.* **9**, e0152 (2011).

57. R. Franke, I. Briesen, T. Wojciechowski, A. Faust, A. Yephremov, C. Nawrath, L. Schreiber, Apoplastic polyesters in Arabidopsis surface tissues - A typical suberin and a particular cutin. *Phytochemistry*. **66**, 2643–2658 (2005).

58. R. B. Franke, I. Dombrink, L. Schreiber, Suberin Goes Genomics: Use of a Short Living Plant to Investigate a Long Lasting Polymer. *Front. Plant Sci.* **3**, 4 (2012).

59. R. B. Franke, Caspary's conductor. *Proc. Natl. Acad. Sci. U. S. A.* **112** (2015), pp. 10084–10085.

60. L. M. Liberman, E. E. Sparks, M. A. Moreno-Risueno, J. J. Petricka, P. N. Benfey, MYB36 regulates the transition from proliferation to differentiation in the Arabidopsis root. *Proc. Natl. Acad. Sci. U. S. A.* **112**, 12099–12104 (2015).

61. D. Roppolo, B. De Rybel, V. D. Tendon, A. Pfister, J. Alassimone, J. E. M. Vermeer, M. Yamazaki, Y. D. Stierhof, T. Beeckman, N. Geldner, A novel protein family mediates Casparian strip formation in the endodermis. *Nature*. **473**, 381–384 (2011).

62. P. S. Hosmani, T. Kamiya, J. Danku, S. Naseer, N. Geldner, M. Lou Guerinot, D. E. Salt, Dirigent domain-containing protein is part of the machinery required for formation of the lignin-based Casparian strip in the root. *Proc. Natl. Acad. Sci. U. S. A.* **110**, 14498–14503 (2013).

63. A. Pfister, M. Barberon, J. Alassimone, L. Kalmbach, Y. Lee, J. E. M. Vermeer, M. Yamazaki, G. Li, C. Maurel, J. Takano, T. Kamiya, D. E. Salt, D. Roppolo, N. Geldner, A receptor-like kinase mutant with absent endodermal diffusion barrier displays selective nutrient homeostasis defects. *Elife*. **3**, e03115 (2014).

64. I. Cheddadi, M. Génard, N. Bertin, C. Godin, Coupling water fluxes with cell wall mechanics in a multicellular model of plant development. *PLoS Comput. Biol.* **15**, e1007121 (2019).

65. H. Cohen, V. Fedyuk, C. Wang, S. Wu, A. Aharoni, *Plant J.*, in press, doi:10.1111/tpj.14711.

66. J. Durr, G. Reyt, S. Spaepen, S. Hilton, C. Meehan, W. Qi, T. Kamiya, P. Flis, H. G. Dickinson, A. Feher, G. D. Bending, P. Schulze-Lefert, D. Salt, J. Gutierrez-Marcos, Two Receptor-Like Kinases Required For Arabidopsis Endodermal Root Organisation Shape The Rhizosphere Microbiome. *bioRxiv*, 816330 (2019).

67. A. Sanchez-Villarreal, J. Shin, N. Bujdoso, T. Obata, U. Neumann, S. X. Du, Z. Ding, A. M. Davis, T. Shindo, E. Schmelzer, R. Sulpice, A. Nunes-Nesi, M. Stitt, A. R. Fernie, S. J. Davis, TIME for COFFEE is an essential component in the maintenance of metabolic homeostasis in Arabidopsis thaliana. *Plant J.* **76**, 188–200 (2013).

68. V. Compagnon, P. Diehl, I. Benveniste, D. Meyer, H. Schaller, L. Schreiber, R. Franke, F. Pinot, CYP86B1 is required for very long chain ω-hydroxyacid and α,ω-dicarboxylic acid synthesis in root and seed suberin polyester. *Plant Physiol.* **150**, 1831–1843 (2009).

69. K. Meyer, A. M. Shirley, J. C. Cusumano, D. A. Bell-Lelong, C. Chapple, Lignin monomer composition is determined by the expression of a cytochrome P450-dependent

monooxygenase in Arabidopsis. *Proc. Natl. Acad. Sci. U. S. A.* **95**, 6619–6623 (1998).